EXPERIMENTAL STUDY OF POSSIBLE USES OF CRUMB RUBBER FOR STRUCTURAL APPLICATIONS

by

ESTEBAN I. PABÓN VÁZQUEZ

A thesis submitted in partial fulfillment of the requirements for the degree of

MASTER OF SCIENCE
in
CIVIL ENGINEERING

UNIVERSITY OF PUERTO RICO
MAYAGÜEZ CAMPUS
2014

Approved by:

José O. Guevara-Guillen, PhD Member, Graduate Committee	Date
Luis E. Suarez-Colche, PhD Member, Graduate Committee	Date
Daniel Wendichansky-Bard, PhD President, Graduate Committee	Date
Silvestre Colón-Ramirez, MS Representative of Graduate Studies	Date
Ismael Pagán-Trinidad, MSCE Chairperson of the Department	Date

ABSTRACT

Currently many nations, including the United States, confront one of the biggest international problems concerning the disposal of solid waste, as scrap tires are when they are not properly disposed. To contribute to the solution of this problem, this research was aimed to study some alternatives scrap tires can have in its use in structural engineering applications through the crumb rubber process.

In order to meet these objectives, two types of experimental tests were performed. The first were used to determine the mechanical properties of the crumb rubber, while the latter to evaluate the possible structural applications. The latter included: (1) the use of the crumb rubber as confinement to increase the compressive strength of slender steel elements, (2) the use of the rubber as infill into steel frames to withstand lateral loads caused by earthquakes, and (3) reinforce the crumb rubber along with steel rebars to create a shear wall with more stiffness to withstand lateral loads caused by earthquakes. The results of these tests showed that: (1) the compressive strength of steel elements with high slenderness can be increased up to 80% using the crumb rubber as a confinement element , (2) the crumb rubber infill panel used in steel frames is sensitive to the slenderness of the wall, making unfeasible to construct a real size wall due to the slenderness increment, (3) the presence of steel in the reinforced crumb rubber shear wall increase the system stiffness and generate an hysteretic behavior, dissipating energy through load cycles.

Finally, the results of the reinforced crumb rubber shear wall were applied to a real building frame as an alternative design to resist the lateral loads induced by earthquakes and were compared to a typical masonry infill frames building. With those models a time history analysis was performed using the structural analysis program SAP2000. It was found that the reinforced crumb rubber shear wall reduced the base shear forces to 40-68 %, resulting in a reduction of the frame sections sizes and costs, facilitating the building design and construction process.

RESUMEN

Actualmente Estados Unidos y muchos otros países enfrentan el problema de la disposición de desperdicios sólidos, entre los que se encuentran los desperdicios de gomas o llantas de automóviles, entre otros vehículos de motor que cada año se acumulan, agravando los problemas ambientales. Debido a este problema, esta investigación estudia alternativas para el uso de la goma chatarra en aplicaciones de ingeniería estructural, a través del proceso de trituración de goma.

Para cumplir con estos objetivos se realizaron dos tipos de pruebas experimentales, donde las primeras se utilizaron para determinar las propiedades mecánicas de la goma triturada, y las segundas para evaluar las posibles aplicaciones estructurales. En el segundo tipo de pruebas se evaluó la posibilidad de: (1) utilizar la goma como confinamiento para incrementar la capacidad compresiva de elementos esbeltos de acero, (2) utilizar la goma como material de relleno en pórticos de aceros para soportar las cargas laterales ocasionadas por sismos, and (3) reforzar la goma triturada con varillas de acero para crear un muro o pared de corte reforzada con mayor rigidez para soportar las cargas laterales ocasionadas por sismos. Los resultados de estas pruebas mostraron que: (1) es posible aumentar hasta un 80 % la capacidad compresiva de elementos de acero con alta esbeltez utilizando la goma triturada como confinamiento, (2) la respuesta a cargas laterales de la goma utilizada como panel de relleno en pórticos de acero es sensitiva a la esbeltez del panel, haciendo que no sea viable construir una pared de tamaño real debido al aumento de esbeltez, (3) la presencia del acero en el muro de corte de goma triturada incrementó la rigidez del sistema y generó un comportamiento histerético a través de los ciclos de carga.

Finalmente se extendió el resultado del muro de corte de goma reforzada a un pórtico de un edificio real, como una alternativa de diseño para la resistencia de cargas laterales inducidas por movimientos sísmicos, y fue comparado con un edificio típico de pórticos rellenos de mampostería. Con estos modelos se realizó un análisis tiempo-historia, y utilizando el programa de análisis estructural SAP2000, se encontró

que el muro de corte de goma reforzada triturada, redujo las fuerzas entre un 40 – 68 %, lo que redundaría en la reducción de los tamaños y costos de las secciones de los elementos del pórtico, facilitando el diseño y la construcción del edificio.

ACKNOWLEDGMENTS

The achievement of this research would not have been possible without the collaboration of the great people who surrounds me. I really appreciate their help and through these lines I want to express my gratitude toward them.

To GOD, to whom belong all things and by whom all things visible and invisible were created, who gave me the strength to achieve this goal.

To my parents, my brother and my fiancée for their support, who have always been there to help me in all situations.

To my mentor, Dr. Daniel Wendichansky, for his help throughout this research. His advices helped me growing in the professional and personal areas.

To the members of my graduate committee, Dr. Luis E. Suárez and Dr. José O. Guevara, for their collaboration with this investigation.

To José Rivera and Yomar Pérez, for their friendship and collaboration with this research and my graduate studies.

To Elvis Ramos, for his help with the experiments construction setup of this research, for his advices and his friendship.

To Monserrate Cruz, for his authorization to work at Laboratory of Materials.

To Nicodemo Crespo, for helping me with the preparation of some specimens for the experimental tests.

To Iván Santiago, for his collaboration on the instrumentations and tests setup.

TABLE OF CONTENTS

LIST OF FIGURES

LIST OF TABLES

CHAPTER 1

INTRODUCTION

1.1JUSTIFICATION OF THIS RESEARCH

Currently United States and many other countries around the world are facing many problems about the disposal of waste material. The United States produces alone 260 million of waste tires annually, without taking into account the 40 million of scrap tires from truck tires. According to the industry more than 800 million scrap tires are currently in stockpile. For these reasons, the Environmental Protection Agency (EPA) estimates that within the next ten years, the majority of the US landfills will be closed due to many factors like regulations, design modifications and costs; making this one of the most crucial environmental problems in the last years (Cadamuro, 2009). Developed countries have a higher growing rate than under-developed countries. As an example, the production of scrap tire has increased to a rate of one tire per person per year (1 tire/per/yr) in the United States and Puerto Rico. In Puerto Rico this situation is aggravated since scrap tires cannot be disposed, as ordered by the law 179. One of the major concerns regarding this topic is how the scrap rubber is disposed on landfills, because it could give rise health problems and development of fires. On the other hand, not disposing it properly leads to illegal landfills setting-up, which become a bigger problem (Botero et. al 2005).

Besides the environmental problems concerning the disposal of scrap tire, there is an additional problem of water accumulation, which is the principal reason for the growth of the mosquito *Aedes aegypti*, vector of the dengue virus. According to the Center for Disease Control and Prevention (CDC), the mosquito lays her eggs on the sides of containers with water and eggs hatch into larvae after a rain or flooding. People also furnish shelters in their houses, as the *Aedes aegypti* preferentially rests in dark cool areas, such as closets, leading the mosquito to bite indoors. According to The World Health Organization (WHO), today dengue ranks as the most important mosquito-borne viral disease in the world, and up to 50 million infections occur annually with 500,000 cases of dengue haemorrhagic fever reported and 22,000 deaths mainly among children.

Knowing all the factors mentioned above, it is important to consider alternatives in the use of scrap tires and one of them is its use in structural engineering applications, in order to improve the performance of the structure under earthquake loads. Even in technologically advanced countries, like US and Japan, the earthquakes have damaged many modern buildings, requiring expensive structural and nonstructural repairs, leading to the development of retrofitting techniques in order to meet with the functionality requirements. These techniques are the conventional strengthening or stiffness techniques like the use of steel jackets, increase the beams or columns shear resistance, applications of Fiber Reinforced Polymers (FRP), and the new and innovative concepts of structural protection by the use of seismic isolation systems and supplemental damping devices (Santiago, 2002).

This investigation aims to determine the feasibility of the use of scrap tires in structural applications, and establish how suitable would be the crumb rubber, with regard to these applications, or any other structural problem. One of the principal points on these investigations is to study the use of the recycled crumb rubber as confinement for a slender compression steel element. Indeed, it is a fact that an unbraced slender compression steel element can fail in sudden way by buckling because the inherent instabilities of the mechanism. This is similar to trying to compress a straw or a very slender stick. As soon as it is loaded, is bended close to half of its length, failing by buckling. However, if it is placed into a mass of some material that provide enough confinement or lateral restriction (this is analogous to put a lateral load or try to hold the straw with the hand), a large load will be necessary to make it fails. On the other hand, the lateral force required to prevent the buckling failure is small. Therefore, providing confinement along the full length of the steel element using a mass of recycled crumb rubber, could increase the ultimate compressive strength, or make the element fails in a plastic fashion. This technique could be used to provide lateral bracing on slender beams that are prone to be affected by lateral torsional buckling.

Also, the rubber can act as a block wall (analogous to a masonry wall or infill masonry panel), providing lateral resistance, to retrofit steel buildings instead of lateral bracings or dampers in order to resist the lateral forces generated by an earthquake. Also, it could be possible to construct small houses or structures using this kind of walls. However, the flexibility of the crumb rubber walls is one of the major problems of it. For this reason, it may necessary to reinforce the recycled crumb rubber wall with steel rebars in order to increase the stiffness, reducing the lateral deformations, and consequently the inter-story drift. In the other hand, compared to reinforced masonry walls building, this system is considerably more flexible, leading to a possible increase in the natural period of the structure. This leads to a reduction of the base shear, using the design spectra philosophy (ASCE 7-05, 2005). Besides, the steel reinforcement could help dissipating energy through hysteretic cycles.

In short, the problem of the scrap tire is very complex. On one side, the problem of allocating more land for landfill use is increasing alarmingly. On the other hand, the diseases linked to the accumulation of water, such as the dengue virus, is other reason for society to address the problem of scrap tire production. Addressing the problems derived from the production of scrap tires, this investigation explores the possible uses of crumb rubber for structural applications: to contribute to solve environmental and health problems, and provide a new solution to conventional structural engineering problems.

1.2 RESEARCH OBJECTIVES

The main objectives of this research are to:

- Determine the mechanical properties of the crumb rubber, as it is currently manufactured by Sofscape Caribe Inc., in order to know the specific properties of the provided batch, and set the starting point to predict the behavior of the rubber in following tests.
- Determine the applicability of the rubber as confining element to avoid the buckling failure of a slender steel element, or to increase the compressive strength.

- Determine the behavior of the crumb rubber as an infill panel subjected to a lateral load and examine if the system exhibits a hysteretic behavior.
- Determine the behavior of the crumb rubber as a Plain Shear Wall. Approximate the Shear Modulus or Stiffness.
- Determine the behavior of a crumb rubber Reinforced Shear Wall with plain steel rebar. Examine if the panel presents a hysteretic behavior and their applicability for a real structure.

CHAPTER 2

LITERATURE REVIEW

Currently, there are some alternatives to manage the disposal of scrap tires in order to avoid their placement into landfills. Velásquez (2001) mentioned four alternatives to accomplish this:

1. Reducing the production of tires by increasing its useful life improving their capacity and performance.
2. Reusing the pneumatics by recapping it, consisting of adhering new layers of tire rubber to make it useful again.
3. Recovering energy through the use of rubber as tire derived fuel (TDF).
4. Recycling the rubber through granulation and other methods. The results of this process are pieces of rubber with different sizes which can be used as aggregate or molded products.

Velázquez pointed out that reusing the rubber by recapping it or prolonging its useful life is a partial solution, because it can be done just for a few times, but finally it will be discarded. Second, the recovering of energy by TDF generates harmful residues for the environment, principally due to smoke emissions loaded with highly contaminant materials. For these reasons, the author recommended as a more feasibility alternative the recycling of the scrap tires, reducing the environmental problem, and making it useful products with economic benefits.

The most common process to recycle the scrap tire is through crumb rubber. Crumb rubber consists of rubber particles free of wire. The particles can vary in size from 2.95×10^{-3} to 1.87×10^{-1} in. After been processed one scrap tire can produce up to 10 to 12 lb. of crumb rubber (Cadamuro, 2009). One of the products derived from the crumb rubber is safety rubber pavers or simply rubber pavers. The pavers can serve as sidewalks, recreational and playgrounds and track surfaces. Other application in which the crumb rubber paver is used is in horse stalls and wash rack areas. Also, the crumb rubber has been used in several other applications such as: retaining wall backfill, aggregate for concrete mixes, landfill liners and rubberized asphalt.

However, the potential health risk the recycled waste tires may have to people is still a concern. Due to its frequent use for outdoor playground and track, the California Integrated Waste Management Board's (CIWMB) approached this concern requesting to the Office of Environmental Health Hazard Assessment (OEHHA) a report (Evaluation of Health Effects of Recycled Waste Tires in Playground and Track products, 2007) to assess the potential health risks in children, taking the previous facilities mentioned above, constructed from recycled waste tires, as the setting for studies. To evaluate for these risks, the OEHHA conducted the following principal studies: (1) evaluation of toxicity due to ingestion or dermal contact, (2) evaluation of the potential impact to the local environment, including the local ecology.

They reported the findings of 46 studies found in scientific literature that analyzed and measured the release of chemical substances from recycled tires using laboratory and field settings for the studies and identifying 49 different chemicals. Using the highest published concentration levels of chemicals released from the recycled tires used, they calculated the likelihood for noncancer health effects for a one-time ingestion of ten grams of tire shreds by a typical three-year-old child. They determined that just the exposure to zinc exceeded the health-based screening value (i.e., value promulgated by a regulatory agency such as OEHHA or U.S. EPA). However, overall, they considered that it is unlikely that a one-time ingestion of tire shreds would produce adverse health effects in the population under study.

For testing the consequences of skin sensitization after rubberized surfaces contact, they contracted a laboratory to perform the testing on guinea pig skin; where they were exposed to rubber. From the results, they observed no skin sensitization, suggesting that these types of surfaces would not cause skin sensitization on children.

In addition, they studied the effect on health these materials may have after been burned. After the fire event occurred at the Yulupa Elementary School in Sonama County, California, the burned soil there was taken as the sample for the study. They collected the soil samples below the playground to test for a variety of chemical substances and compared the results with the basal levels from the rest of the soils of the United States. The results of the collected soil samples showed that chemicals found on these soils were at or below the reference levels, suggesting a low risk to the local ecology. They mentioned the results of U.S. EPA testing performed with the air of the burning site demonstrating no health risk problem for the clean-up workers. It was also shown, that the soil/rubber mixture removed from the site did not represent a hazardous waste.

One of the possible uses of the crumb rubber proposed in this investigation is the use of crumb rubber as slender steel element confinement for compressive loads. The principal problem in this mechanism is the action of rebars as columns, because their slenderness can cause early failure by buckling. Salmon et al. (2008), mentioned that a compression flange of a beam can be seen as a column and treated like it. The difference between those two lie on the restriction provided by the web of the beam, which limits the possible buckling towards one of the sides of the flange. However, no restrictions in the out-of-plane beam's direction are provided to avoid a possible buckling failure. Therefore, the buckling failure can be avoided by providing lateral bracing with low stiffness, because a low lateral force is required to maintaining the stability of the compression flange. Yura (2001) discussed the fundamentals of bracing and pointed out that the lateral force required to achieve a fully plastic fashion failure is in the range of 0.3 to 10 percent of the compression force on the element. A rule of thumb adopted often is to use 2 % (Lawless and Hawk, 2013). Although the crumb rubber has low stiffness, it is possible to provide some level of continuous lateral bracing by confining the compression element into the mass, increasing the ultimate load or, at best, causing the steel fails in a fully plastic way.

Following a similar idea, the closest study to this research was conducted by Cadamuro (2009). Cadamuro studied the effect of confine steel rebars in a mass of crumb rubber to create a composite pile. Cadamuro constructed two different configurations of piles. The first one was a bare pile made of crumb rubber, and the second one was constructed with 5 #4 rebars to reinforce the pile. After conducting the test, the unreinforced crumb rubber pile reached a maximum stress of 242.42 psi, while the reinforced pile failed at a maximum stress of 2,424.24 psi. Therefore, the investigation concluded that it is feasible to use this composite pile for some applications. There is a substantial increment in the maximum stress for failure, and it was also found that this maximum stress is consistent with timber piles.

There is no information in the literature about the use of crumb rubber as masonry walls, masonry infill panels, or in retrofitting techniques. Thus, in this investigation, the blocks of crumb rubber will be treated as masonry with their corresponding properties, and the appropriate literature will be reviewed, in order to establish how effectively is to compare the strength and behavior of both materials.

For a long time researcher have been evaluating the behavior of infilled frames. In general, infilled frames are analyzed using models that replace the infill wall by an equivalent pin-jointed diagonal strut, as seen in Figure 1. The idea behind this concept is that the infill wall stiffness is provided by the width of the equivalent strut, implying that as it increases the overall frame stiffness increases as well. Early followers of this concept were Polyakov (1960) and Holmes (1961). Holmes, through several numerical simulations and parametric analysis, proposed a strut with a as a third of the diagonal length r_{inf}.

Stafford Smith (1966) introduced a theoretical relationship for the width of the diagonal strut based on the relative stiffness of infill and frame and using the parameter λ_h:

$$\lambda_h = \sqrt[4]{\frac{E_m * t * \sin(2\theta)}{4 * E_c * I_c * H}} \qquad \textbf{(1)}$$

where

E_m = modulus of elasticity of masonry.

E_c= modulus of elasticity of the frame column.

t = thickness of the infill panel.

I_c = moment of inertia of the column.

H = height of the infill.

θ = angle of the of the infill diagonal.

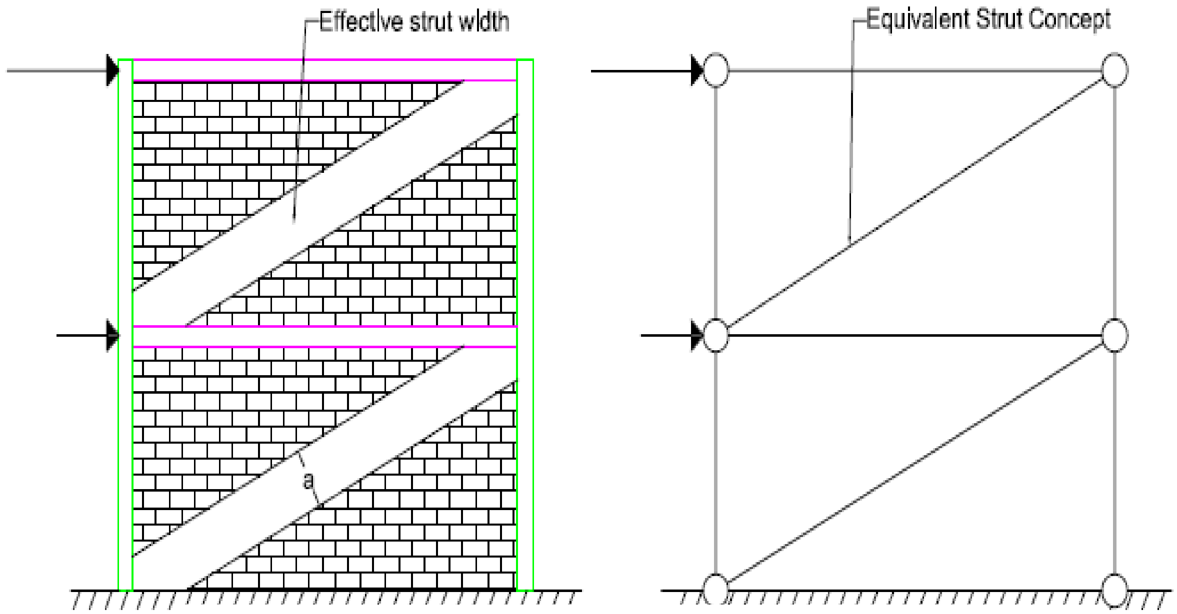

(a) Laterally loaded Infilled Frame ; (b) Equivalent strut concept

Figure 1. Equivalent Strut Concept

Smith and Carter (1969) proposed the following equation to calculate the width of the strut:

$$a = 0.58 * \left(\frac{1}{H}\right)^{-0.445} * (\lambda_h * h_c)^{0.335 * r_{inf} * \left(\frac{1}{H}\right)^{0.064}} \qquad \textbf{(2)}$$

where

h_c = column height

Mainstone (1974), suggested the following expression, using the parameter λ_h (this expression was later adopted by the Federal Emergency Management Agency (FEMA) papers):

$$a = 0.175 * r_{inf} * (\lambda_h * h_c)^{-0.4} \qquad \textbf{(3)}$$

Kadir (1974) concluded that the dimension of the strut is influenced by the top beam, in addition to the frame columns. To take this into account, he proposed the introduction of a parameter λ_g:

$$\lambda_g = \sqrt[4]{\frac{E_m * t * \sin(2\theta)}{4 * E_b * I_b * H}} \quad (4)$$

where

E_b = modulus of elasticity of the beam.

I_b = moment of inertia of the beam.

Using the parameters λ_h and λ_g he calculated the width of the equivalent strut as:

$$a = \frac{\pi}{2} * \left(\frac{1}{4 * \lambda_h^2} + \frac{1}{4 * \lambda_g^2}\right) \quad (5)$$

Liaw and Kwan (1984), based on experimental results obtained from steel frames with masonry infills, suggested the following expression:

$$a = \frac{0.95 * H * \cos(\theta)}{\sqrt{\lambda_h * h_c}} \quad (6)$$

Paulay and Priestley (1992), following the Holmes idea, proposed an equivalent strut width of a fourth of the infill diagonal length. Many researches had studied the infilled frame behavior in order to determine the strength capacity and many equations had been proposed. For this research the FEMA 306 methodology reported in the 1998 publication was used to evaluate the strength capacity of the masonry infill frames and it is going to be discussed in the next chapters.

In terms of failures modes, Leuchars and Scrivener (1976) defined three types of failures inherent to the panels: (1) Shear, sliding failure bed, (2) Diagonal tension cracking through masonry and mortar, (3) Local crushing of the masonry in a compression corner. They revealed that this process begins with an elastic behavior, in which the system reaches 50% of the ultimate strength. The masonry panel starts exhibiting different deformations than the frame after the shear forces slide the wall block beds. This causes the walls to separate from the columns, except at the corners, thus generating the equivalent diagonal.

Meanwhile, Paulay and Priestley mentioned that infilled frames at low levels of in-plane lateral forces, act in a fully composite fashion, as a structural wall with boundary elements. As Leuchars and

Scrivener described, the panel tries to deform in a shear mode separating from the frame after the increase of the lateral deformation. Then, the compression diagonal or strut makes contact only at the corners of the frame, at a level of 50-70 % of the ideal lateral shear capacity of the frame. After the separation, the authors recommended to use 0.25 of the diagonal length for the width of the strut. The reason for this is that if a lower strut width is chosen for the design, the rigidity of the braced frame will decrease, producing a lower seismic response as mentioned previously. Therefore, it is conservative to choose the maximum strut width, because the final design will be based on higher loads.

CHAPTER 3

EXPERIMENTAL TESTS FOR THE USE OF CRUMB RUBBER

3.1 INTRODUCTION

In the existing literature there are relevant studies concerning the mechanical properties of the crumb rubber used for playground surfaces. Currently, the information available about this particular is basically found on the internet web pages from some of the manufacturers of this product. For this research, the crumb rubber material used was obtained from playground blocks and tested at the Structural Laboratory of the University of Puerto Rico at Mayagüez to determine the mechanical properties due to the lack of information regarding this matter. These blocks were donated from the manufacturer Sofscape Caribe Inc., from Vega Baja, Puerto Rico. However, the properties of the material used could fluctuate due to the source of the raw material, manufacturing process, storage place, among other factors.

It is necessary to know the mechanical properties of the crumb rubber to establish its possible use of in structural applications. To accomplish this, the first sections of this chapter present the methodology of two experimental tests: (1) Specific weight, an important property which identifies a material, and (2) Axial cyclic load (ACL) test intended to determine the mechanical properties. The remaining sections will show the configuration or design of the performed tests to identify possible uses of the crumb rubber. For this, two main tests were developed: (1) Confined (with crumb rubber) Compression Steel Rebars tests, and (2) Crumb Rubber walls tests. Figure 2 shows the flowchart of the test plan, which contains all the experimental tests performed in this research and discussed in this thesis.

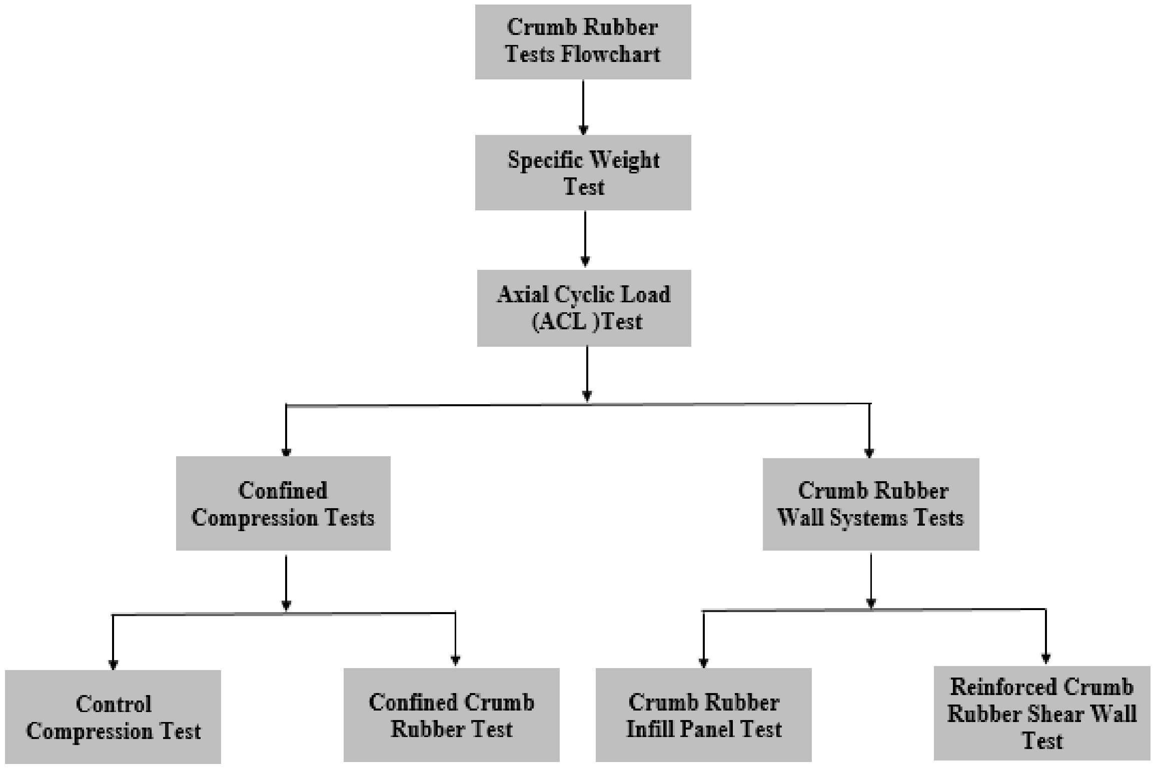

Figure 2. Test plan flowchart.

3.2 SPECIFIC WEIGHT

Specific weight is an important characteristic used to identify a certain material and to indicate the degree of uniformity among different sampling units or specimens. Physically and mathematically is defined, as the weight per unit of volume of the material.

In this investigation, this property was obtained through the volume displacement technique. This technique consists of weighing a piece of the material and immersing it into a calibrated test tube with a known liquid volume. For this test, four irregular pieces of rubber were taken from the batch and weighed. Finally, they were immersed into the calibrated test tube, filled with water, to measure the volume of the rubber specimens.

3.3 MECHANICAL PROPERTIES OF THE CRUMB RUBBER: AXIAL CYCLIC LOAD TEST

The crumb rubber has not been used for structural purposes. Due to the variability of the source and manufacturing of the material, there are several questions that need to be answered, before proposing a formal use for it. To corroborate the manufacturer's properties and explore new ones, a cyclic load test was developed. This test provides information about the compressive properties, like the modulus of elasticity and compressive strength of the material when the entire cross section is uniformly loaded in the axial direction at uniform rates of straining or loading. Also, it provides information about the tension and yield strength, the ability of the material to dissipate energy through hysteresis, and to determine applying load velocity affects the load behavior response.

The test was performed using two layout configuration (Configuration A and B), as seen in Figure 3, to asses if anisotropy modify the load response of the specimens. Table 1 shows all the information regarding the specimen such as: layout configuration, load cycles and the velocity rate. The cross sectional area shown in the plan views in Figure 3 was calculated as a rectangular area. Figure 4 shows the setup used in the axial cyclic load test, which consists of: (1) Deluxe Testing Machine, Tensile and Compression Testing with load capacity of 4,000 lb, (2) Load Cell with capacity of 1,000 lb to measure the load carried by the specimen, (3) Linear Variable Differential Transformer (LVDT) with maximum deformation of 6 in to measure the deformation of the specimen, and (4) two rigid steel plates (top and bottom) to uniformly distribute the load on the specimen. All the data collected in this thesis by LVDTs and load cells was recorded using the DasyLab software, which is a data acquisition system for laboratory or experimental tests.

The load was applied at different intervals, depending if the specimen could withstand tension forces. For specimens with tensions, the load was applied at intervals of 100 lb, with five repetitions. For compression only, the load was applied at intervals of 200 lb, with same amount of repetitions. To apply the tension loads, a coat of epoxy was used to bond the rubber specimens to the steel plates.

Table 1. Cyclic load test specimen layout and load configuration.

Specimen	Configuration	Cross Section Area	Load Cycles	Velocity Rate
		(in^2)		(in/min)
ACL-1	A	8.75	Tension/Compression	0.2
ACL -2	B	4.375	Tension/Compression	0.2
ACL -3	A	8.75	Compression	0.2
ACL -4	B	4.375	Compression	0.2
ACL -5	A	8.75	Compression	0.8
ACL -6	B	4.375	Compression	0.8

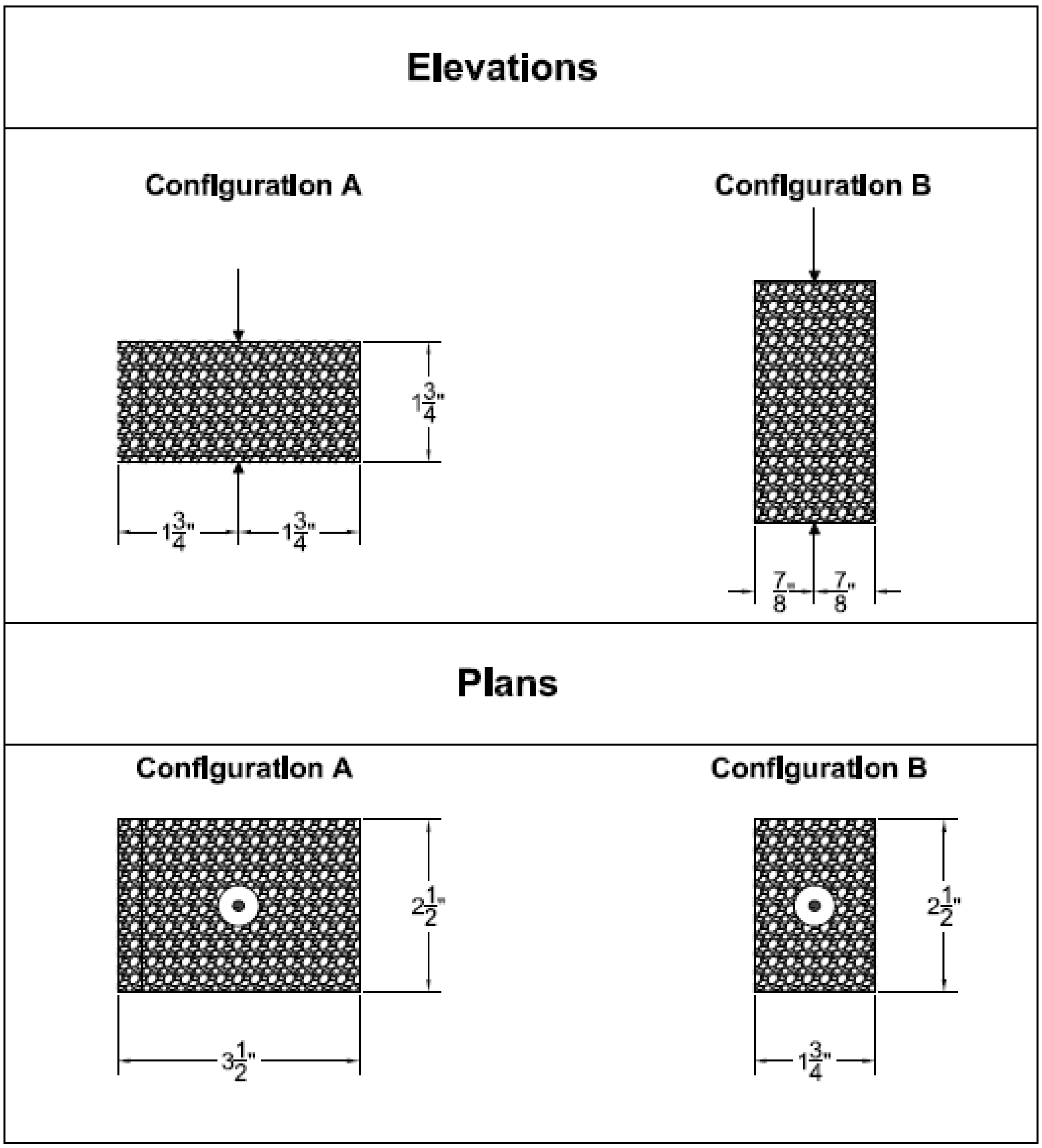

Figure 3. Axial cyclic load test configurations dimensions.

Figure 4. Cyclic load section test layout.

3.4 COMPRESSION TESTS ON CONFINED STEEL REBARS WITH CRUMB RUBBER

To begin with the proposed uses for the crumb rubber, the first test presented here evaluates whether the rubber confinement improves the compression strength of the slender steel elements, or fully restraints the element along its length avoiding a buckling failure.

Before implementing the confined test, a control compression test was performed on three rebars without confinement. All the specimens had the same diameter and were just their length was modified in order to represent the variations on the slenderness ratio. The setup for this test was the same used for the cyclic load test, except for the use of the LVDT, because the goal was finding the maximum load (see Figure 5). The compression load was applied at a constant velocity of 0.2 in/min until the specimen failure.

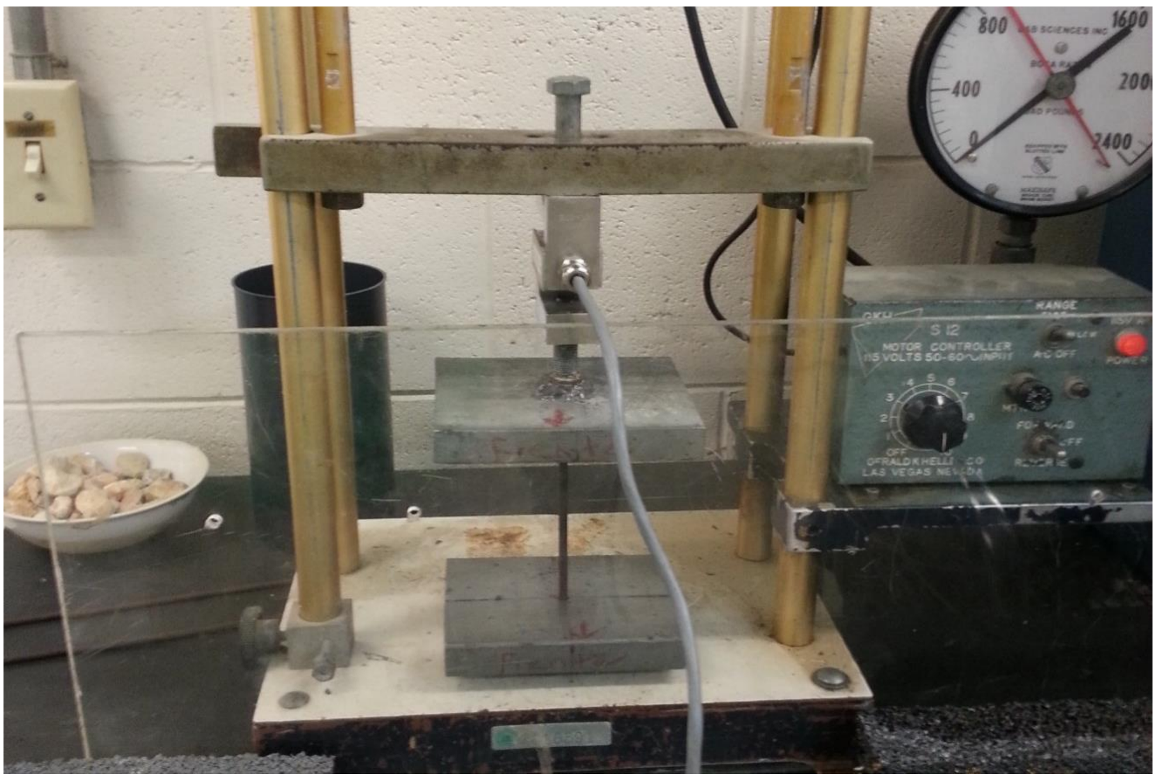

Figure 5. Unconfined compression steel rebars test setup.

The confined test (see Figure 6) used the same setup as the unconfined test. For additional details, Figure 7 presents a diagram about the cross section of this test and shows how the load was applied. Semicircles contacting the rebars with the steel plates can be seen in Figure 7. These semicircles were constructed to avoid eccentricity on the specimens. The properties of the unconfined and confined system are summarized in Table 2 and Table 3, respectively. The confinement area is calculated as the net cross section area (Figure 7) minus the rebar area. All the rebars had a diameter of 0.19 in. diameter, for an area of 0.03 in².

Figure 6. Confined compression rebars test setup.

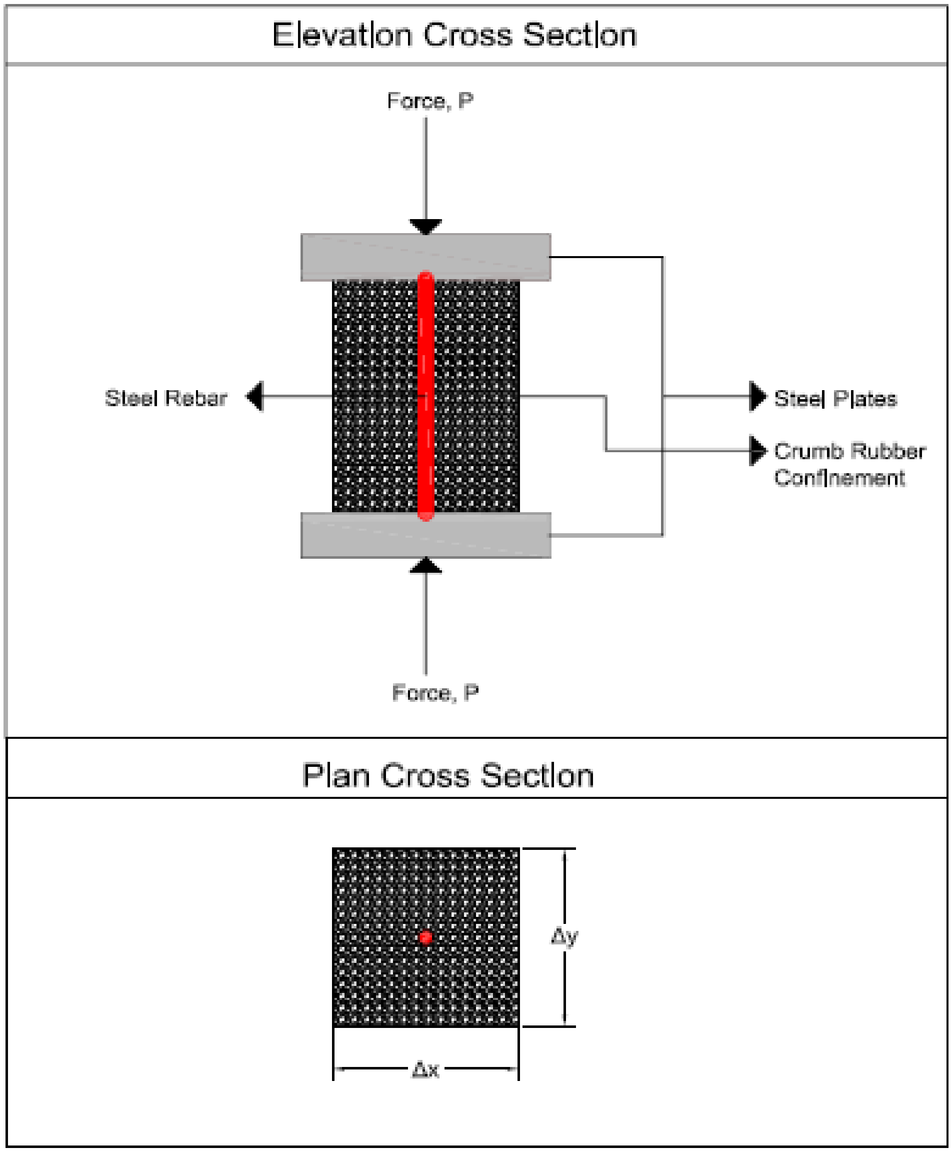

Figure 7. Confined steel rebar test elevation and plan cross section.

Table 2. Unconfined rebar compression test properties.

Specimen	Rebar Length	Slenderness KL/r
-	(in)	-
UR-1	5.88	123.04
UR-2	4.81	100.79
UR-3	4.63	96.86

Table 3. Confined rebar compression test properties.

Specimen	Δx	Δy	Confinement Area	Rebar Length	Slenderness KL/r
-	(in)	(in)	(in²)	(in)	-
CR-1	1.63	1.75	2.8	5.88	123.04
CR-2	1.63	1.75	2.8	4.81	100.79
CR-3	1.63	1.63	2.59	4.63	96.86
CR-4	1.63	1.63	2.59	8	167.54
CR-5	1.63	1.63	2.59	9	188.48
CR-6	1.63	1.63	2.59	8.25	172.77
CR-7	1.63	1.63	2.59	9	188.48
CR-8	3	3	8.95	9.25	193.72
CR-9	3	3	8.95	7.63	159.69

CR = confined rebar

Δx = width of the cross sectional area
Δy = length of the cross sectional area

3.5 CRUMB RUBBER WALL TESTS

To evaluate further crumb rubber applications, additional tests were performed using the crumb rubber as a wall panel. Two wall configurations were tested: (1) plain crumb rubber infill panels, and (2) plain and reinforced crumb rubber shear wall. The purpose of this test was to evaluate the behavior of crumb rubber panels acting as walls. Crumb rubber panels could be used as infill frames or shear walls. The ability of the systems to resist the lateral forces by having the adequate stiffness and providing energy dissipation through inelastic load cycles was assessed.

In order to evaluate the capacity of crumb rubber panels as walls, a rigid pinned steel frame was designed, as seen in Figure 8, allowing the rubber panel to withstand the entire lateral load. Figure 9 shows the final setup, which consists of: (1) Hydraulic Jack, with load capacity of 10,000 lb. to apply the load, (2) Load Cell with capacity of 1,000 lb. to measure the load on the specimen, (3) Linear Variable Differential Transformer (LVDT) with a maximum deformation of 6 in to measure the deformation of the specimen, and (4) a rigid steel frame fixed with bolts to the strong concrete slab. The rigid steel frame was constructed using two rectangular steel columns plates with dimensions of 5 in x 4 in x 3/4 in, and two steel plates with dimensions of 9 in x 4 in x 3/4 in for the top beam and floor base. This system was attached to the strong floor, using four angles welded to a steel base plate (see Figure 8). Finally, the steel base plate was fixed to the strong concrete slab using four bolts as seen in the same figure. It is worth to note that the hydraulic jack was fixed to a strong *I* shape column, as seen at the right corner of Figure 9, which is part of a strong steel frame, which is in turn connected to the strong concrete slab. Meanwhile, the rigid frame was fixed to the strong slab with four nut and bolts, two at the front and two at the back of the frame. The differences between the crumb rubber tests were the arrangement inside the steel frame or how the load is transferred to the rubber panel.

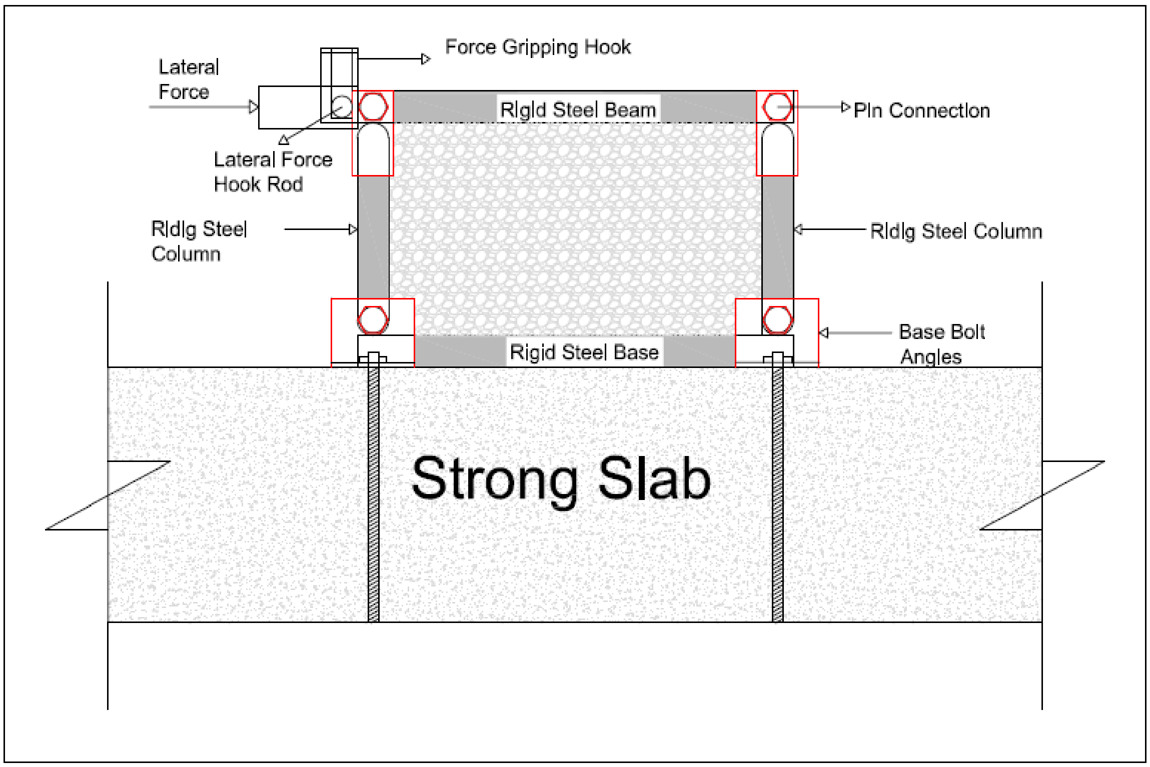

Figure 8. Crumb rubber wall setup diagram.

The load was applied back and forward until the specimen failed or some other unexpected condition occurred. On the first cycle the frame was pushed (forward action) up to 100 pounds and then

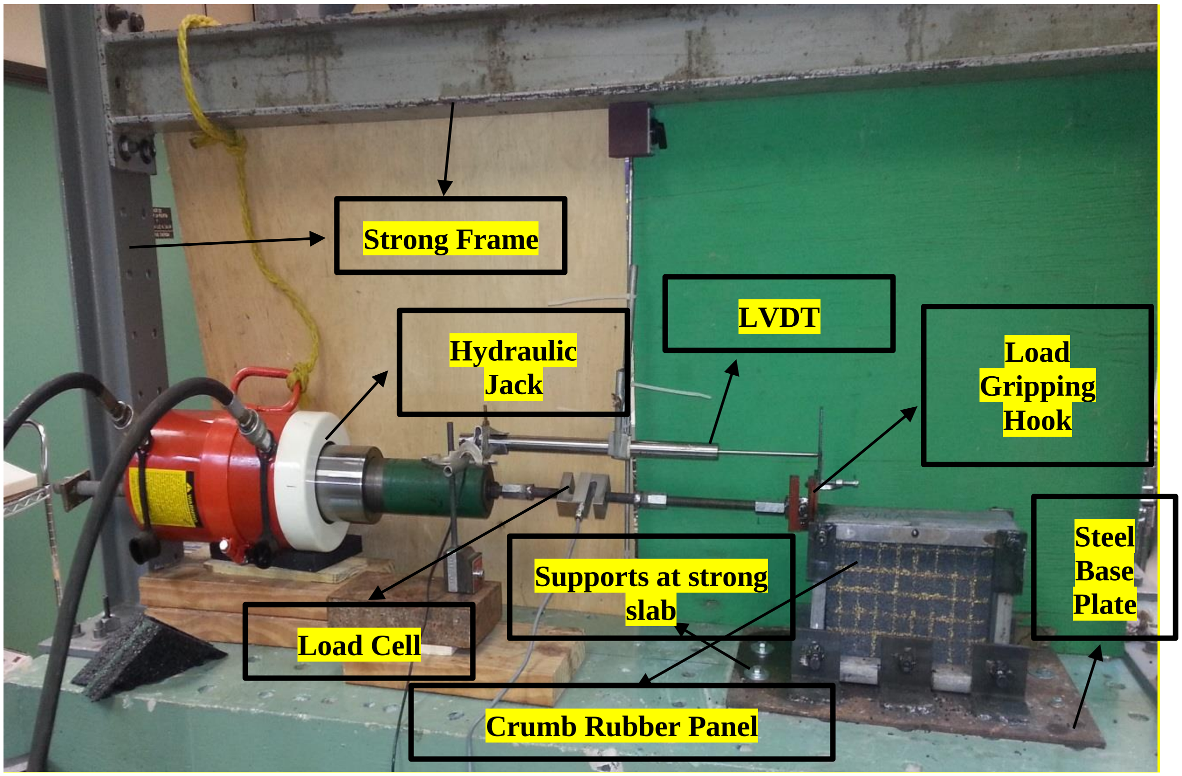

Figure 9. Crumb rubber wall test general setup.

3.5.1 CRUMB RUBBER INFILL FRAME TEST

The first test performed in the crumb rubber walls category was the Crumb Rubber Infill Frame test, and was aimed to evaluate the behavior of the crumb rubber acting as infill. An infill frame is a type of frame-wall system in which the wall makes contact with the beam and columns during the action of the lateral load, as mentioned previously. During the test, two major conditions were evaluated: (1) infill frame without lateral boundary (2) infill frame with lateral boundary. The boundary was a restriction imposed to the wall side corners, as seen Figure 10, with the objective of verifying whether the behavior of the infill is affected or not by the presence of this condition. Table 4 summarizes all the infill panel specimen properties. As part of the study, the maximum lateral deformation was obtained, and the effect of the variations to the thickness of the wall panel was evaluated to check how it affects the behavior by sudden buckling failures.

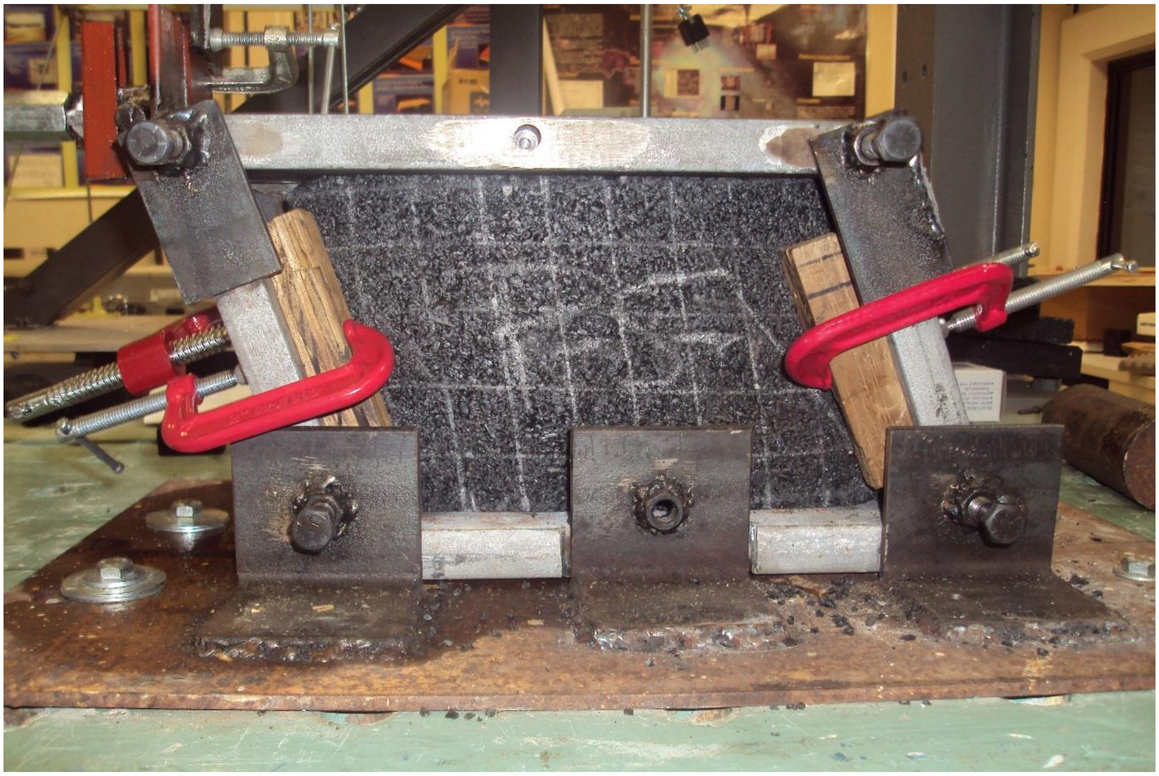

Figure 10. Infill frame with boundary condition.

3.5.2 REINFORCED CRUMB RUBBER SHEAR WALL TEST

The Reinforced Crumb Rubber Shear Wall Test was the last test performed in the crumb rubber wall category. It was intended to investigate the behavior of this wall configuration when steel reinforcement is used to enhance the system properties, and to determine the Shear Modulus (G) of the crumb rubber. The main goal of the test was to determine whether the reinforced system is capable of providing energy dissipation through hysteresis cycles, and if it can be used to increase the lateral for seismic applications. Therefore, force-displacements curves were generated to: (1) determine the stiffness of the shear wall systems, (2) examine the hysteretic behavior, (3) obtain the yield point of the reinforced specimens.

To accomplish it, four specimens were tested. The first one was a plain wall attached to the beam and the base plate (see Figure 11) with two steel plates that were located above and below of the rubber

Table 4. Infill panel specimen properties.

Specimen	T	Boundary Condition	L	L/T
-	(in)	-	(in)	-
IF-1	0.75	NLB	8.75	11.67
IF-2	1	NLB	8.75	8.75
IF-3	1.75	NLB	9	5.14
IF-4	1.75	LB	9	5.14
IF-5	1.75	LB	9	5.14
IF-6	1.5	LB	9	6
IF-7	1	LB	9	9

IF = infill frame panel.

T = thickness of the infill panel.

NLB = no lateral boundary provided.

LB = lateral boundary provided.

L/T = measure of the slenderness of the infill panel.

panel, as an intermediate plate, to bond the whole system and fill the gap between the rubber and the beam (this gap was left to allow free rotation on the frame, avoiding the columns from locking with the top beam), and transfer the load from the hydraulic jack to the rubber. These steel plates were bonded to the rubber panel, and then, on the other side, another coat of epoxy was added to bond the specimen to the frame. In order to have a shear wall action, a gap of 1 in. was left between the steel columns and the rubber specimens, for the four specimens.

The other specimens were reinforced with steel rebars, and placed without bonding the rubber to the beam and floor with epoxy, using the intermediate plates to fill the gap left too. The idea behind eliminating the epoxy is to create the shear action through the steel rebars (Figure 12). Table 5 summarizes the properties of the specimens.

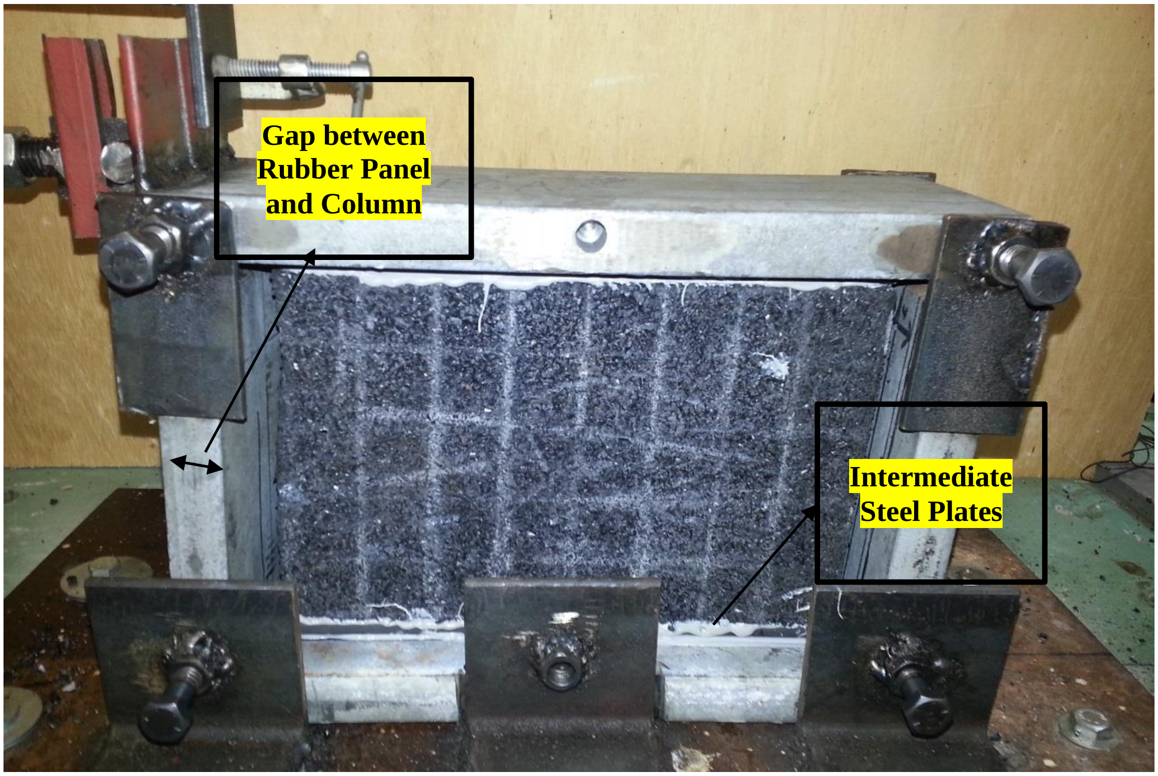

Figure 11. Plane crumb rubber shear wall.

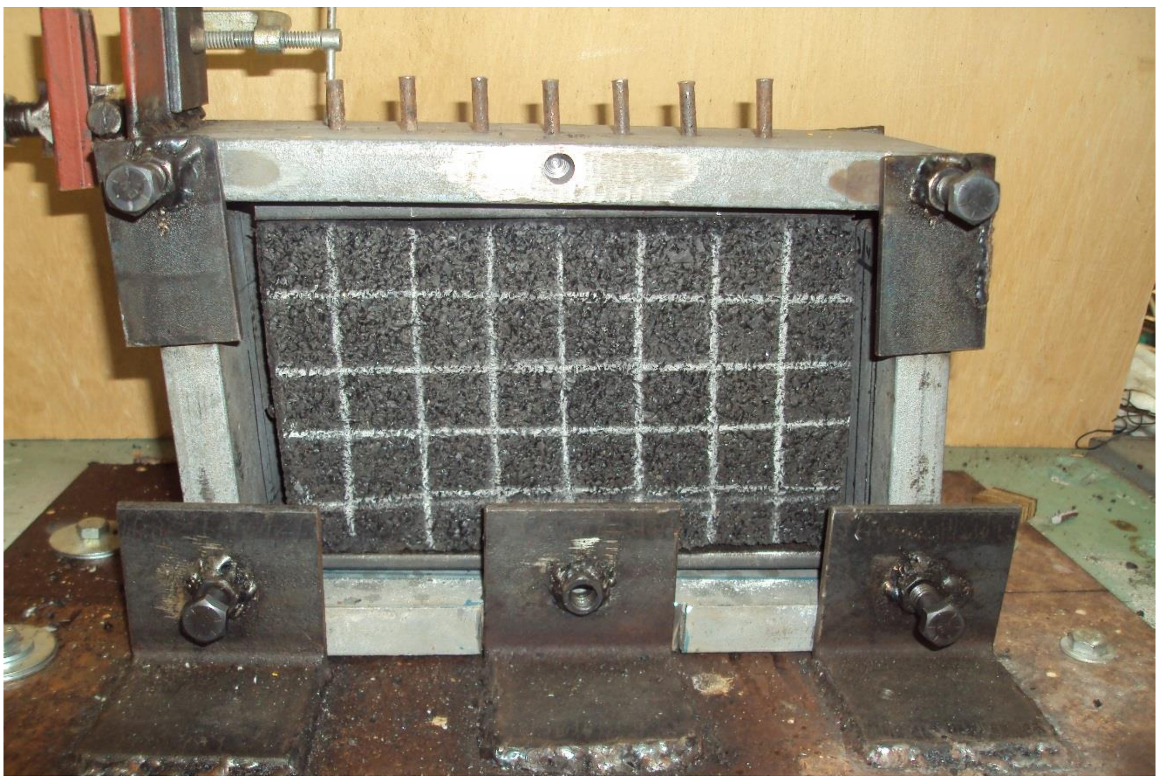

Figure 12. Reinforced crumb rubber setup.

Table 5. Reinforced crumb rubber specimen's properties.

Specimen	T	L	Wall Area	Rebar Diameter	Number of Rebars	Wall Steel Area
-	(in)	(in)	(in^2)	(in)	-	(in^2)
RCR-1	1.75	8	14	NS	NS	NS
RCR-2	2	8	16	0.125	7	0.09
RCR-3	2	8	16	0.191	7	0.20
RCR-4	2	8	16	0.375	3	0.33

RCR = reinforced crumb rubber

T = thickness of the wall panel

L = length of the wall panel

NS = no steel

CHAPTER 4

EXPERIMENTAL RESULTS

4.1 INTRODUCTION

This chapter discusses the experimental results obtained from the tests discussed in Chapter 3. The following tests were the performed: (1) specific weight, (2) axial cyclic load test to determine several mechanical properties of the rubber, (3) confined rebars compression test to evaluate whether the crumb rubber confinement increases the ultimate strength of the rebars, and (4) cyclic lateral load on crumb rubber wall specimens to determine the feasibility of using rubber panels as steel buildings walls.

4.2 SPECIFIC WEIGHT

The experimental results obtained from the specific weight are summarized in Table 6. Specific weight of the crumb rubber was determined using different pieces of rubber from the batch. From the four samples tested, the average value was 61.04 lb./ft^3. Several manufacturers, as RB Recycled Rubber Products and Sofscape Caribe, established a range of specific weight values between 55 to 65 lb./ft^3. The results obtained are within this range.

4.3 AXIAL CYCLIC LOAD TEST

The ACL test was designed to determine the following mechanical properties of the crumb rubber: (1) Compression strength, (2) Tension strength, (3) Modulus of Elasticity, (4) Isotropy, (5) Hysteresis energy dissipation, (6) Time dependent response. To accomplish it, six specimens were tested

Table 6. Specific weight summary.

Specimen	Specimen Volume	Initial Volume of Water	Final Volume of Water	Change of Volume	Weight	γ	γ
	(in³)	(cm³)	(cm³)	(cm³)	(g)	(g/cm³)	(lb/ft³)
1	15.31	1600	1775	175	171.1	0.98	61.04
2	15.31	1600	1780	180	175.14	0.97	60.74
3	15.31	1600	1780	180	174.9	0.97	60.65
4	15.31	1600	1780	180	178.09	0.99	61.76
						γ_{avg} =	61.05

γ = specimen unit weight

γ_{avg} = average unit weight

under a specific load cycle type. The next sections will present and discuss the results obtained from this test, which are summarized in Table 7.

Table 7.ACL test summary results.

Specimen	Configuration	Cycle Load Type	Velocity	Ultimate Tension (Tu)	Ultimate Compression (Cu)	Ultimate Strain (εu)
-	-	-	(in/min)	(psi)	(psi)	ε (%)
ACL-1	A	Tension/ Compression	0.2	30	N/A	14.81[1]
ACL-2	B	Tension/ Compression	0.2	N/A	109	37.7
ACL-3	A	Compression	0.2	N/A	118	38
ACL-4	B	Compression	0.2	N/A	91	39.7
ACL-5	A	Compression	0.8	N/A	123	44.5
ACL-6	B	Compression	0.8	N/A	133	50
			Average	**30**	**114.8**	**41.98[2]**

ACL = axial cyclic load

1. Maximum tension strain

2. Average compression stress is based on specimens ACL 2-6

*For configurations A and B see Figure 3

4.3.1 MAXIMUM COMPRESSION AND TENSION STRAIN AND STRESSES

The maximum tension stress from the test was 30 psi, and it was obtained from the ACL-1 specimen. On the other hand, the maximum and average compression stress was 133 and 114.8 psi, respectively. The minimum compression stress was 91 psi, on the specimen ACL-4. An eccentricity was noted while testing this specimen, which is attributed to this minimum performance. When the maximum and average compression stresses are compared with the tension stress, it can be noticed that the tension stress is just 22.5 % and 26 % of the maximum and average compression stress, respectively, which is almost negligible. In terms of deformations, the maximum compression strain recorded was 50 %, and the maximum tension strain was 15 %. The average compression strain average was 41.98 %, showing a high deformation capacity as the rubber in general. On the other hand, the tension strain exhibited a low strain behavior compared to the compression strain due to the poor performance of the rubber under tension stresses. Figure 13 shows a deformed compression tested specimen; it can be see a bulge at the sides of the specimen which is typical of compression members. Meanwhile, Figure 14 and Figure 15 show the cracks at the ultimate stage of load. At glance, the cracks are aligned at 45° from the horizontal. According to the mechanics of materials, this is the expected plane of failure for concentric axial tests.

Additionally, the system did not exhibit a dissipation of energy through the inelastic cyclic of hysteresis. Hysteresis is a characteristic of the non-linear materials, in which it dissipates energy providing inelastic deformations. This results in the decreasement of the applied load. This is an important virtue that any structure located at a high risk seismic zone should has, in its overall performance, in order to sustain the onslaught of an earthquake. This characteristic can be seen in the load-deformation or stress-strain curves, and can be measured or defined as the area below the curve. This means, that a material with great energy dissipation will exhibit a large area below the stress-strain curve.

For this test, it can be said, that the crumb rubber cannot dissipate energy because its load response is linear during all cycles, as seen in Figure 16, which means that the crumb by itself is a good option for constructing or repairing structures for seismic application.

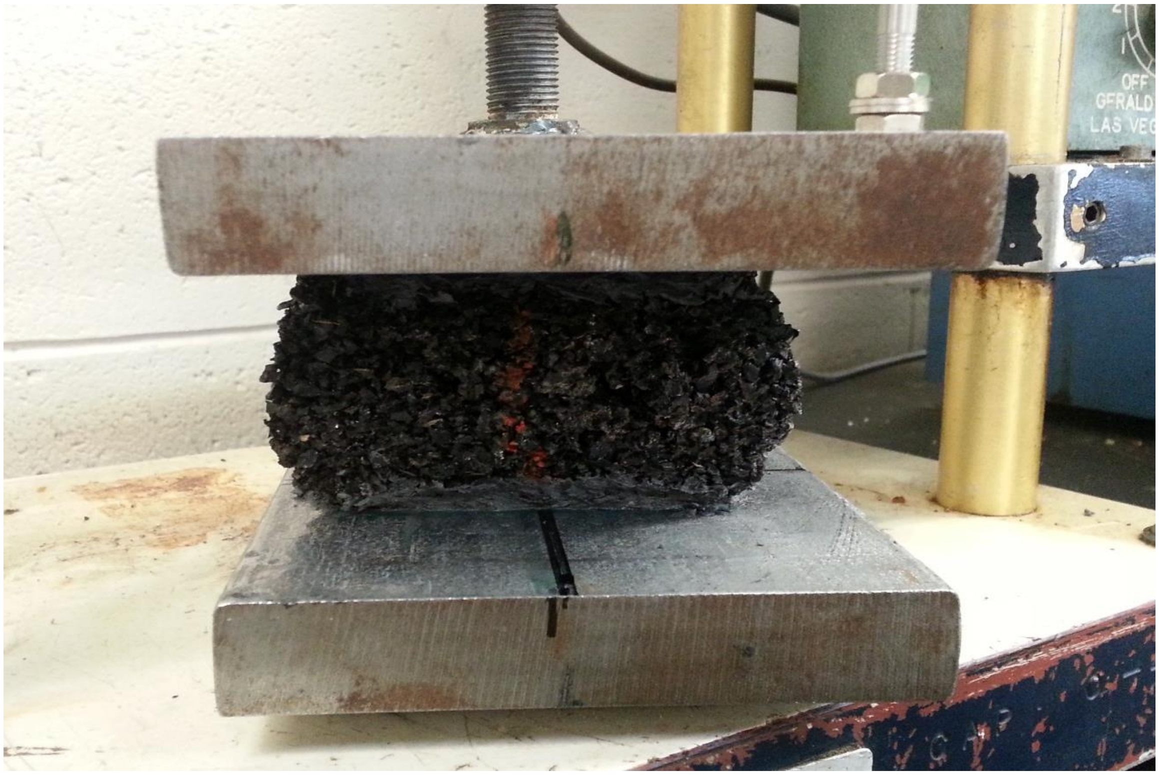

Figure 13. ACL test compression deformed specimen.

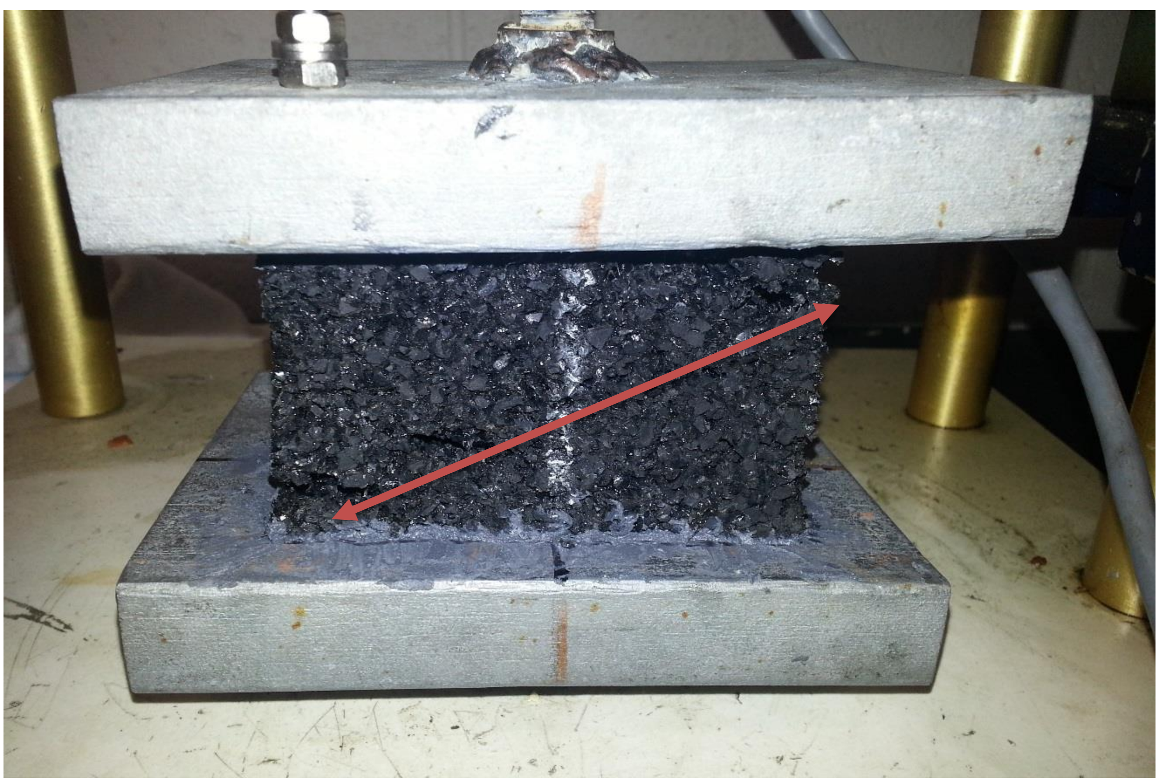

Figure 14. ACL: tension failure crack.

Figure 15. ACL: compression failure crack.

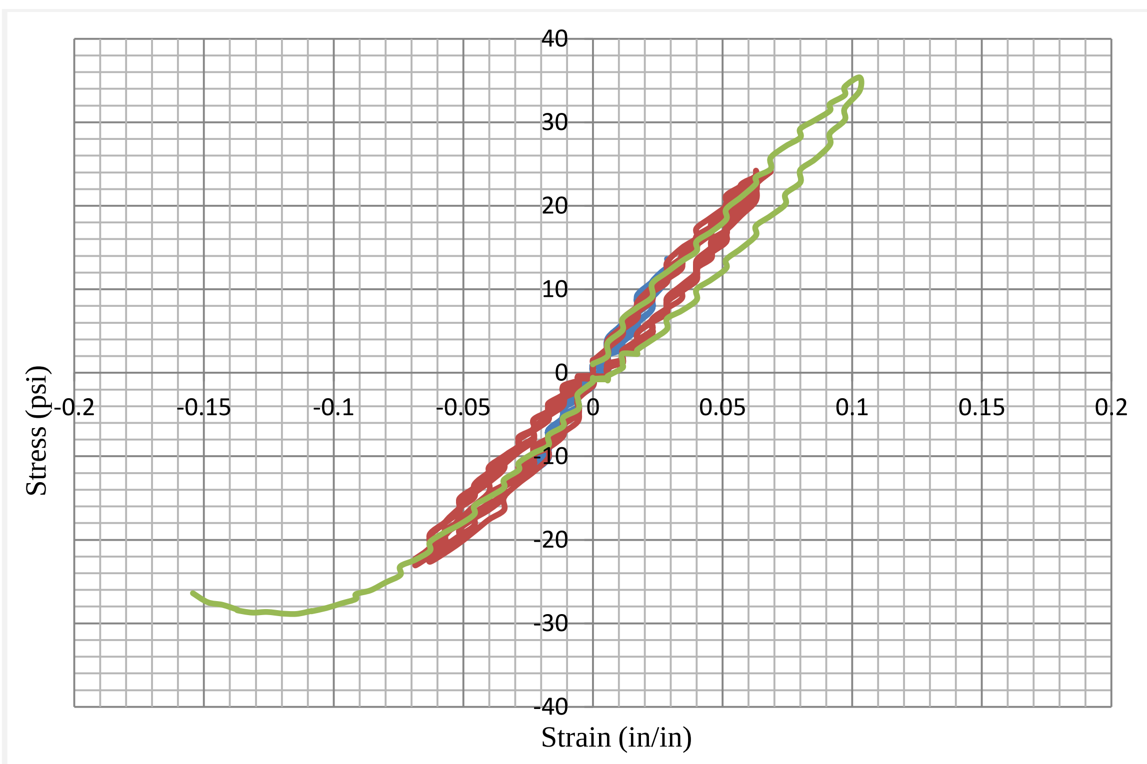

Figure 16. ACL test Stress vs. Strain curve.

4.3.2 MODULUS OF ELASTICITY

The data collected with the load cell and LVDTs was used to construct the curves for all the ACL test specimens. From these curves the modulus of elasticity was computed, using the initial modulus method, given that the material is highly linear during more than an half of the cycle test, as seen in Figure 16. Table 8 presents the modulus of elasticity for all the specimens. The maximum modulus was 424.84 psi, while the minimum was 257.08 psi, with an average of 335.54 psi. The difference between each specimen is attributed to the level of compaction of the crumb rubber, or accidental eccentricities due to test setup. To manufacture the rubber pavers pieces of crumb rubber are mixed with epoxy to mold the pavers. The weight unit of the rubber block can be increased by compressing this concrete mix. Therefore, as the weight unit of the rubber block increases by compressing the mix, the stiffness increases as well. Fluctuations in this process could affect the mechanical response of the crumb rubber paver.

Table 8. Modulus of Elasticity ACL test curves

Specimen	**Modulus of Elasticity (E)**
-	(psi)
ACL - 1	424.84
ACL - 2	351.67
ACL - 3	353.89
ACL - 4	307.52
ACL - 5	257.08
ACL - 6	318.24
E_{avg}	**335.54**

ACL = axial cyclic load

E_{avg} = average modulus of elasticity

4.3.3 ISOTROPY

An isotropic material is one that has the same physical and mechanical properties in all directions. In this test two configurations were used. From Figure 3 it can be noticed that Configuration B is the same as Configuration A, but rotated 90°. In other words, the blocks of crumb rubber, having the same dimensions, were placed into ACL test in different ways to test the isotropy of the material. The results shown in Table 7 can demonstrate that the crumb rubber is an isotropic material. For example, specimens ACL-5 and 6 had an ultimate compression stress of 123 and 133 psi, respectively.

4.3.4. TIME DEPENDENT RESPONSE

The response of some materials is affected by the velocity of load application. Because the other subsequent test involved the use of cyclic loads, this property was evaluated in order to check if the use of a higher load application rate affects the final results. As seen in Table 7, that the ACL-5 and 6 were tested at a higher velocity (0.8 in/min) compared to the other specimens, which were tested under a slow velocity (0.2 in/min). No significant changes were noticed when examining the results. For example, the specimen ACL-3 had an ultimate compression stress of 118 psi, while the ACL-5 had 123 psi (both using the same configuration). The small differences are due to the variance of the material itself. From this test it can be established, that the material did not experience dramatic changes in the load response behavior, which suggested that the crumb rubber is a non-time dependent material.

4.4 CONFINED REBARS COMPRESSION TEST

The results of the confined rebar compression test will be presented as explained before in Chapter 3. The first section will present the control or unreinforced (UR) specimens or unreinforced with no confinement. The second section will present, summarize and discuss the results obtained in the confined compression tests, taking into account the differences and the possible uses and restrictions.

4.4.1 UNCONFINED REBARS COMPRESSION CONTROL TEST

The results obtained in this test are summarized in Table 9. The table describes the slenderness of the specimens and the results are compared with those predicted by the critical load equation (Euler's formula) as shown in the third column of the table. The factor of slenderness, *K*, was chosen equal to 1 because the tests were conducted with pin conditions. Before conducting the tests, the critical load was calculated from the Euler equation and the theoretical critical stress was determined (see columns 4 and 5). The experimental results of the test are presented in the sixth column, and in the last column the percent of difference between the experimental values and the predicted by the Euler equation are shown. Figure 17 shows a photo of the typical buckling failure during an UR test.

Table 9. Unconfined rebars compression control summary test.

Specimen	KL/r	$Pcr = \frac{\pi^2 * E * A}{\left(\frac{KL}{r}\right)^2}$	F_{cr}	Pcr_{exp}	Fcr_{exp}	Percent of Difference
-	**-**	**(lb.)**	**(ksi)**	**(lb)**	**(ksi)**	**%**
UR-1	123.04	541.73	18.91	541	18.88	0.15
UR-2	100.79	807.35	28.18	694	24.22	14.05
UR-3	96.86	874.13	30.51	667	23.28	23.70

UR = unconfined rebar.

KL/r = rebar slenderness.

Pcr = maximum compressive load given by Euler's expression.

Fcr = maximum compressive stress given by Euler's expression.

Pcr_{exp} = maximum experimental compressive load.

Fcr_{exp} = maximum experimental compressive stress.

For specimen UR-1 the result confirms Euler's equation: the rebar behaved exactly as Euler's equation predicted. For the specimen UR-3 and UR-3, meanwhile, the experimental results show a 14 to

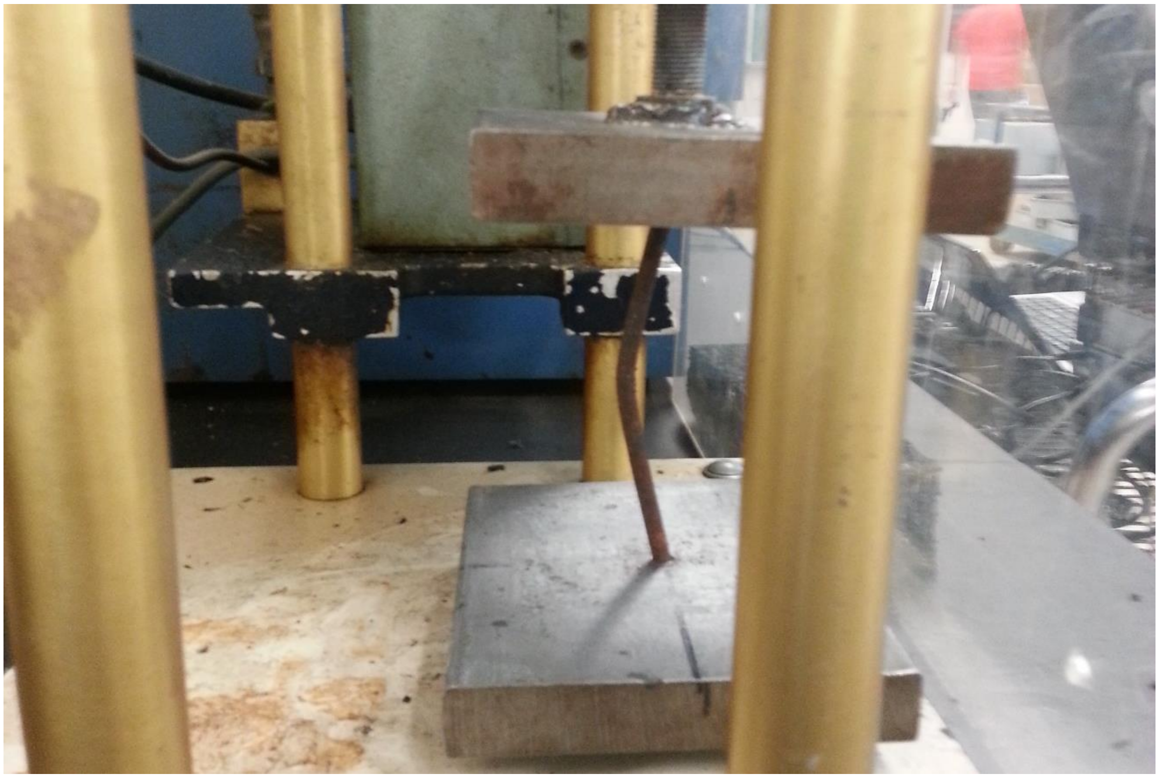

Figure 17. UR buckling failure.

24 % of difference. However, if these specimens are examined in detail it can be noticed that, as the slenderness ratio decreased, the percent of difference incremented. That is consistent with the steel buckling theory, where for smaller values of slenderness ratio, the outer fibers of the element subjected to compression yield before the critical load is reached and the Euler expression is no longer valid. In addition, initial out-of-straightness of the column, residual stresses, eccentricity in the load applications, among others, tend to cause buckling at stresses less than the Euler critical stress (Williams, 2011). In conclusion, the Euler expression gives higher values of the critical load than the measured ones for smaller values of slenderness ratio. Nevertheless, in this small slenderness range, the expression predicts very well the behavior for the steel rebars.

4.4.2 CONFINED CRUMB RUBBER STEEL REBARS COMPRESSION TEST

These sections will present the results of the confined compression test (see Figure 6 and Figure 7) where the steel rebars were confined with the crumb rubber. For this test a series of nine specimens were used with variation in slenderness ratio and confinement area (for the specimen properties, see Chapter 3). As discussed in the previous section, the critical load and stress were calculated using the slenderness ratio of each specimen. It is worth mentioning that this critical load is the maximum load that each element can withstand without any restraint along their length. The results obtained are compared with the critical load to evaluate the improvement, if any, of using the confinement of the crumb rubber as a fully lateral support along the whole length.

Table 10 summarizes the results for the confined crumb rubber steel rebars compression test, and in Figure 18 is shown a three dimensional drawing with the dimension's properties. From the results it can be stated that the confinement improves the compressive strength of the specimens. However, the following are several points that should be discussed, in order to better understand the results of this test: (1) Specimens CR-6 and 7 show a negative percent of increment, which means that these elements did not reach the Euler critical load. This effect is associated to accidental eccentricity in the setup, because the specimen CR-5, which has the same slenderness ratio as the specimen CR-7, had an increment of eight percent of the compressive strength, and this tendency is repeated along the test. (2) In general, elements with more confinement area exhibit a better improvement on the compressive strength. Elements with 2.8 in^2 of confinement area had a maximum of 80% of increment, and the other one was 18%. With 2.59 in^2 of confinement area, there is a more variable behavior, which can be attributed that it was the lowest confinement area. With less confinement area, the element tends to behave like the Euler equation predicts. Even so, with this amount of confinement area, a 30% of increment was reached. Finally, the specimens CR-8 and 9 were tested using an 8.95 in^2 of confinement area and both showed an increment greater than 50%. (3) As mentioned previously, elements with smaller slenderness ratio exhibit more plastic behavior, diverging from the Euler expression and this is consistent with the results, because in general, specimens with larger slenderness ratio showed more percent increment. For example, the percent of increment for the specimen CR-1 was 80% versus the 18% of the CR-2. Looking at specimens CR-8 and 9, the same behavior is presented. However, this tendency was not the same for the specimens confined with 2.59 in². The most likely reason to have this problem is the lesser confinement area, and accidental eccentricity in the setup. The construction process is one of the factors that may have contributed to the element eccentricity. To prepare the specimens, a bore hole was made to the crumb rubber mass in order to insert the rebar. This process was difficult because the crumb rubber possessed geometrical imperfections, and there was not an accurate way to verify if the rebar came out perfectly straight through the crumb rubber mass, which leaded to eccentricities. Also, another probable reason for eccentricities was the possible problems with the straightness of the rebars. Figure 19 shows the typical deformed shape of the CR test specimens, which confirms the bucking failure mode, according to the above.

Table 10. Confined crumb rubber steel rebars compression test summary results.

Specimen	**Ac**	**KL/r**	$\mathbf{Pcr = \frac{\pi^2 * E * A}{\frac{KL}{r^2}}}$	**Fcr**	**Pcr_{exp}**	**Fcr_{exp}**	**PI**
-	**(in²)**	**-**	**(lb)**	**(ksi)**	**(lb)**	**(ksi)**	**%**
CR-1	2.8	123.04	541.73	18.91	975	34	80%
CR-2	2.8	100.79	807.35	28.18	950	33.2	18%
CR-3	2.59	96.86	874.13	30.51	1136	39.6	30%
CR-4	2.59	167.54	292.16	10.2	321	11.2	10%
CR-5	2.59	188.48	230.84	8.06	250	8.7	8%
CR-6	2.59	172.77	274.72	9.59	179	6.2	-35%
CR-7	2.59	188.48	230.84	8.06	108	3.8	-53%
CR-8	8.95	193.72	218.53	7.63	350	12.2	60%
CR-9	8.95	159.69	321.6	11.22	486	17	51%

CR = confined rebar.

Ac = crumb rubber confinement area.

KL/r = rebar slenderness.

Pcr = maximum compressive load given by Euler's expression.

Fcr = maximum compressive stress given by Euler's expression.

Pcr_{exp} = experimental maximum compression load.

Fcr_{exp} = experimental maximum compressive stress.

PI = percent of increment: percent of load increment due to crumb rubber confinement.

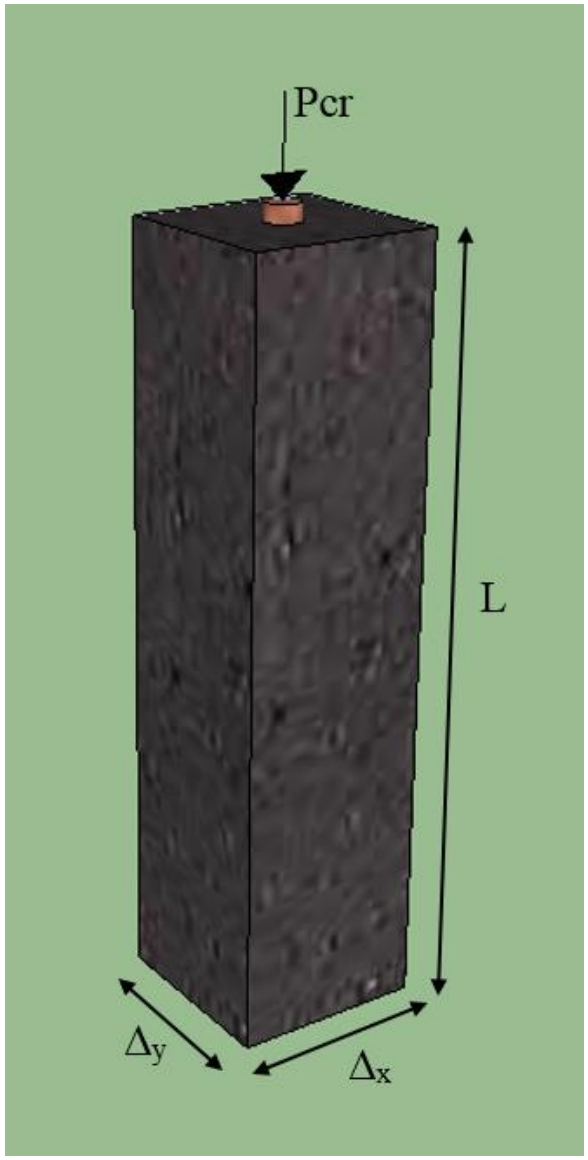

Figure 18. CR test drawing.

It was mentioned previously, that Cadamuro investigated the effect of confine steel rebars with crumb rubber to create a reinforced crumb rubber pile. As part of this investigation, six reinforced crumb rubber piles were tested. These piles were constructed with a cross sectional area of 23.5 in², and reinforced with 5 #4 steel rebars (Figure 20). In the first test group, they were constructed 12.5 in. length and the second one, 15 in. length. The compression test was performed using these two groups and the results are summarized in Table 11.

Figure 19. CR buckled deformed shape.

After compression was applied, maximum load was recorded. For purposes of this research, the compression load and the cross sectional area were divided by the numbers of rebars, to compare the results with those obtained in this investigation. Then, with the load and cross sectional area normalized by the number of rebars, the critical load and percent of increment were calculated to compare how effective was the confinement in the Cadamuro's investigation.

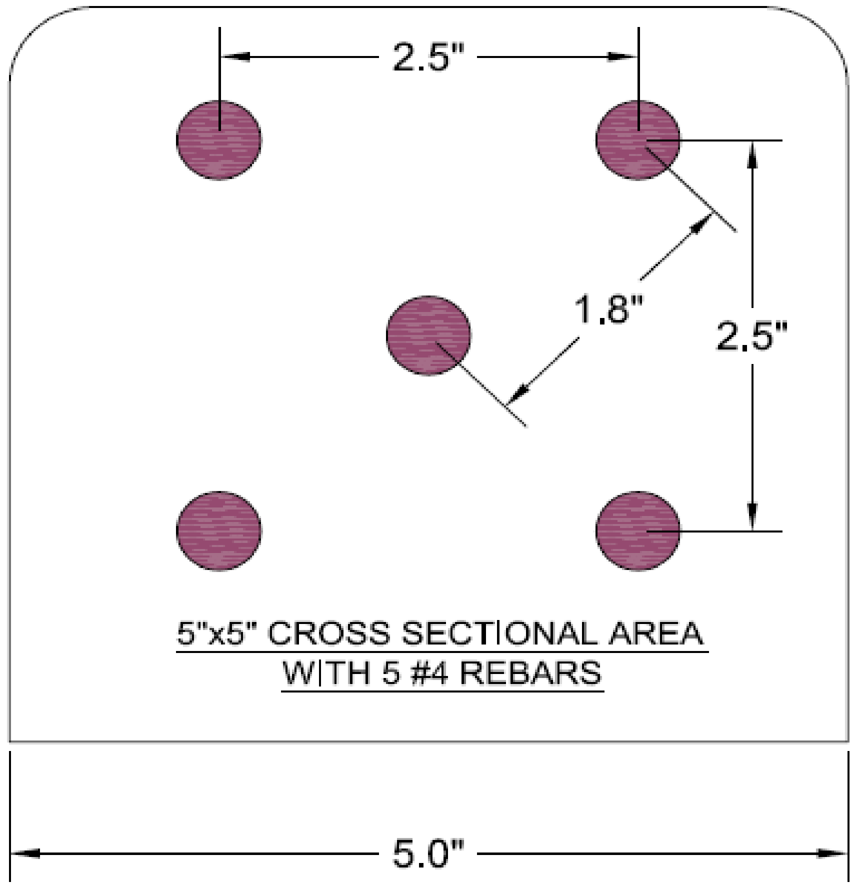

Figure 20. Cadamuro reinforced crumb rubber pile cross section.

The investigation of Cadamuro showed a similar trend as the CRC test. From it results, it is clearer that the slenderness plays an important role. The specimens 7 and 9, with a slenderness ratio of 120, presented an average of 123 percent of increment, versus the specimens 4 and 6, in which the average percent of increment was 62 percent. Therefore, the results suggest that slender elements will experience a greater capacity increment. On the other hand, while the element is more slender, an inelastic buckling starts to control the failure mode, causing the confinement to be less necessary.

Finally, in Figure 21 is shown a plot of the buckling stresses. The plot presents three series: (1) Euler's buckling curve, (2) CRC's test curve, and (3) Cadamuro's test curve. From the figure it can be noticed that the curve developed in this investigation is more conservative. Additionally, from the CRC test's series it can be appreciate that the curve follows the trend of the Euler's curve, shifted upward. If

Table 11. Cadamuro's buckling test analysis results.

Specimen	L	KL/r	$Pcr = \frac{\pi^2 * E * A}{\frac{KL}{r^2}}$	Fcr	Pcr_{pile}	Pcr_{exp}	Fcr_{exp}	PI
-	(in)	-	(lb)	(ksi)	(lb)	(lb)	(ksi)	%
4	12.5	100	5619.89	28.62	41000	8200	41.76	46%
6	12.5	100	5619.89	28.62	50000	10000	50.93	78%
7	15	120	3902.7	19.88	42000	8400	42.78	115%
9	15	120	3902.7	19.88	45000	9000	45.84	131%

L = length of the steel rebar.

KL/r = rebar slenderness.

Pcr = Euler's critical load for one # 4 steel rebar.

Fcr = Euler's critical stress for one # 4 steel rebar.

Pcr_{pile} = Cadamuro's experimental ultimate compression load on the reinforced pile.

Pcr_{exp} = experimental ultimate load on each rebar (is the Ppile divided by the number of rebar, in this case, five rebars).

Pcr_{exp} = experimental critical stress, defined as the Pcrexp divided by the steel rebar.

PI = percent of increment: increment ratio of the ultimate load, from a bare compression test, to a confined compression test.

* For #4 rebars, the cross sectional area is 0.20 in^2.

less slender specimens were used, it was logical to expect that the curve tended towards a yield plateau, because the failure mechanisms begin to behave, increasingly, more inelastic. However, the purpose of this test was to investigate how slender elements could be improved using confinement along their length, under compression loads.

4.5 CRUMB RUBBER INFILL FRAME TESTS

This section presents and discusses the results of the behavior of the crumb rubber as an infill frame, and the results are presented in Table 12, and in Figure 22 is shown a three dimensional drawing to show in more detail the properties of the system and the lateral boundaries. From the results and looking at Figure 23, it can be established that the crumb rubber panel, acting as an infill frame, is very sensitive to the

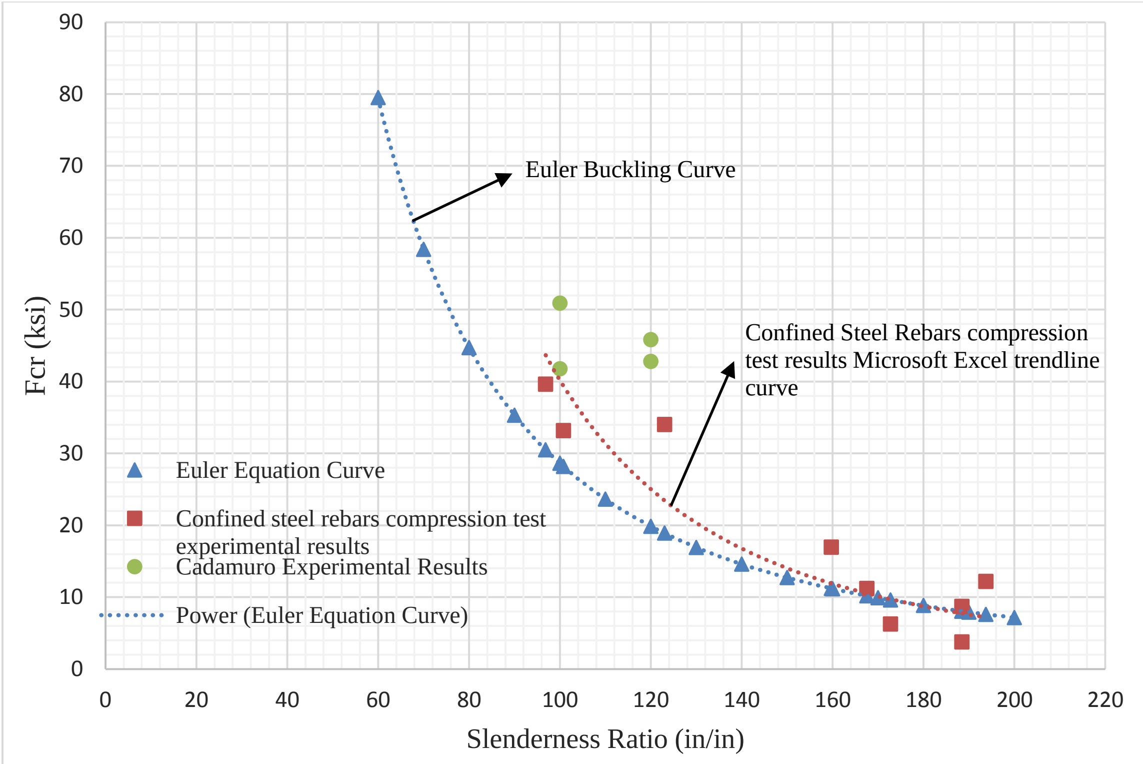

Figure 21. Confined steel rebars compression stress buckling curves.

to the slenderness ratio and the boundary condition, since a small increase in the slenderness decreases quickly the strength of the panel. During the test, the first specimens were tested without lateral boundary condition. With the load increments, the panels started to slip with respect to the columns. This problem caused additional eccentricity on the lateral load application, and the panels started to move out-of-plane, as seen in Figure 24. At this moment, specimens without boundary failed, and the test was stopped. Due to this problem, it was decided to add a boundary element (see Figure 10) to avoid out-of-plane movement and bending moments, and force the wall to work in-plane.

Finally, if a closer look is taken at the results, it is clear that the lateral boundary improved the behavior of the panels. For example, if the stresses (σ_x) presented in column seven of Table 12 are compared, specimens with 1.5 in or more of thickness versus those with 1 in or less are 1.6 times greater in average. That means that this decrease in slenderness represents a 160% of increment in the strength. Is

Table 12. Crumb rubber infill frame test summary test's results.

Specimen	Boundary Condition	T	L	L/T	F_x	σ_x	Δ_X	ε_x	k	G
-	-	(in)	(in)	(in/in)	(lb.)	(psf)	(in)	(in/in)	(lb/in)	(psf)
CIF-1	NLB	0.75	8.75	11.67	87	13.26	1.3	0.15	66.92	89.23
CIF-2	NLB	1	8.75	8.75	98	11.2	0.8	0.09	122.5	122.5
CIF-3	NLB	1.75	9	5.14	360	22.86	1.8	0.2	200	114.29
CIF-4	LB	1	9	9	60	6.67	1.35	0.15	44.44	44.44
CIF-5	LB	1.75	9	5.14	430	27.3	2	0.22	215	122.86
CIF-6	LB	1.75	9	5.14	450	28.57	2	0.22	225	128.57
CIF-7	LB	1.5	9	6	390	28.89	2	0.22	195	130

CIF = crumb rubber infill frame panel.

Boundary = restriction imposed at the side ends of the rubber panel to avoid out-of-plane displacements.

T = thickness of the infill panel.

NLB = no lateral boundary provided.

LB = lateral boundary provided.

L/T = measure of the slenderness of the infill panel.

Fx = maximum lateral force.

σ_x = lateral stress on the wall ,defined as lateral load divided by the wall cross sectional area

Δ_X = maximum lateral deformation.

ε_x = lateral strain of the wall.

k = lateral stiffness of the wall (F_x/Δ_x).

G = lateral stiffness, expressed in terms of stress and strain (σ_x/ε_x).

important to point out, that this test was stopped when the specimen failed by buckling or when 2 in. of lateral deformation was reached. Therefore, this 160% could increase if greater deformation is allowed. In terms of stiffness, all the specimens behave in a similar way, except the CFI-1 and 4. These differences are associated for specimen CIF-1 to the slenderness of the element and the absence of the boundary, and for CIF-4, to the accidental eccentricity and the slenderness of the element. Figure 25 shows a plot of the lateral infill rigidity in terms of the lateral stresses, as discussed above.

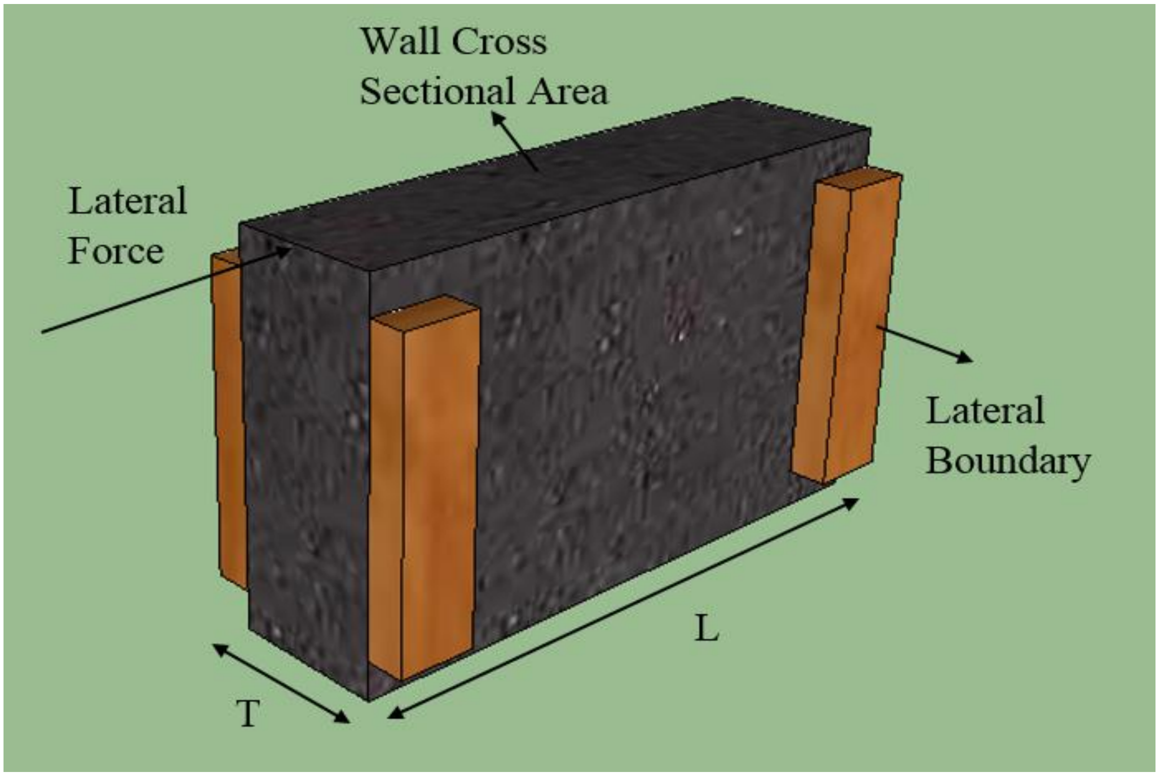

Figure 22. Crumb rubber infill frame three dimensional drawing.

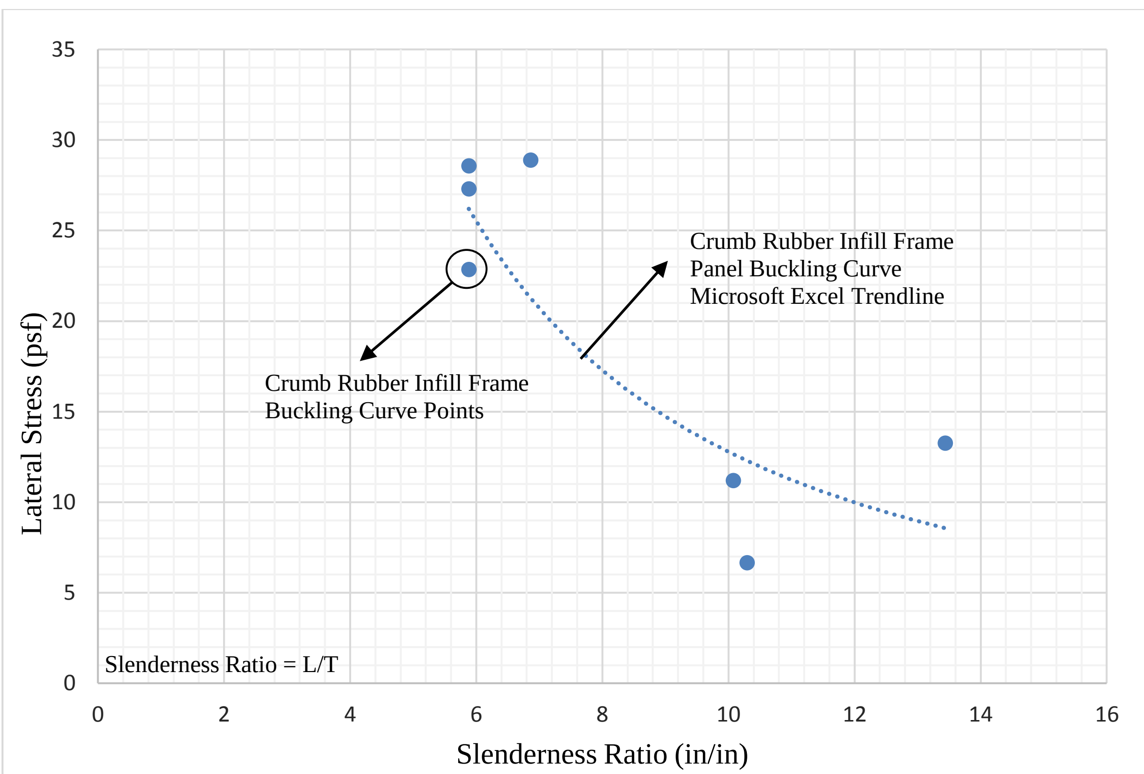

Figure 23. Crumb rubber infill frame panel buckling curve.

Figure 24. Out-of-plane deformation on crumb rubber infill frame without lateral boundary.

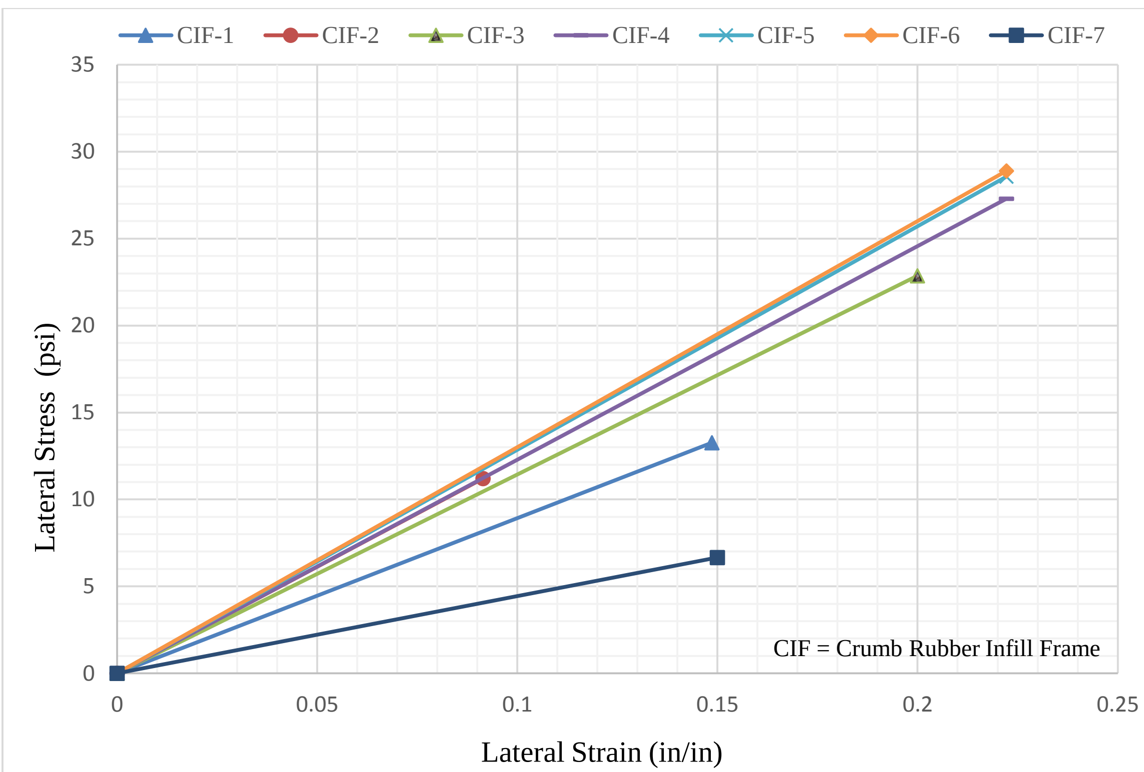

Figure 25. Lateral crumb rubber infill frame stiffness.

4.6 IN-PLANE RESISTANCE OF REINFORCED CRUMB RUBBER SHEAR PANEL

The last test performed in this investigation was the in-plane resistance of Reinforced Crumb Rubber (RCR) Wall, in order to explore the possible uses of the crumb rubber. For this test, four specimens were tested. The first was a plain crumb rubber wall (no steel reinforcement) used to compare the results with reinforced ones, and to obtain the shear modulus (G). Table 13 shows the summary of results obtained from the test, and in Figure 26 is shown a three dimensional drawing of the reinforced crumb rubber specimens with more details.

Table 13. In-plane loaded reinforced shear wall test results.

Specimen	**T**	**Wall Area**	**Steel Area**	**Δx_y**	**Fx_y**	**Δx_u**	**Fu**	**k_1**	**k_2**	**Gk_1**	**Gk_2**
-	(in)	(in^2)	(in^2)	(in)	(lb.)	(in)	(lb)	(lb/in)	(lb/in)	(psi)	(psi)
RCR-1	1.75	14	0	NA	NA	0.61	279.0	457.4	-	261.4	-
RCR-2	2	16	0.09	0.4	382	1.94	940.3	955.0	362.5	477.5	181.3
RCR-3	2	16	0.2	0.32	468	3.22	1760.0	1462.5	445.5	731.3	222.8
RCR-4	2	16	0.33	0.25	641	3.35	2800.0	2564.0	696.5	1282.0	348.2

RCR = reinforced crumb rubber.
T = thickness of the infill panel.
A = shear cross sectional wall area.
As = steel reinforcement area.
Fxy = in-plane force on the reinforced specimens at yield.
Δx_y = in-plane deformation on the reinforced specimens at yield.
Fu = ultimate load.
ΔX = ultimate deformation.
k1 = initial lateral stiffness.
k2 = second length lateral wall stiffness.
Gk_1 & Gk_2 = analogous k1 & k2 lateral stiffness in terms of stress and strain (k_1/T)
* The length and height of all specimens were 8 in and 5.5 in respectively.

4.6.1 PLAIN SHEAR WALL SPECIMEN RESULTS

The force vs. deformation plot of the plain specimen (RCR-1) shown in Figure 27, exhibits in essence a linear elastic behavior throughout all the cycles, resulting in little or no dissipation of energy

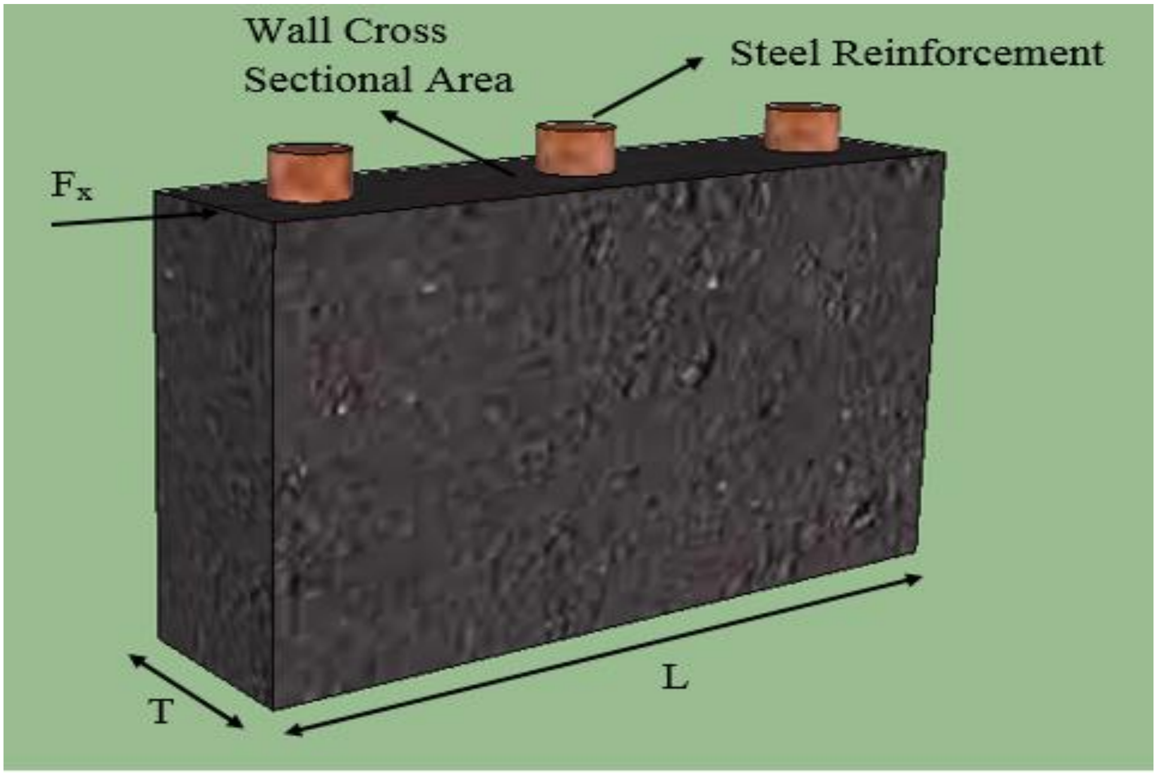

Figure 26. RCR shear wall test 3D drawing.

through hysteretic cycles. Recognizing the linearity exhibited, the shear modulus of a crumb rubber acting as shear wall or shear element was calculated resulting in 181.17 psi. For the plain specimen, the maximum recorded shear stress, τ, was 19.93 psi, with a shear strain, γ_x, of 0.11. These values were not the maximum value the specimen could withstand because the test was stopped at the onset of the debonding between the specimen and the steel plates without any signs of cracks on the rubber as seen in Figure 28, due to the bending moment, inherent to the load action.

Analytically, for masonry walls fixed walls at top and bottom (see Figure 29), the top displacement, Δx, is given by the following equation (Narendra, 2010):

$$\Delta x = \frac{P * h^3}{12 * Ew * I} + \frac{3 * P * h}{A * Ew} \quad (7)$$

where

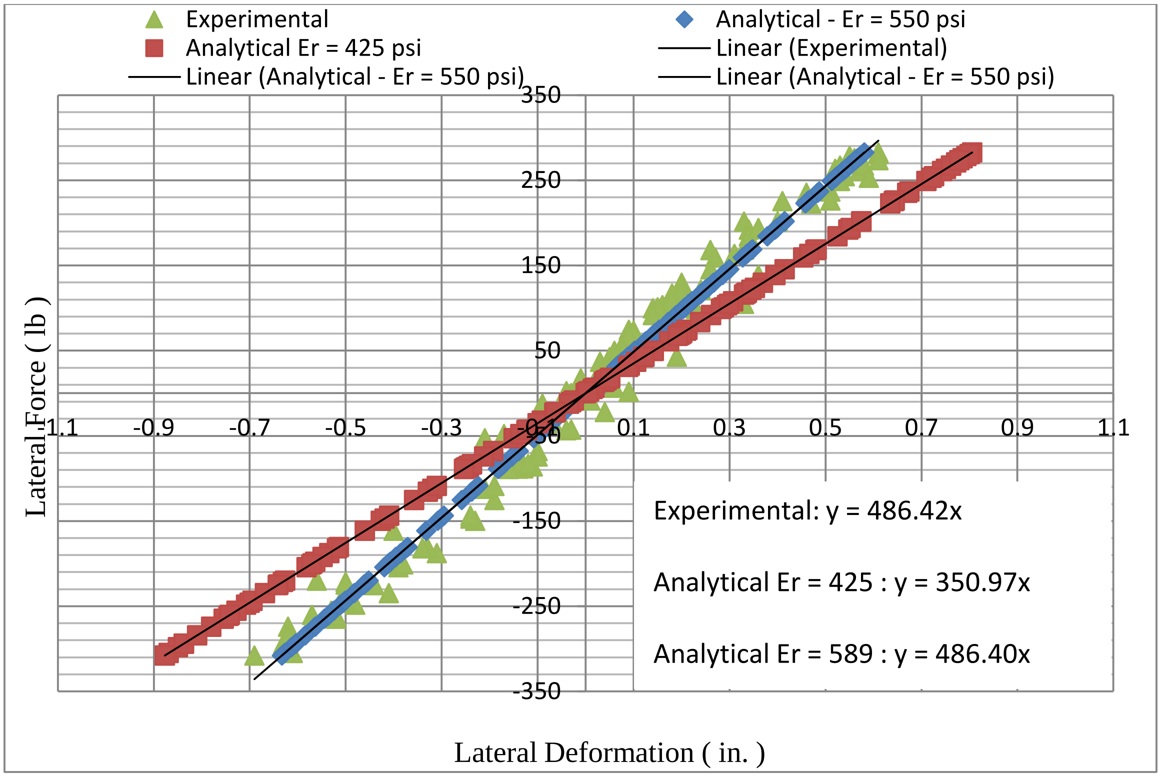

Figure 27. Plain crumb rubber shear wall test curve.

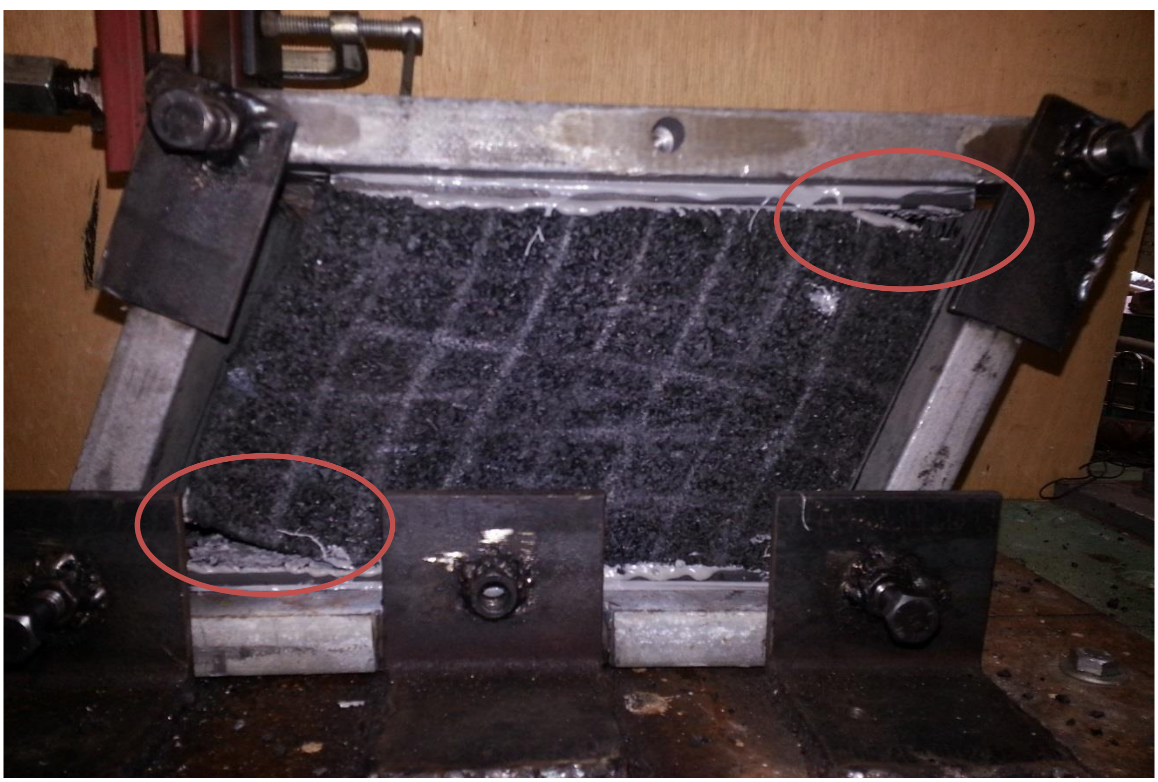

Figure 28. RCR plain shear wall deformed shape and corner debonding.

P = lateral load

h = height of the wall

Ew = modulus of elasticity of the material of the wall

I = moment of inertia of the wall

A = cross sectional area of the wall

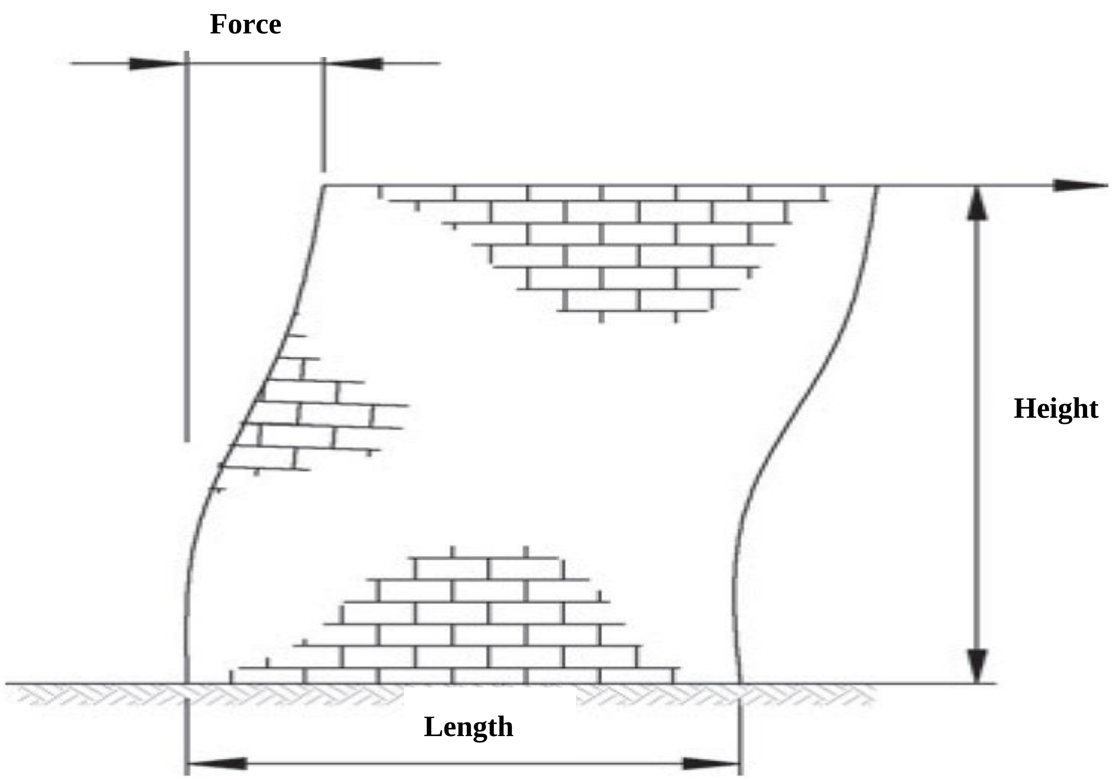

Figure 29. Narendra top and bottom fixed shear wall deformed shape.

Knowing the modulus of elasticity and the area of the wall it is possible to obtain the displacement for a given force. Looking for similarities in the behavior of the crumb rubber shear wall and masonry, the experimental results were plotted together with the results of the equation (7). From the ACL test, the maximum modulus of elasticity obtained for the crumb rubber was 425 psi, although the results were very variable, as discussed previously, with a maximum difference of 65 % with the lowest modulus obtained.

Putting this maximum modulus of elasticity into the equation (7), it does not fit the experimental results as expected (see Figure 27). Therefore, a linear regression analysis was performed with the aid of Microsoft Excel to determine the correct modulus that fit the equation and this resulted in a modulus of 589 psi. This modulus represents a difference of 38 % percent above the maximum value obtained in the ACL test. From the results several factors can be mentioned to explain the discrepancy between the experimental results and equation (7): (1) it is possible that the rubber used for the shear test possessed a higher modulus of elasticity than the rubber used for the ACL test, because during the process of manufacturing several variables could have been affected (like the strength of the epoxy used to bond the rubber particles, the level of compaction of the mix, etc.), which would change the strength of a particular block of crumb rubber, (2) equation (7) is an approximation to obtain the lateral deformation of a masonry wall fixed at top and bottom; therefore this equation may not be a good approach to predict the behavior of the crumb rubber, and (3) comparing the deformed shape of fixed top and bottom shear wall in Figure 29 with the deformed shape of the RCR-1 specimen shown in Figure 28, it cannot be established that both system deform in the same way, although they look similar.

In summary, if the modulus of elasticity of the crumb rubber cannot reach higher values, it is likely that equation (7) does not fit the experimental results of the crumb rubber shear. On the other hand, if the modulus of elasticity can reach higher values than those obtained from the ACL test, it is possible that, indeed, equation (7) be a good approximation to predict the deformation of crumb rubber shear wall element.

4.6.2 REINFORCED SHEAR WALL SPECIMEN RESULTS

The reinforced specimens exhibit different behaviors, as seen in Figure 30 to Figure 32. At glance, it can be noticed that there is a yield point, and after this point the system decreases its stiffness, behaving as a bilinear system. This behavior, in turn, generated hysteretic cycles which resulted in energy dissipation.

These cycles increase proportionally to the amount of steel reinforcement because when the initial stiffness is greater, the area under the curve is also greater.

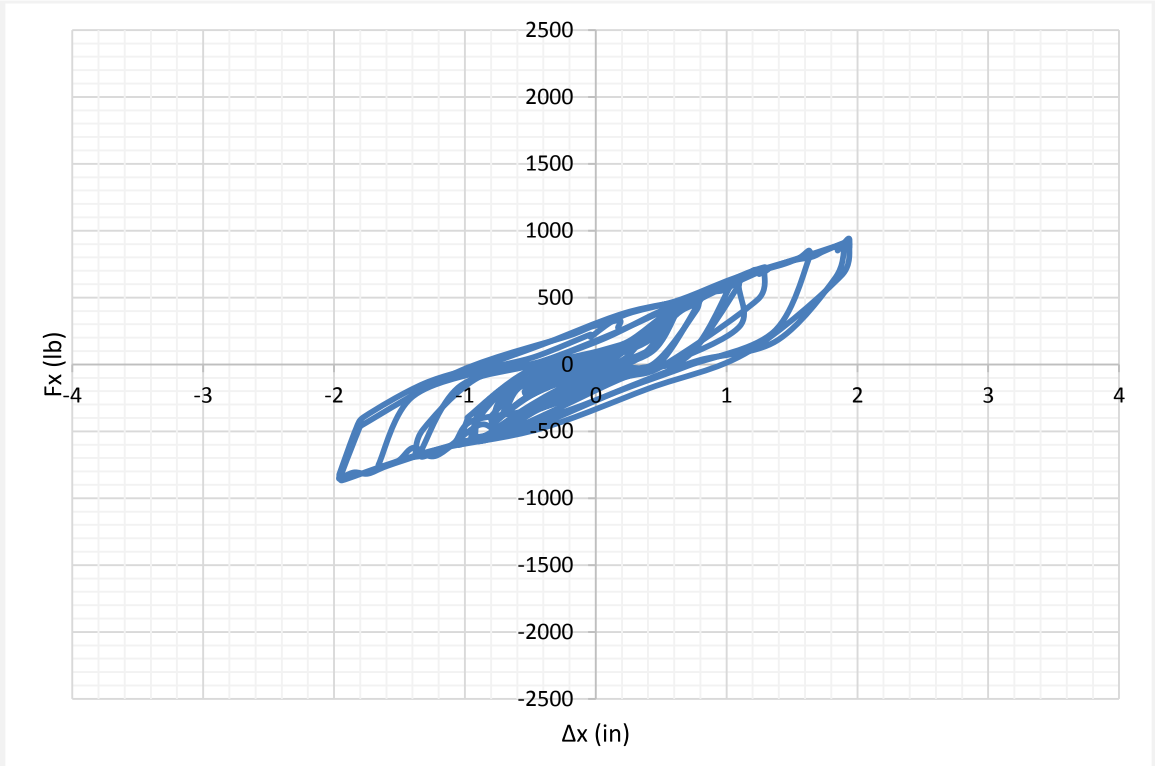

Figure 30. RCR-2 specimen test curve.

Noting the bilinear behavior, it was proceeded to construct a plot with the four specimen curves. The yield and ultimate point of the curves were calculated drawing lines parallels to the slopes of the two stretches of the curves shown in Figure 30 to Figure 32. In Table 14 are summarized the values selected from the experimental curves to construct the plot, where: (1) the level of load represents the load stage, (2) τ is the lateral load divided by the wall cross sectional area, (3) Lateral strain defined as the lateral displacement divided by the original length.

Finally, with the values of the table, the plot shown in Figure 33 was constructed. From the plot, it can be noticed that the second part of the curves show a similar trend than the plain specimen line.

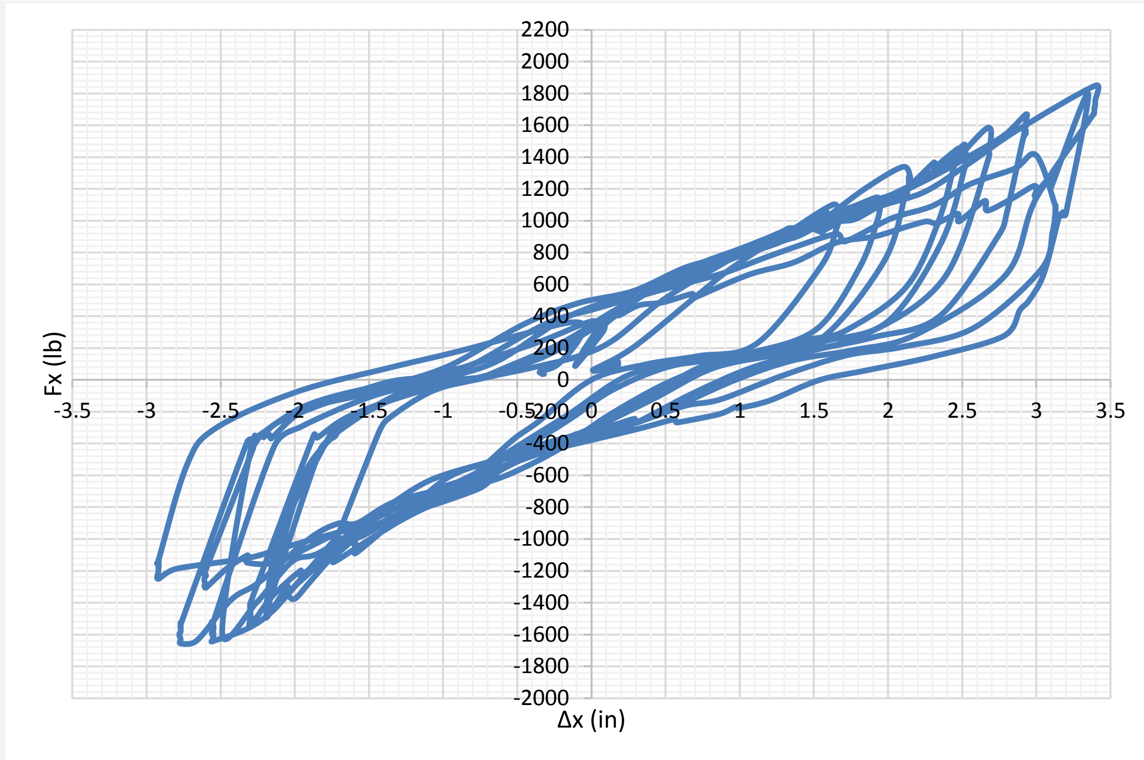

Figure 31. RCR-3 specimen test curve.

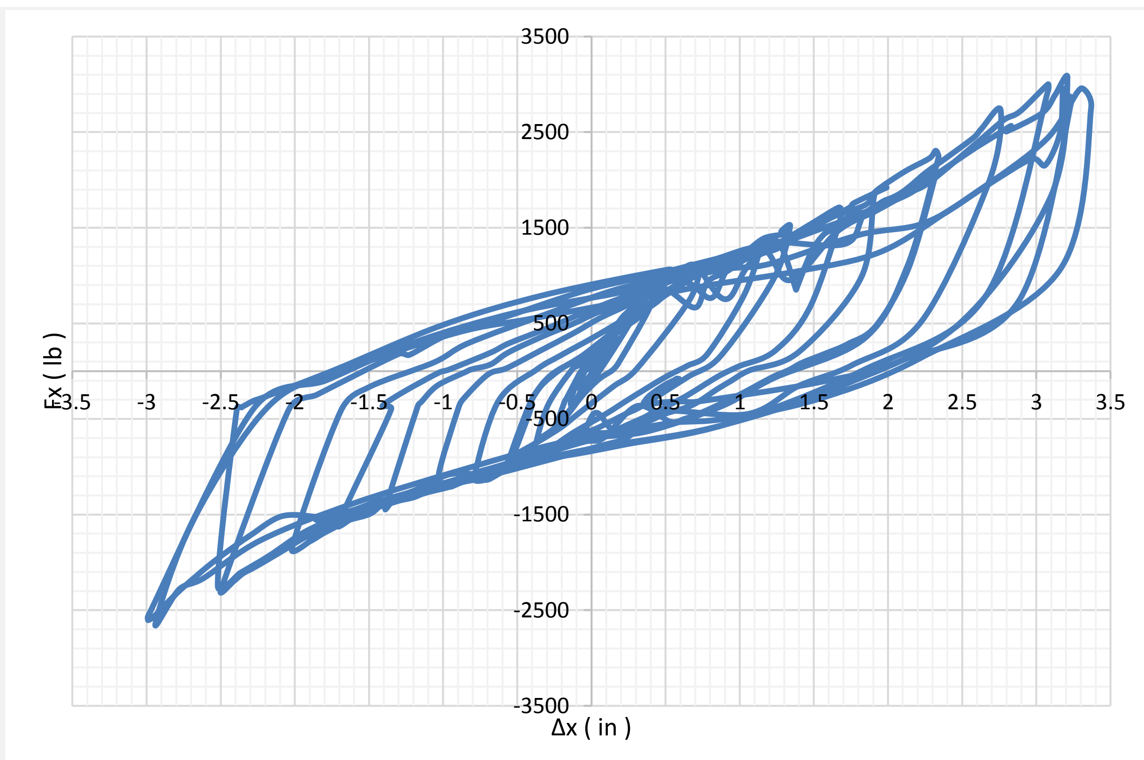

Figure **32**. **RCR-4 specimen test curve.**

Table 14. RCR shear wall bilinear curves points.

Specimen	Level of Load	τ (psi)	Lateral Strain
RCR-1	Maximum Load	19.93	0.08
RCR-2	Yield	23.88	0.05
	After Yield	58.77	0.24
RCR-3	Yield	33.13	0.04
	After Yield	104.3	0.40
RCR-4	Yield	40.06	0.03
	After Yield	175.00	0.42

τ = shear stress at level of load.
Lateral strain = lateral strain at level load.

Furthermore, in Table 13 are presented the slopes of this part of the curves (Gk_2), and it seems to confirm this assertion. For example, the average Gk_2 for the reinforced specimens is 251 psi. Comparing this average with the 261 psi (Gk_1) of the plain specimen, it represents a 3.85 % of difference. Then, it is fair to say that the second part of the curve seems to be due to the contribution of the rubber block. In other words, in the second part of the curve, the steel stops contributing to the overall stiffness of the system, which means that the steel is behaving in an elasto-plastic way, as the theory in general predicts.

Another aspect worth to mentioning is the increase in strength gained due to the use of reinforcement. For example, RCR-4 specimen slope (Gk_1) was 1282 psi, while RCR – 1 was 261 psi. Considering that the RC-4 has the maximum amount of reinforcement used, the increase in stiffness was 4.92 times the stiffness of the plain specimen. Meanwhile, the maximum ductility was obtained from the RCR-4 specimen, and resulted in 13.46. Ductility is the ability of a material to deform permanently before fracturing, and is mathematically defined as:

$$\mu = \frac{\Delta u}{\Delta y} \qquad (8)$$

where

Δu = ultimate displacement

Δy = displacement at the yield point

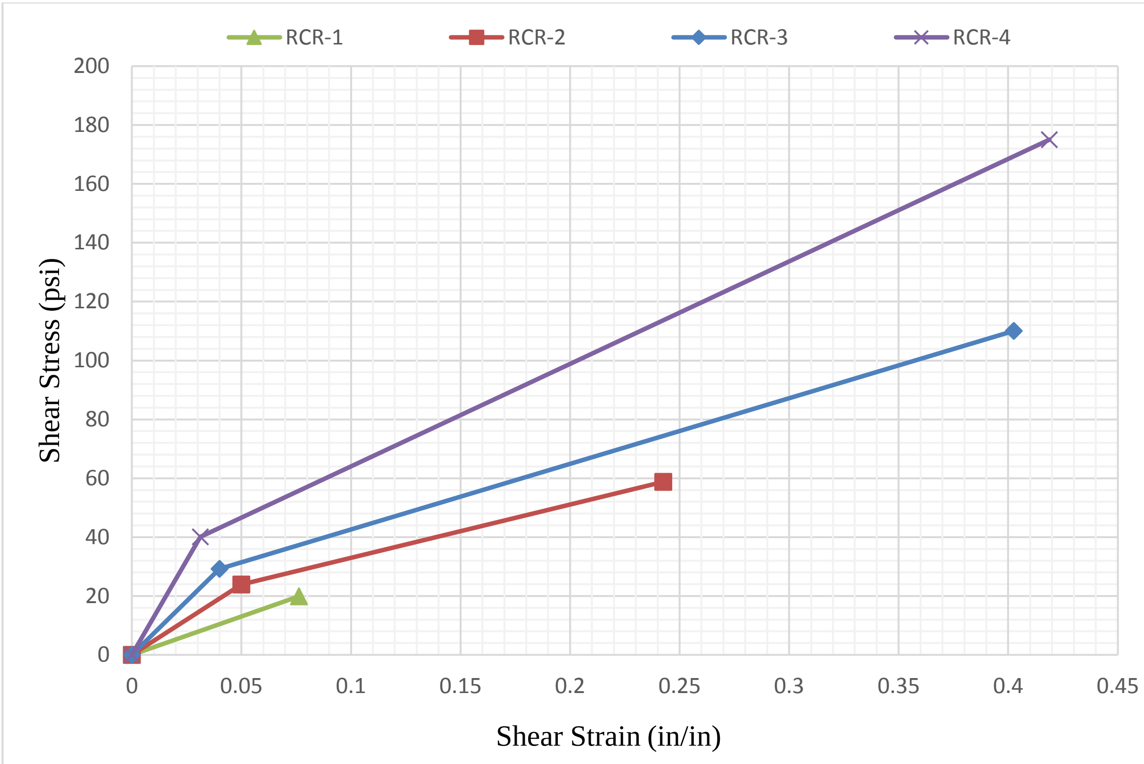

Figure 33. RCR shear wall lateral response curves.

The relevance of ductility in structures is the ability of warning before breaking. For example, a building constructed with ductile elements and subjected to extreme loads will show signs of deformation, warning the occupants from a possible or imminent collapse, giving them time to evacuate.

The failure mode is controlled by the steel plasticization at the supports on the rigid steel plates, as observed in Figure 34 through Figure 36 of specimens RCR – 3 and RCR – 4. Specifically, two facts can be pointed out from these figures: (1) when the rebars were extracted from the rubber block, it was observed that the deformed shape exhibited large deformation at the ends (where the support makes contact with the rebar), and an overall deformation similar to a fixed-fixed column subjected to a displacement in one of the supports (see Figure 35), (2) with the rebars out, it was noticed that the rebars basically cut the rubber block in two parts (see Figure 34).

Additionally, from the experimental Force vs. Deformation curves (Figure 30 to 32), it can be noticed the degradation of the hysteretic system after several cycles of load. As seen in Figure 35, one

Figure 34. RCR-3 specimen failure.

Figure 35. RCR-3 specimen rebars failed deformed shape.

Figure 36. RCR-4 deformed shape.

of the rebars was broken due to the shear stress exerted, and several were about to be broken. This discussion leads to establish that the energy dissipation generated by the system hysteresis is a consequence of several factors such as: (1) the yielding of the rebars at the joints, (2) the breakage of the rebars, and (3) the cutting of the rubber block by the movement and deformation of the rebars. It is important to note is the fact of the rebars redundancy, when the numbers of bars are greater, a greater amount of brakeage is necessary to generate a rupture mechanism failure.

Finally, to compare the results of the reinforced specimens with each other, two plots were generated in terms of the reinforcement ratio. The reinforcement ratio, ρ, is the same property used for concrete, defined as the area of steel per unit of area of concrete. In this case, it is the ratio of steel to the crumb rubber wall area. Mathematically it is defined as:

$$\rho = \frac{Ast}{b * h} \tag{9}$$

where

As_t = total area of steel reinforcement

b = thickness of the crumb rubber wall

h = length of the crumb rubber shear wall

The two plot constructed were: (1) the yield shear stress versus the reinforcement ratio (Figure 37), and (2) the yield lateral strain versus the reinforcement ratio (Figure 38). The reinforcement ratios are presented in terms of percent. A linear trend can be noticed in both plots. The advantage of this behavior is that the yield shear stress and the corresponding yield lateral strain can be predicted with the reinforcement ratio. After plotting the points, a linear regression analysis was performed with the aid of Microsoft Excel, from which the equation of the lines to calculate the yield shear stress and strain, as a function of the reinforcement ratio was obtained. Below are shown the two equations:

$$\tau_y = 1{,}061 * \rho + 17.4 \ \ (psi) \qquad \textbf{(10)}$$

$$\gamma_y = 0.0561 - 1.22 * \rho \qquad \textbf{(11)}$$

In summary, the RCR shear wall can dissipate energy and avoid the buckling problems, presented in the infill frames due to the slenderness ratio of the wall. Additionally, the use of reinforcement improves considerably the rigidity of the wall, making it possible to use this configuration in buildings walls. The next chapter will present an analysis of these results applied to a real structure, and will show an implementation of the proposed RCR shear wall for steel frame buildings.

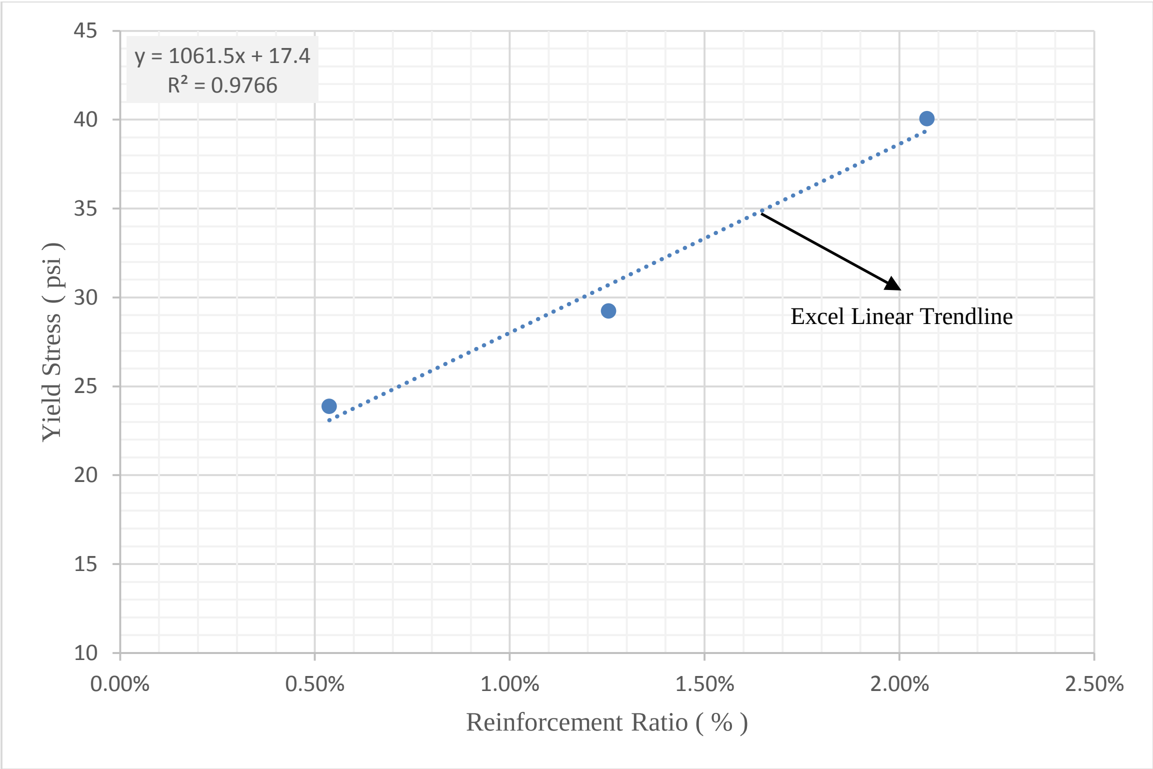

Figure 37. Reinforcement ratio - yield stress curve.

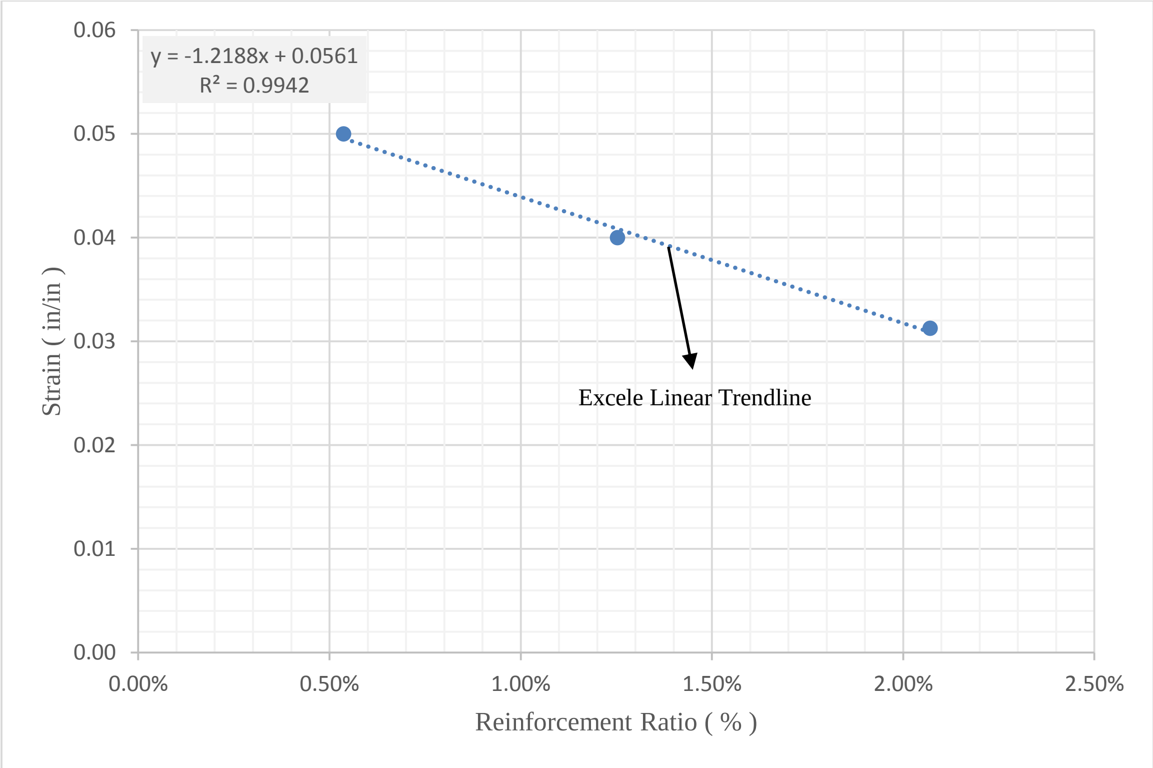

Figure 38. Reinforcement ratio - yield strain curve.

CHAPTER 5

EARTHQUAKE APPLICATION OF THE REINFORCED CRUMB RUBBER WALL

5.1 INTRODUCTION

This chapter aims to show a possible use for the scrap tire in structural engineering helping, in this way, to solve the current problem of its disposal. Another problem that we are currently confronting is that old buildings were constructed with typical plain masonry infill frames, which are seismically deficient (do not satisfy the requirements of the current design codes). The problem with its use in seismic applications is that the masonry exhibits a linear behavior that leads to a sudden failure and also increases the forces on the structures, as will be shown later, due to the high rigidity that characterizes the masonry. Therefore, many building needs retrofitting.

The specimens tested as part of the RCR test showed a high ductile response under cyclic load. A model of RCR as shear wall is proposed to resist the lateral forces induced by seismic movements as alternative way to retrofit seismically deficient structures (as plain Masonry Infill Frame or MIF) and to provide a new solution for future constructions . In order to perform the seismic evaluation of the proposed model and to compare it with the typical MIF building a time history analysis was conducted using the SAP2000 program.

5.2 ANALYTICAL MODELS

To compare both systems (Reinforced Crumb Rubber Shear Wall vs. Masonry Infill Wall), the following procedures were performed: (1) selection of the frame to be analyzed, (2) design of the RCR shear wall system building to resist the lateral loads to determine the earthquakes and wind loads, following the provisions of the ASCE 7-05, primary reference of the IBC 2009 (adopted code in Puerto Rico, (3) proposing a MIF building to resist the lateral loads, using the same size and number of walls obtained from the RCR shear wall lateral load design, and (4) performing of a time history analysis for both models using three different earthquake acceleration records, with the SAP200 software, in order to determine the advantages of using the rubber system instead of the masonry infill system.

5.2.1 BUILDING CONFIGURATION

The proposed building represents a structure that can be used for many typical applications, in order to resist the earthquakes forces, such as: pharmaceutics, factories, storage, and residential, among others. The building consists of four bays of 25 ft length in the X direction, and two bays of 30 ft. in the Y direction. The building has three floors; the first is 13 ft tall, and the two upper floors are 12 ft tall, with a 6 in concrete slab. All the beams and columns are W 14 x 61 and W 10 x 45, respectively. Figure 39 and Figure 40 summarize all the dimensions of the proposed building.

5.2.2 BUILDING DESIGN WITH RCR SHEAR WALL

The proposed building was designed to resist earthquake loads according to the Equivalent Lateral Load Analysis established by the ASCE 7-05, using the following procedure: (1) definition of the RCR Shear wall system configuration and determination of its strength, (2) determination of the lateral loads using the ASCE 7-05 Equivalent Lateral Load Analysis procedure, and (3) design verification.

5.2.2.1 SHEAR WALL SYSTEM CONFIGURATION AND STRENGTH

Chapter 4 discussed the fact that the large deformations at the joints, led to the bilinear plastic behavior of the crumb rubber shear wall as seen in Figure 41. Indeed, there are six plastic zones at the

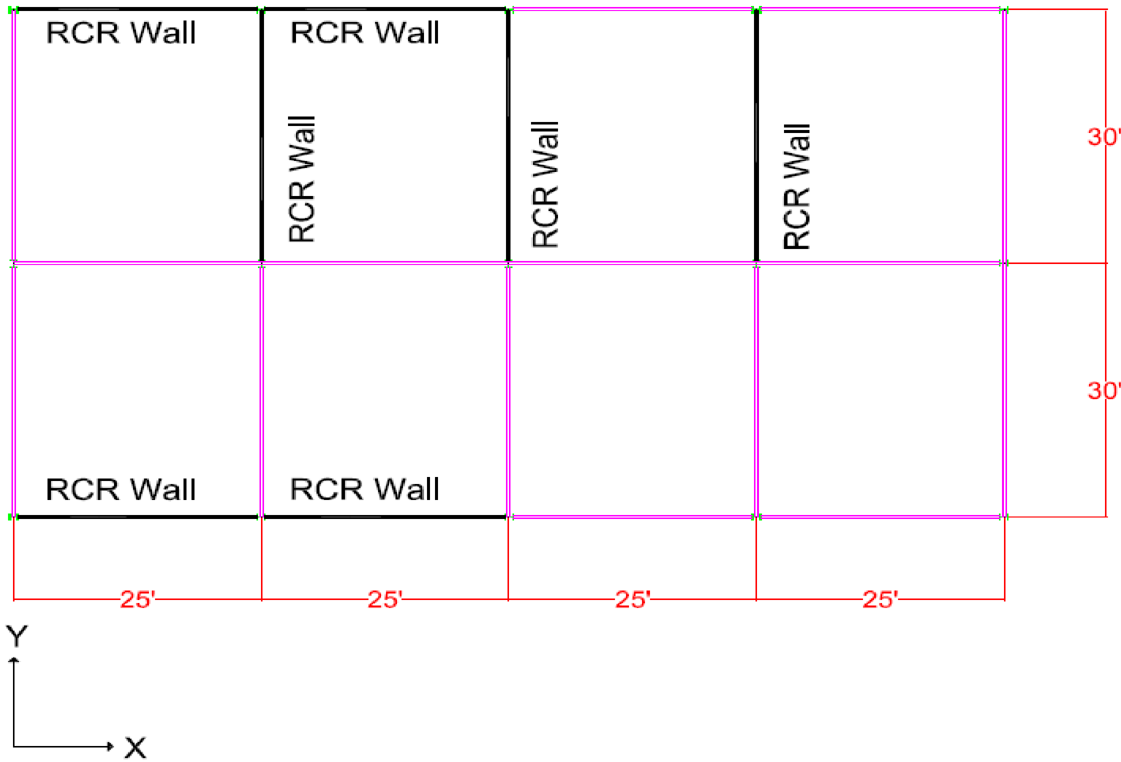

Figure 39. Proposed building model plan view.

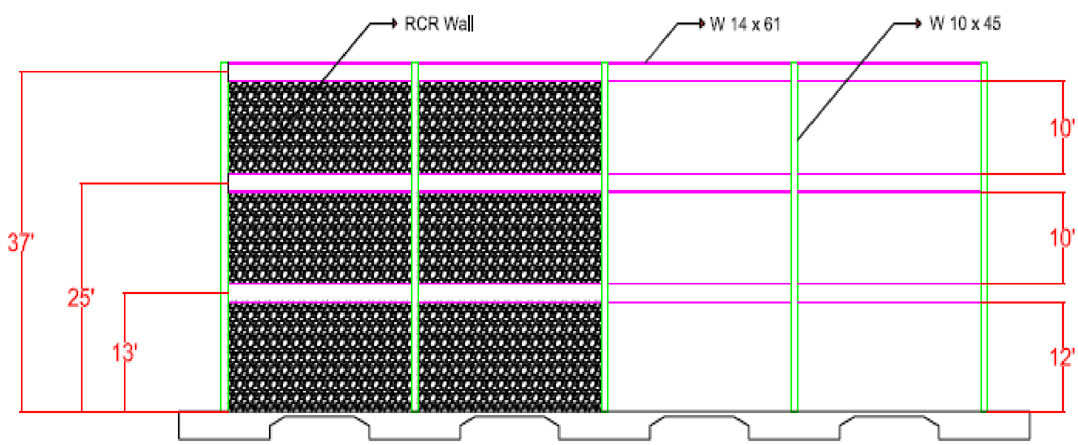

Figure 40. Principals frames on X direction.

contact point between the rebars and the beam plates. Extending this principle to a system with three rigid steel plates, and two RCR blocks as shown in Figure 42, and applying a force at the plate, the new system will have the same deformation, but twice the initial strength. This configuration has 12 plastic zones shown in Figure 42, which is twice the number of the single system.

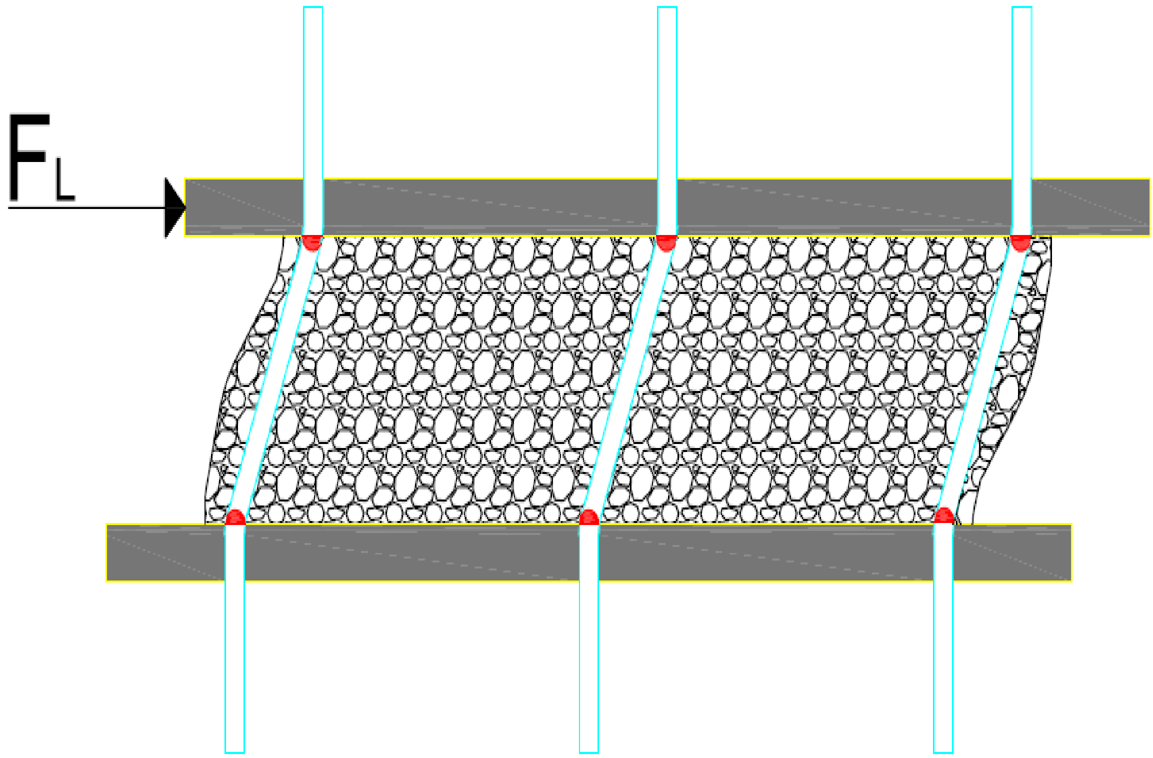

Figure 41. Single shear deformed shape and plasticization.

Consequently, if a number of *n* blocks were placed between plates along the two sections of Figure 42, a force *n* times greater would be necessary to induce the same deformation, because is the same concept of parallel springs or a shear building with columns. Besides, if more blocks are placed in the out of plane direction, the overall stiffness of the system would remain equal to the sum of all the parallel springs. Similar to a shear building, the rigid steel plates represented a rigid diaphragm, in which the load was applied equally throughout the system. Therefore, the total stiffness of the system can be defined as:

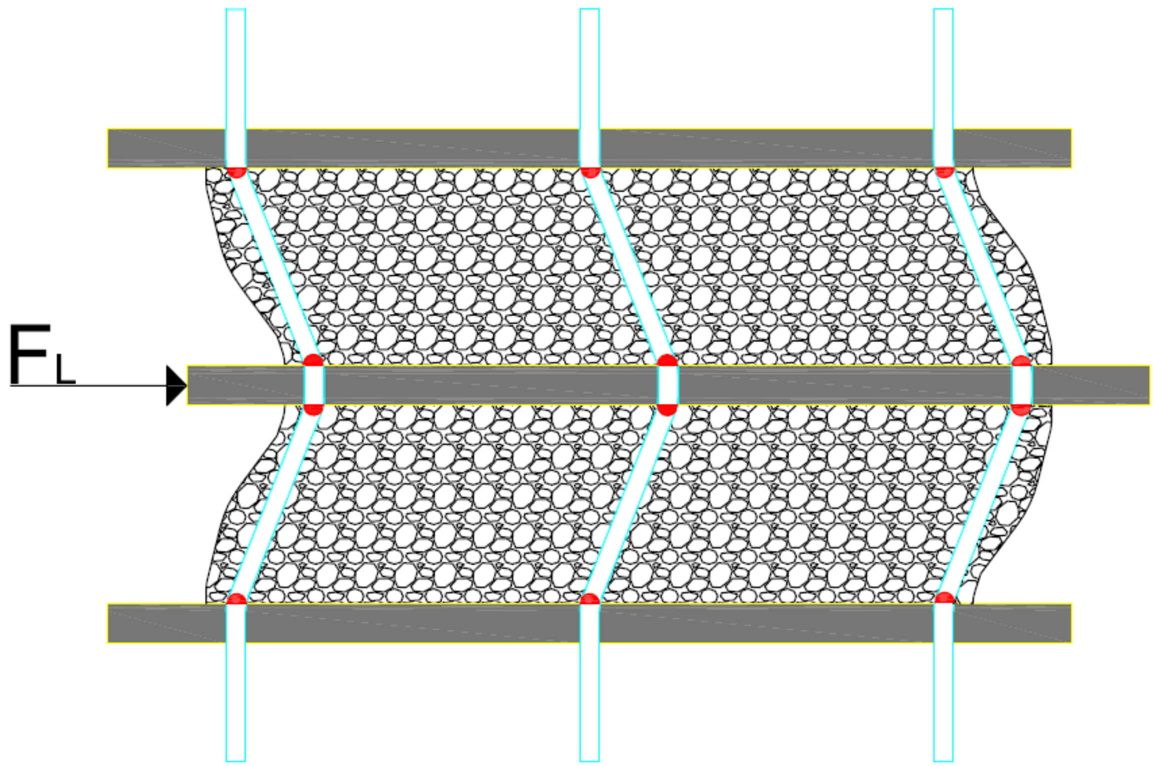

Figure 42. Proposed double shear system for building walls.

$$K_t = \sum_{i=1}^{n} k_i \tag{12}$$

where

K_t = total system stiffness

k_i = stiffness of the spring *i*

In the case of the RCR blocks, all blocks have the same stiffness. Thus, this equation can be rewritten as:

$$K_t = \# \, blocks * k_b \tag{13}$$

where

 # blocks = total number of blocks placed between plates

k_b = stiffness of a single block.

Therefore, in the same way, the yield force of the system could be determined from the expression:

$$F_t = \#\, blocks * F_y \tag{14}$$

where

F_y = yield force of a single block

However, in the previous chapter the results of the RCR test were expressed in terms of stress. The maximum force of the system using this approach is obtained with the following equation:

$$F_t = \#rows * \tau_y * A_w \tag{15}$$

where

A_w = the cross sectional wall area.

rows = number of vertical rows of blocks (for the proposed double shear system the number of rows is two).

The expression is multiplied by the number of rows because this number increases the strength of the system, providing more area or blocks to resist the lateral forces.

In essence, equations (14) and (15) represent the same approach, because it can be demonstrated that one can be obtained from the other. For example, the cross sectional area can be expressed as:

$$A_w = \left(\frac{\#blocks}{\#row}\right) * A_i \tag{16}$$

where

 # blocks/#rows = total number of blocks on one row (for the double shear system, there are two rows)

A_i = area of a single block

and the yield shear stress as:

$$\tau_y = \frac{F_y}{A_i} \tag{17}$$

Therefore, substituting equations (19) and (20) into equation (15), leads to:

$$Ft = \#rows * \tau_y * Aw = \#rows * \left(\frac{F_y}{A_i}\right) * \left(\frac{\#blocks}{\#\, rows} * A_i\right) = \#\, blocks * F_y$$

Equation (15) presents a simple way to determine the strength of this system that avoids the process of determining the quantity of blocks in a particular RCR shear system. It is important to establish that if the ultimate strength of the system is needed, the same approach can be used just changing the yield values for the ultimate values.

After establishing that it is possible to increase the strength of the double shear system, presented in Figure 42, first by having two rows of blocks and second by the number of blocks placed along the rows, the shear wall shown in Figure 43 is proposed, whose lateral response depends on the strength of the double shear system, placed in the diagonal of the wall. From the point of view of a frame, this system is analogous to a braced frame system, because the double shear system acts as a strut with a force, *Ft*, and stiffness, *Kt*. Hence, the building frame to be analyzed (see Figure 40) can be modeled as a braced frame, as shown in Figure 44, with a double shear system stiffness characteristics. For the proper functioning of the system, the following conditions must be meet: (1) the central plate must be connected using a pin at joint 5 (see Figure 43) to transmit the force through the rebars, and a gap must be left with the joint 2 to avoid the loading of the plate by itself, like a normal brace, and (2) the external plates must be pinned at the joints 1 and 3 to transmit the shear system strut force to the base or to the previous floor column, and they must be connected at joint 4 and 6 with a rollers that allow movement of the upper corner independent of the plates to avoid the loading of the plates by the brace effect. In that way, the central plate is pushed or pulled by the upper beam, and thus the forces are transmitted to the rebars. Finally, the rebars transmitted the forces to the external plates, which accordingly transmitted the forces to the base or lower column.

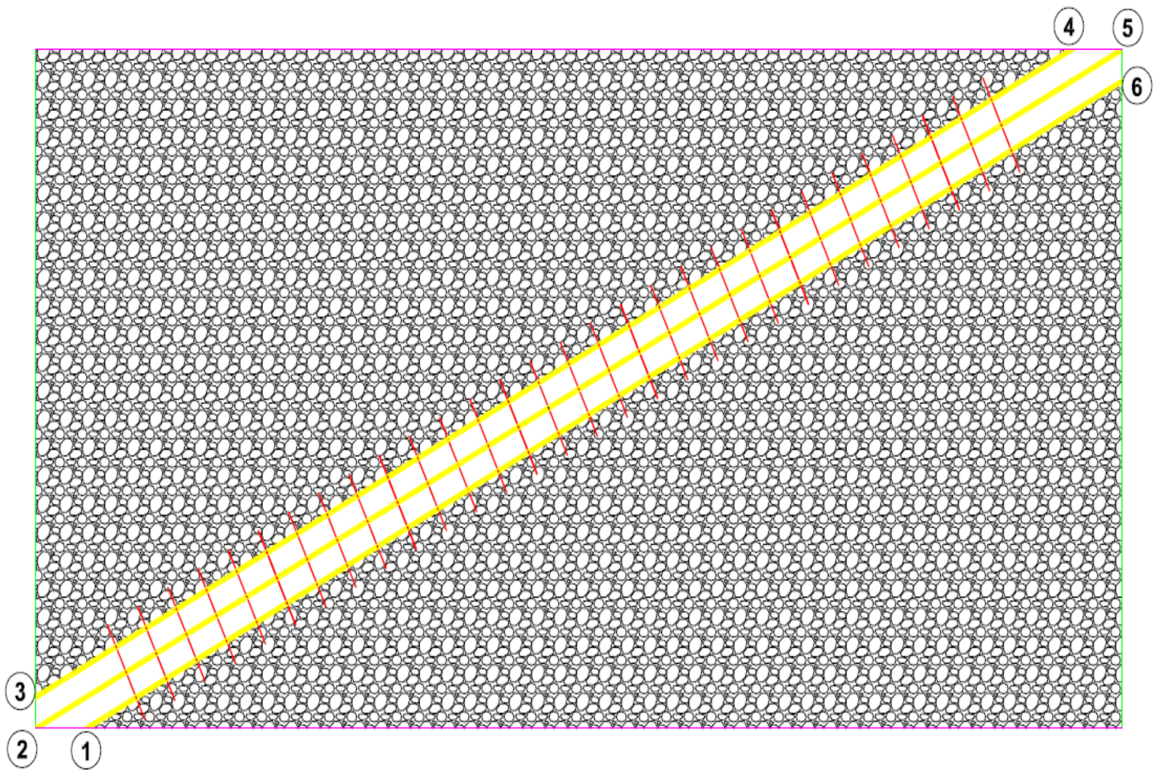

Figure 43. Proposed shear wall system.

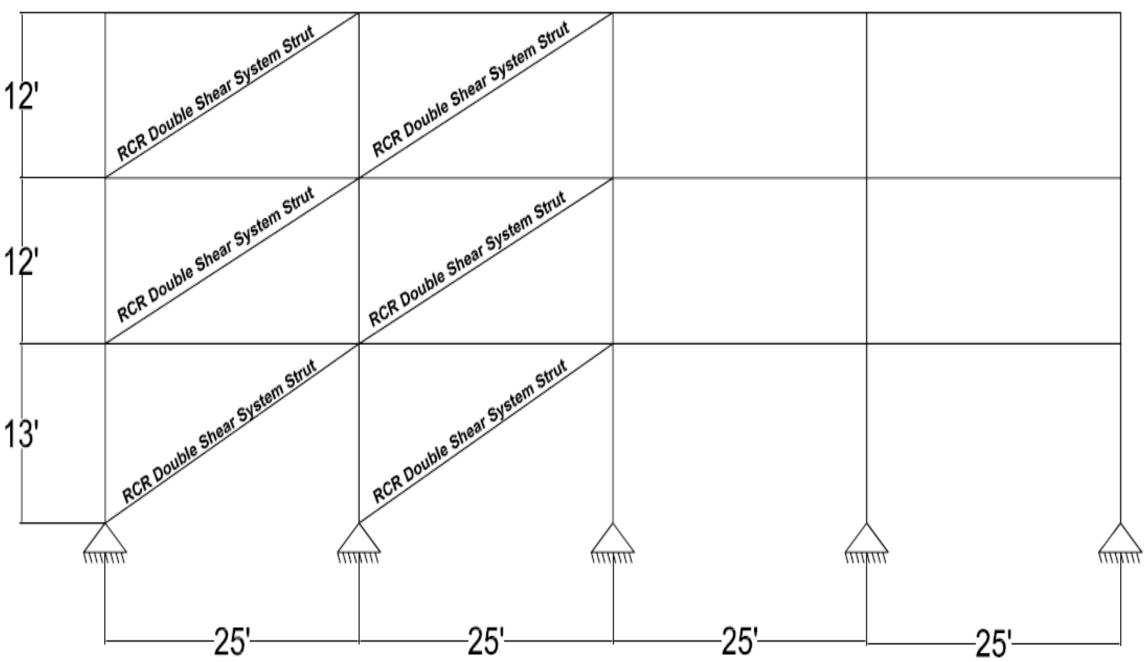

Figure 44. Strut frame analysis model for RCR shear wall system.

5.2.2.2 PRE-DESIGN OF THE ANALYZED FRAME

Before verifying the design of the building, it was necessary to conduct a pre-design in order to have a reasonable double shear strut size to finally get the actual loads in the building. To apply the Equivalent Lateral Force Analysis of ASCE 7 to determine the frame loads, it was necessary to estimate the natural period of the structure, as will be shown later. In the section 12.8.2.1 of the ASCE 7-05 there is a provision to calculate the approximate natural period of a structure. Given that the lateral force is sensitive to the natural period, and consequently, also sensitive to the stiffness and mass of the structure, this provision is not a good approach for this research because the calculation depends more on the structure type instead of the specific mass and stiffness of the structure, as established by the structures dynamics theory, through the following equation:

$$T = 2\pi \sqrt{\frac{M}{K}} \tag{18}$$

Therefore, the structures design loads will be different than the expected ones if the ASCE 7 provision is used to obtain the natural period.

To accomplish the pre-design of the building for lateral loads, the following procedure was performed:

1) Seismic weight determination: the effective seismic weight of the building was calculated using the ASCE 7-05, and the self-weight of the slabs and walls above all beams. For the effective weight, only 25 % of the live load was considered. Table 15 summarizes the effective weight contributions. Summing up all these factors, the effective weight of the building was 3,870 kips. The weight was uniformly distributed over the building.

Table 15. Proposed building effective weight contributions.

Slab Load (kips)	Walls Load (kips)	Super Imposed Load (kips)	Live Load (kips)
2700	675	270	900

3) Analyzed frame selection: Figure 39 shows the symmetry in the X direction. For this reason the effective weight was equally distributed in the two frames, thereby the frame shown in Figure 40 was analyzed using an effective weight of 1,935 kips, which is half of the building weight.

4) Base shear estimation: to estimate the size of the double shear for the pre-design, it was determined to estimate the base shear as 10 % of the effective weight, which represents 193.5 kips. This base shear was distributed along the three floors of the frame using the equations 12.8-11 and 12.8-12 of ASCE 7-05 :

$$Fxi = Cvx_i * V \tag{19}$$

$$Cvx_i = \frac{w_x * {h_x}^k}{\sum_{i=1}^{n} w_i * {h_i}^k} \tag{20}$$

where

Cvx_i= vertical distribution factor,

V = total design lateral force or shear at the base of the structure

w_i *and* w_x = the portion of the total effective seismic weight of the structure (W) located or assigned to level i or x

h_i and h_x = the height (ft or m) from the base to level i or x

k = an exponent related to the structure period as follows: for structures having a period of 0.5 s or less, k = 1; for structures having a period of 2.5 s or more, k = 2; for structures having a period between 0.5 and 2.5 s, k shall be 2 or shall be determined by linear interpolation between 1 and 2. For the pre-design, k was taken as 1, because the period of the structures is unknown.

The forces acting on the three levels of the frame shown in Figure 44 were obtained using the equations (19) and (20) the analyzed frame. Table 16 summarizes all the factors and forces for pre-design. To distribute the force in the most evenly way possible, the force floor, F, was divided by the number of nodes of the floor (see F/Joint column). Figure 45 shows the model created to analyze the frame for pre-design, with the seismic forces acting at the joints.

Table 16. Base shear floor distribution for pre-design.

Floor	Height	Weight	wi*hi^k	Cvx	F	F/Joint	Floor Shear
-	(ft.)	(kips)	(Kips -ft.)	(%)	(kips)	(kips)	(kips)
3	37	645	23865	49%	95.46	19.09	95.46
2	25	645	16125	33%	64.50	12.90	159.96
1	13	645	8385	17%	33.54	6.71	193.50
	Σ	1935	48375	100%	193.50		

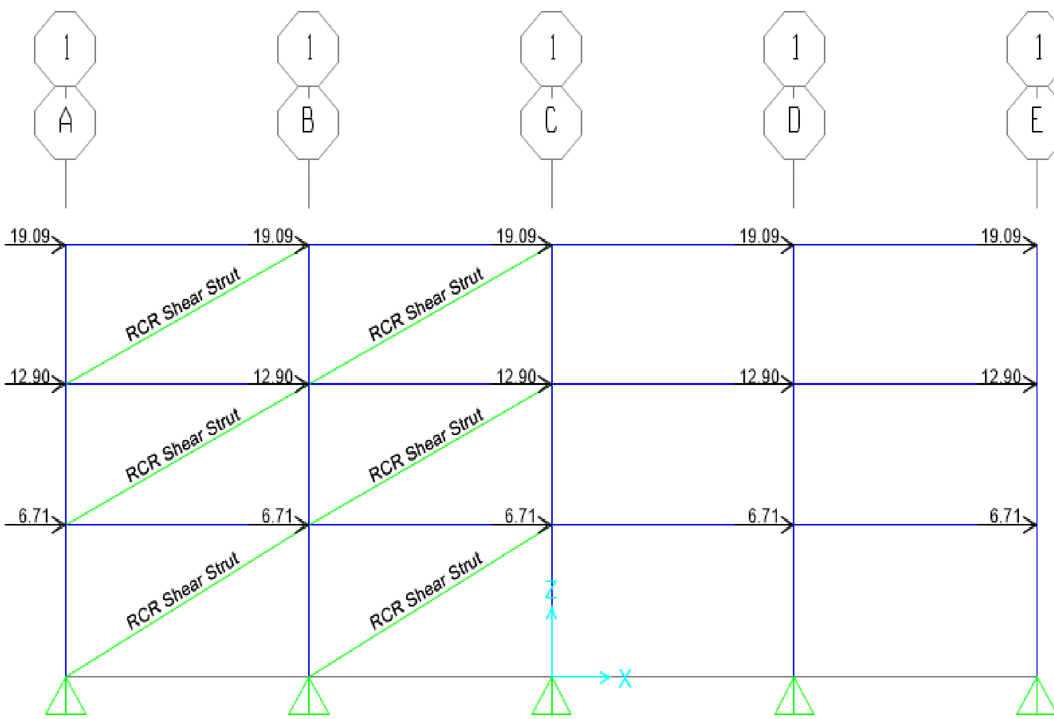

Figure 45. SAP200 model distributed forces for pre-design.

Finally, to analyze the maximum forces, F_{max}, acting on the links, the SAP200 model was run with the following load combinations of the ASCE 7-05:

$$Fmax = 1.2D + E + L \tag{21}$$

$$Fmax = 0.9D + E \qquad (22)$$

where

D = dead load

E = earthquake load

L = live load

From the analysis it was found that the maximum force in the strut was 122 kips. For purposes of design equation (14) can be rewritten as follows:

$$tmin = \frac{V_{max}}{2 * \tau_y * L_{eff.}} \qquad (23)$$

With the shear yield stress of 40 psi obtained from the RCR-4 specimen, and using an effective wall diagonal length, *Leff*, of 280 in, it was obtained that the minimum thickness, t_{min}, of the wall required to withstand 122 kips of shear was 5.44 in. In order to use a standard or typical number, a 6 in thickness RCR wall was adopted, with a reinforcement ratio of 2.07 %. The effective length was used, because it is impossible to place rebars through the whole diagonal length.

5.2.2.3 DESIGN VERIFICATION OF THE ANALYZED FRAME ACCORDING TO ASCE 7-05

After determining the 6 in thickness RCR shear wall in the pre-design, the design was verified using the Equivalent Lateral Load Analysis procedure described in Section 12.8 of the ASCE 7. All the equations presented in this section are based on the ASCE 7-05 edition. For this analysis, the following procedure was performed:

1) Calculation of initial stiffness: The initial stiffness of the RCR shear wall was calculated dividing equation (14) by the 0.25 in yield deformation of the RCR-4 specimen. Using an effective length of 280 in, resulted in a cross sectional area of 1,680 in². From the equation (14) a maximum force of 134 kips, for a stiffness of 536 k/in was obtained.

2) Determination of the fundamental period: A modal analysis was conducted in SAP2000 to determine the period, *T*, of the structure. The result of the analysis showed that the RCR shear wall frame had a fundamental period of 0.70 seconds.

3) Determination of the Importance factor: an Occupancy Category III building was chosen. This gives a factor of I = 1.25.

4) Localization of the structures: the structure was located at Mayagüez, Puerto Rico, whose spectral accelerations S_s and S_1 are 1.19 and 0.39, respectively.

5) The next parameters were obtained from the ASCE 7-05 as follows, and are summarized in Table 17:

    a. sites coefficients were determined using Tables 11.4-1 and 11.4-2

    b. site coefficients and adjusted maximum considered earthquake spectral response acceleration parameters with equations 11.4-1 and 11.4-2

    c. design spectral acceleration parameters using equations 11.4-3 and 11.4-4

Table 17. ASCE 7-05 spectrum parameters.

Fa	Fv	SMs	SM_1	SD_S	SD_1
1.02	1.62	1.21	0.63	0.81	0.42

6) Selection of factor *R*: considering the high ductility behavior exhibited in the RCR test of the reinforced specimens, a factor R = 8 was chosen.

7) Design response spectrum periods equations from section 11.4.5:

$$T_s = \frac{SD_1}{SDs} \quad (24)$$

$$T_L = 12, for\ Puerto\ Rico \quad (25)$$

8) Construction of the seismic response spectrum: Figure 46 shows the seismic design response spectrum for a site with all the properties mentioned above. From the figure, for a period of 0.70

seconds, the seismic response coefficient is 0.094. The seismic response spectrum was constructed using the seismic response coefficient from section 12.8.1.1, described as follow:

for T > TL

$$Cs = \frac{SD_1 * T_L}{T^2 * \left(\frac{R}{I}\right)} \tag{26}$$

for Ts < T ≤ Ts

$$Cs = \frac{SD_1}{T * \left(\frac{R}{I}\right)} \tag{27}$$

for T ≤ Ts

$$Cs = \frac{SDs}{\frac{R}{I}} \tag{28}$$

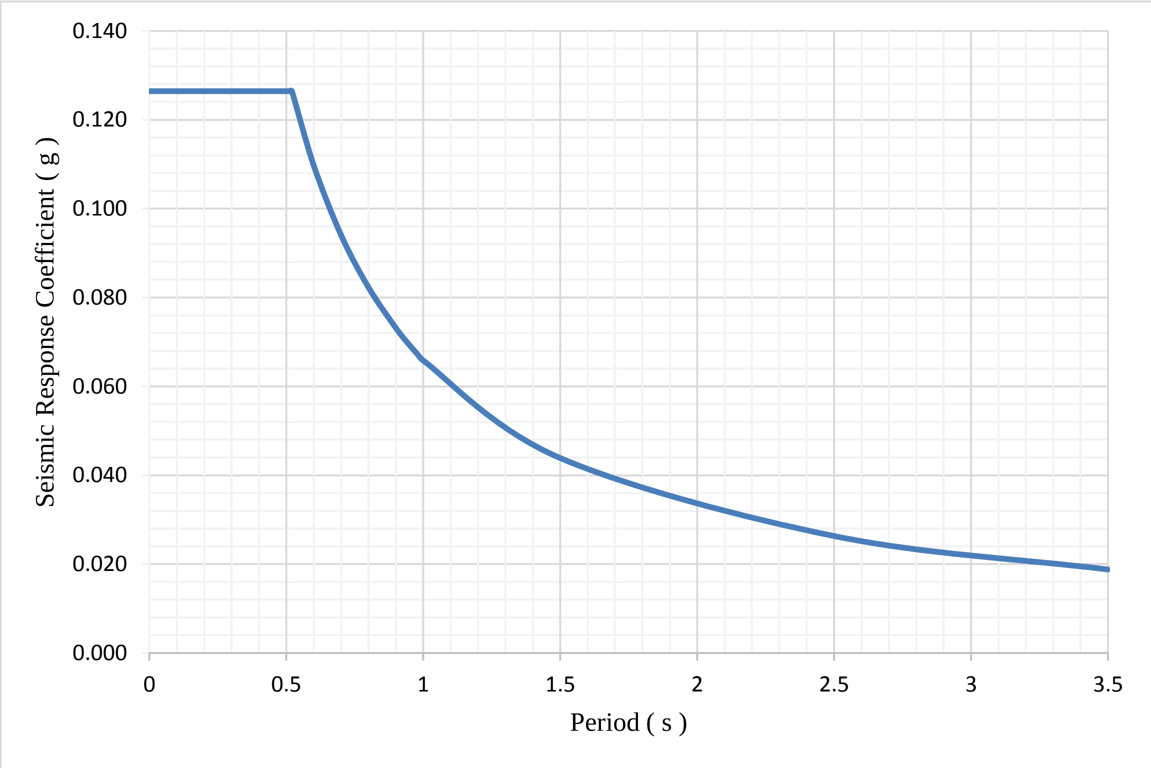

Figure 46. Design response spectrum

9) Determination of the base shear, *V*: from the design spectrum, and using the period of the structure, the seismic response coefficient was obtained and finally the base shear was calculated using equation 12.8-1:

$$V = Cs * W \tag{29}$$

where

W is the effective weight of the frame.

Recalling that the effective seismic weight of the frame was 1,935 kips, the result of this calculation is a design base shear of 181.92 kips. Because this base shear is less than the base shear calculated for the pre-design, a wall with a 6 in thickness can resist the forces predicted by the Equivalent Lateral Load Analysis.

10) Distribution of lateral force: to verify the inter-story drifts, equations (19) and (20) were used to calculate the force distribution through the three floors to finally obtain the elastic displacements of the frame. Table 18 are presents the seismic forces on the frame, which are similar to those from the pre-design.

Table 18. Design force distribution on analyzed frame.

Floor	**Height**	**Weight**	**wi*hi^k**	**Cvx**	**Force**	**Force/Joint**
-	(ft.)	(kips)	-	-	(kips)	(kips)
3	37	645	34243.77	51%	92.53	18.51
2	25	645	22248.14	33%	60.12	12.02
1	13	645	10836.71	16%	29.28	5.86
	Σ =	1935	67328.62	100%	181.92	

11) Determination of story drifts: the design story drift, Δ, was calculated as the difference of the deflections at the centers of mass at the top and bottom of the story under consideration. However, to consider the inelastic deflections, the ASCE 7 provides the following equation in section 12.8.6 to calculated the ultimate displacement u_x:

$$u_x = \frac{C_d * u_{xe}}{I} \tag{30}$$

where

C_d = the deflection amplification factor in Table 12.2-1 of ASCE 7-05.

u_{xe} = the deflections determined by an elastic analysis.

I = the importance factor.

Because the system proposed in this investigation is not a conventional one, it was decided to use a Special Steel Concentrically Braced Frame from the table, for which C_d = 5.5, to convert the elastic displacements determined by the analysis to the expected non-linear displacements. To compare these displacements, Table 12.12-1 gives the equations to calculate the maximum allowable displacement for a specific structural system and occupancy category. The maximum allowable drift for the RCR shear wall was calculated as follows:

$$\Delta_a = 0.020\ h_{sx} \tag{31}$$

where

h_{sx} = height of the floor analyzed.

This equation establishes that the allowable drift is 2 % of the story height. Using the equations (30) and (31), and the SAP2000 analysis, the following quantities were computed: (1) elastics deflections u, (2) total deflection, u_x, (3) story drifts in inches and percent, Δ, and (3) allowable story drift, Δ_a. The results of the analysis are summarized in Table 19. From the table, it can be noticed that the maximum drift was 0.79 %, and occurred in floor two, which is less than the allowable 2 %, drift. This means that the frame has no drift problem.

Table 19. Design frame drifts.

Floor	u_{xe}	u_x	Δ	Δ	Δ_a
-	(in)	(in)	(in)	(%)	(in)
3	0.7	3.08	0.748	0.52%	2.88
2	0.53	2.332	1.144	0.79%	2.88
1	0.27	1.188	1.188	0.76%	3.12

u_{xe} = deflections determined by an elastic analysis in SAP2000.

Δ = interstory drift.

Δ_a = allowable interstory drift

5.2.3 MASONRY WALLS STIFFNESS AND STRENGTH

The strength and stiffness of a plain masonry wall depends on the effective width, a, of the diagonal compression strut shown in Figure 17. To obtain the effective width of a masonry infill panel, the recommendations given in FEMA 306 were followed. The equivalent strut represented by the actual infill thickness that is in contact with the frame (t_{inf}) and the diagonal length (r_{inf}) and an equivalent width is given by the following equation:

$$a = 0.175\ (\lambda * h_{col})^{-0.4} \tag{32}$$

where

$$\lambda = \left(\frac{E_{me} * t_{inf} * \sin(2\theta)}{4 * E_{fe} * I_{col} * h_{inf}}\right)^{\frac{1}{4}} \tag{33}$$

and

h_{col} = column height between centerlines of beams, in.

h_{inf} = height of infill panel, in.

E_{fe} = expected modulus of elasticity of frame material, psi.

E_{me} = expected modulus of elasticity of infill material, psi.

I_{col} = moment of inertial of column, in^4.

r_{inf} = diagonal length of infill panel, in.

t_{inf} = thickness of infill panel and equivalent strut, in.

θ = angle whose tangent is the infill height-to-length aspect ratio, radians

$$\theta = \tan^{-1}\frac{h_{inf}}{L_{inf}} \quad (34)$$

where

L_{inf} = length of infill panel.

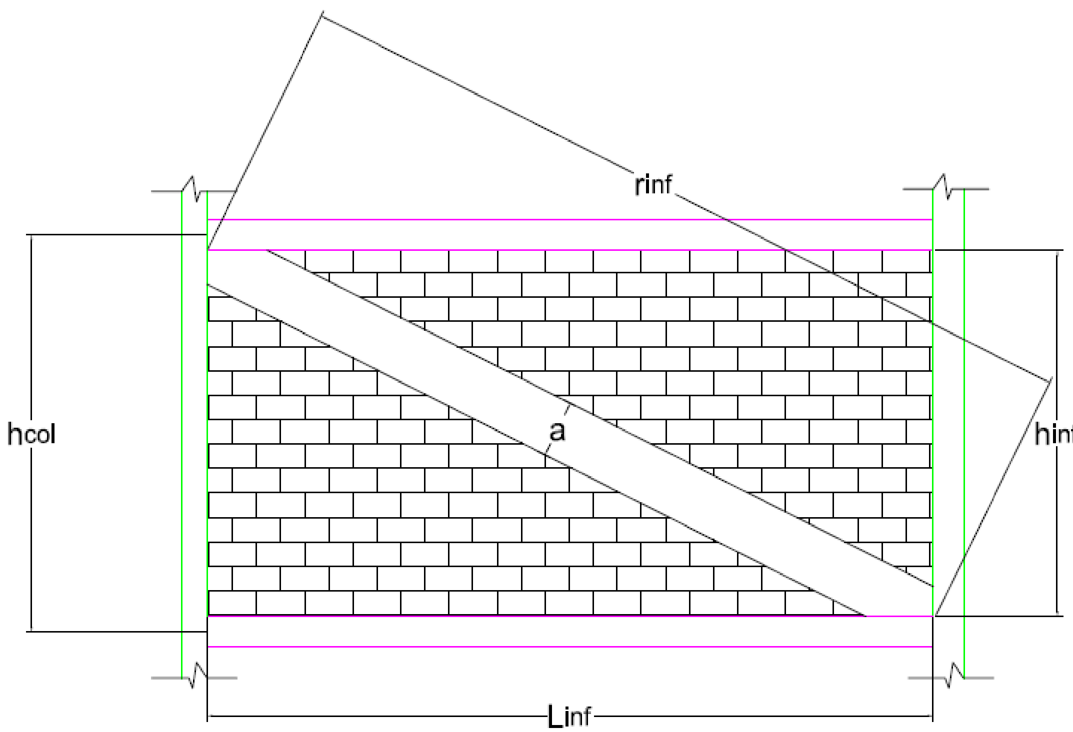

Figure 47. Masonry infill wall layout and properties.

The properties of the masonry infill wall frame to be analyzed are presented in Table 20. Using the previous equations and the properties of Table 20, the width of the equivalent strut resulted in 24.24 in and the stiffness was 1,121.94 kips/in. Using the same model presented in Figure 44 with the stiffness of the masonry calculated in this section, a modal analysis was performed with SAP2000, which resulted in a fundamental period of 0.54 seconds. The strut stiffness was calculated using the axial stiffness equation for bar elements, as follows:

$$K = \frac{E * A}{L} \tag{35}$$

On the other hand, the ultimate compression was calculated according to the following equation, presented in FEMA 306, section 8.3:

$$Rc = a * h_{inf} * f'm_{e90} \tag{36}$$

where

a = equivalent strut width, defined in equation (32)

t_{inf} = infill thickness

$f'm_{e90}$ = expected strength of masonry in the *horizontal* direction, which may be set at 50% of the expected stacked prism strength f'me.

Table 20. Masonry infill wall properties.

h_{inf}	L_{inf}	r_{inf}	t_{inf}	h_{col}	t_{inf}	Θ	I_{col}	$f'm_e$	Em_e
(ft)	(ft)	(ft)	(ft)	(ft)	(ft)	(rad)	(in4)	(psi)	(ksi)
12	24.17	323.78	6	13	30	0.46	248	1170	2223

The result was that the masonry infill wall was able to withstand 96 kips in compression, and it was assumed that no other failures occurred. The masonry strength and the factors to convert lower-bound properties to expected values were obtained from Table 7-1 and Table 7-2 of the FEMA 356, respectively.

5.2.4 EARTHQUAKES FOR TIME HISTORY ANALYSIS

Three earthquakes were selected to study the effects of different frequencies on the RCR shear wall and compare it with the masonry infill frames. The three earthquakes selected were: (1) 1947 El Centro at Imperial Valley, California, (2) 1994 Northridge at North-Central San Fernando, California, and (3) 1989 Loma Prieta at San Francisco, California. In Figure 48-Figure 50 are shown the plot of the three earthquakes response spectra using a damping ratio of 5 % which is a typical value for structural applications.

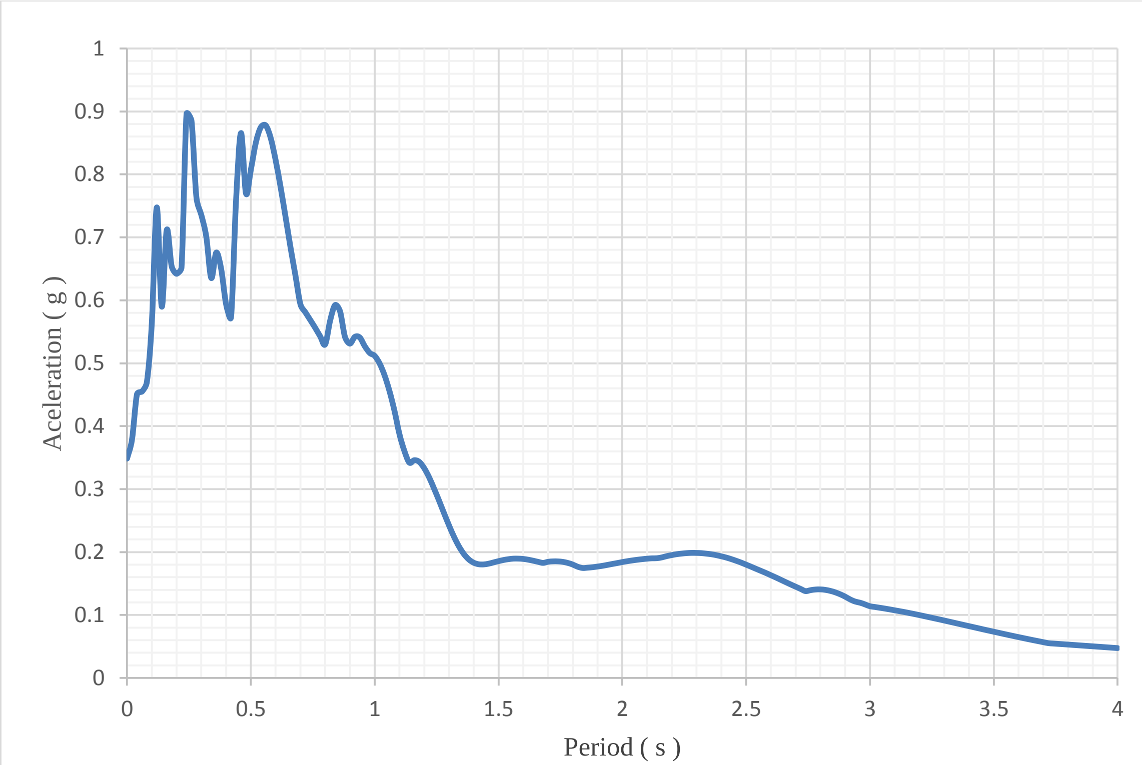

Figure 48. El Centro response spectrum.

5.3 TIME HISTORY ANALYSIS

To show the benefits of using the RCR shear wall systems over the typical masonry infill frames, a time history analysis was performed on both. The same geometrical properties were used and only the lateral stiffness of the systems was changed to account for the material and section properties of the walls.

5.3.1 TIME HISTORY ANALYSIS CONSIDERATIONS

To run the time history analysis, the following considerations were taken into account to represent the conditions of the analyzed building:

a. The model was constructed using diagonal struts, represented by links elements in SAP2000, with the corresponding stiffness.

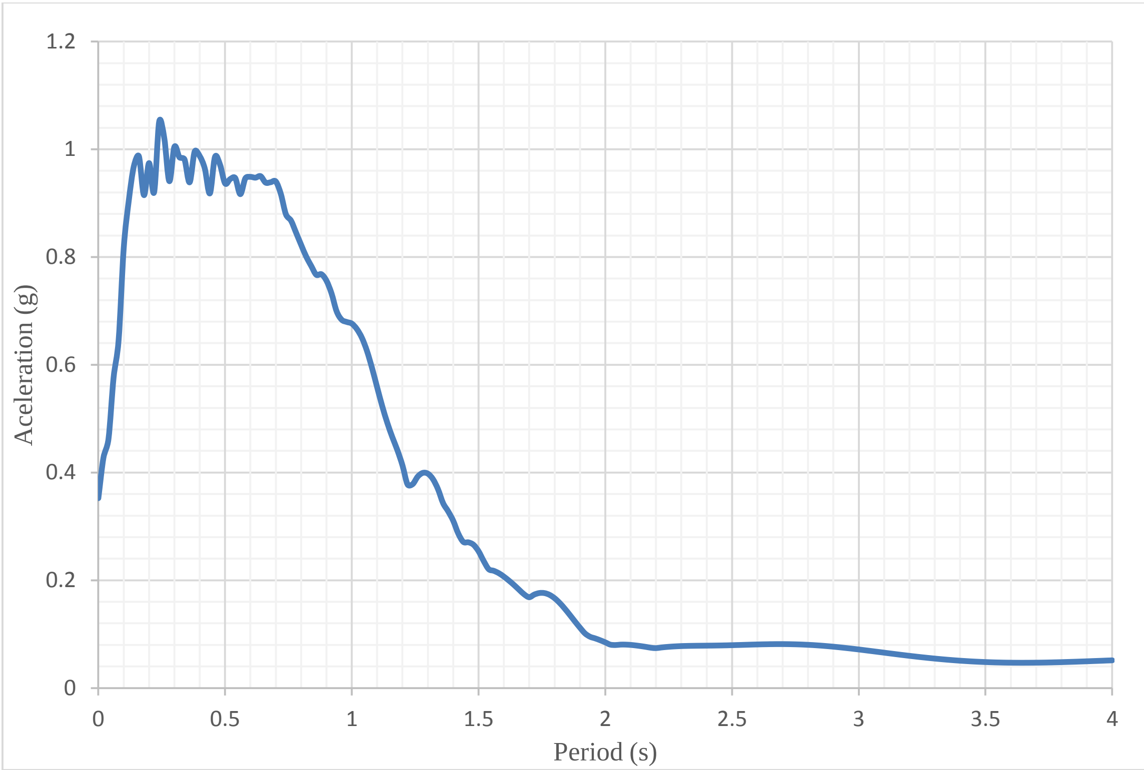

Figure 49. Loma Prieta response spectrum.

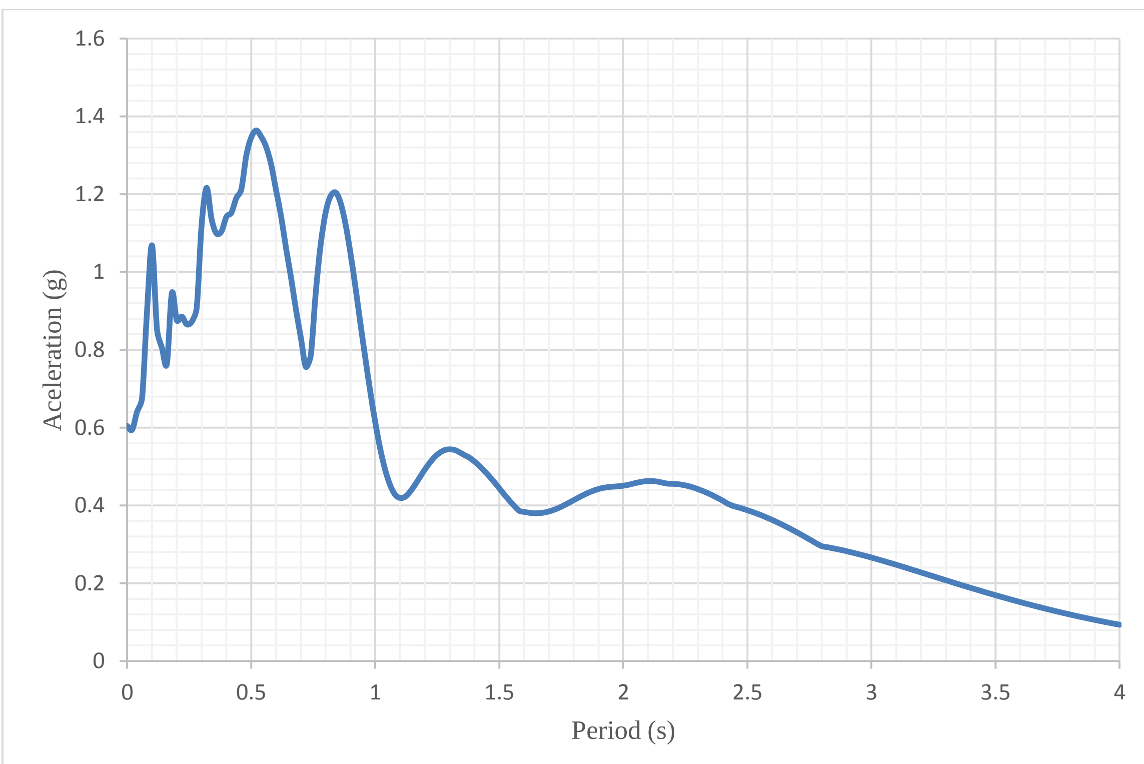

Figure 50. Northridge response spectrum.

b. The mass of the model was obtained dividing the effective weight by the number of joints of the model, presented in Figure 51, to distribute the mass uniformly. The model has 15 joints; therefore, for an effective weight of 1,935, this represents a mass of 0.33 kips-s^2/ft. per joint.

c. A constant viscous damping ratio of 5 % was used.

d. All the building connections were pinned to avoid transfer of the lateral load to the frames, thus transmitting the entire load through the braces.

e. A non-linear time history analysis was performed on the model with RCR shear walls, while a linear time history analysis was performed in the MIF model, due to the elastic and brittle nature of the plain masonry.

f. For the non-linear time history analysis performed on the RCR shear wall system, a force-displacement constitutive model was created to represent the behavior of the wall based on the experimental results. The first part of the bilinear model represents the initial stiffness, and the yield force was presented in section 5.2.2.3. The yield strength of the system was 134 kips, with a yield deformation of 0.25 in. The ultimate strength was calculated by multiplying the ultimate stress of the RCR-4 (175.00 psi) specimen by the double shear system cross sectional area (1680 in^2) and the number of rows (2 rows for the double shear system), and the resulted force was 588 kips with an ultimate deformation of 3.35 in. Figure 52 presents the force-displacement constitutive model for the RCR shear wall. It is plotted in both directions (positive and negative), because is a shear system that behaves in the same way back and forth.

5.3.2 TIME HISTORY ANALYSIS RESULTS

After concluding the time history analyses, three aspects of the responses were reviewed to compare the effects of the earthquakes on both systems: (1) Base Shear, *V*, and Top Acceleration, (2) Force-Displacement curves: hysteretic behavior, and (3) Story Drifts.

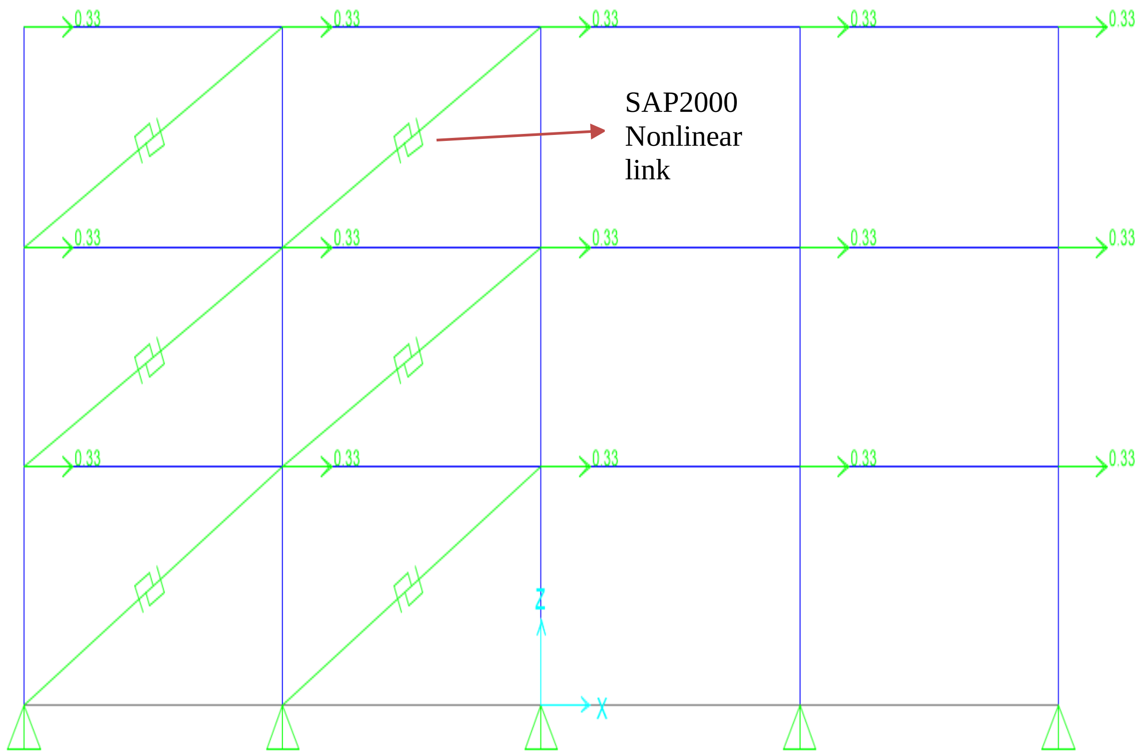

Figure 51. Frame mass assignments.

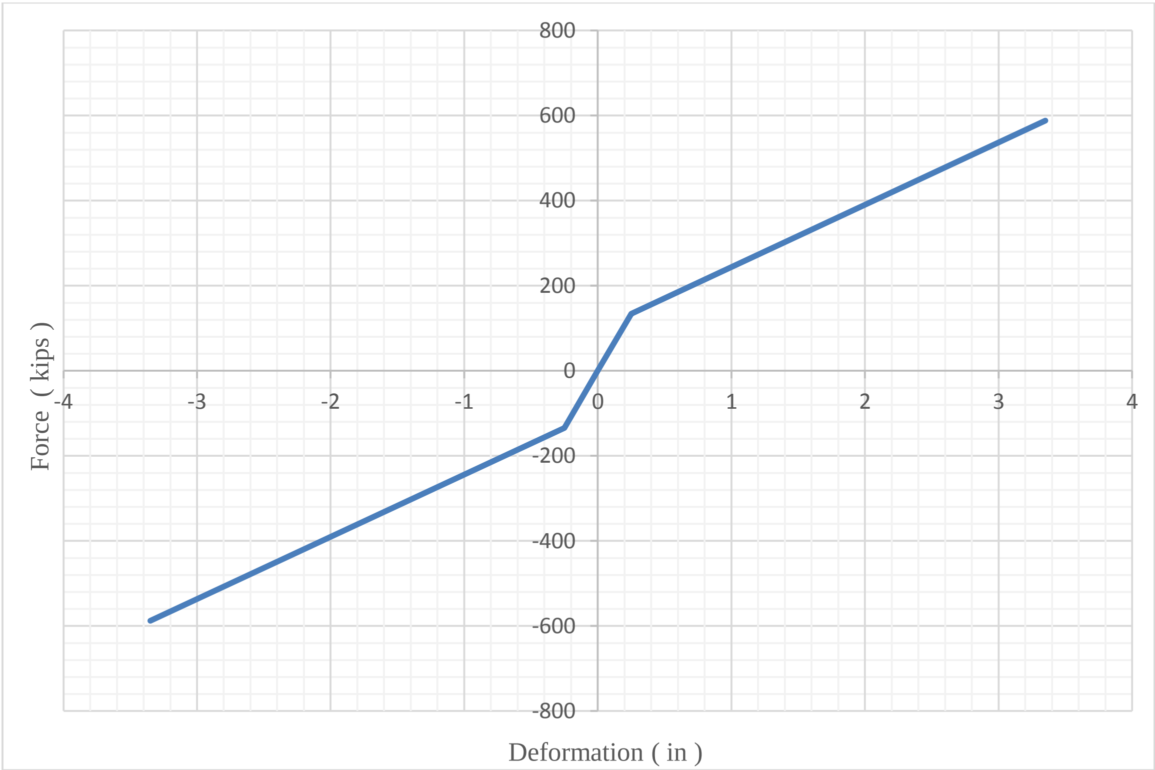

Figure 52. Force-displacement RCR shear wall constitutive model.

5.3.2.1 BASE SHEAR AND TOP ACCELERATION

For a better understanding of the results obtained from the time history analysis in this section they are presented in tables and graphs. The results are discussed below:

a) The following results are presented in Table 21 and Table 22: (1) The spectral acceleration S_a obtained from the earthquakes spectra in section 5.2.4, entering to the plot with the fundamentals periods of both systems (0.54 and 0.70 seconds, for MIF and RCR shear wall, respectively), (2) The maximum base shear V obtained from the analysis. (3) The ratio V/W between the base shear and the effective seismic weight (1,935 kips), and (4) the percent of difference between spectral acceleration for the first natural period and the base shear – effective weight ratio.

b) The base shear response for both systems is presented in Figure 53 to Figure 55.

c) The top acceleration response for both systems is show in Figure 56 to Figure 58.

Following the response spectrum theory, for a single linear degree of freedom system, the base shear can be obtained as:

$$V = S_a * W \tag{37}$$

Thus, the spectral acceleration can be compared with the base shear – effective weight ratio rewriting equation (37) as:

$$S_a = \frac{V}{W} \tag{38}$$

Table 21. Base shear analysis results: RCR.

Earthquake	S_a	V	V/W	Percent of Difference
-	(g)	(kips)	(g)	(%)
Centro	0.59	467	0.24	-59
Loma Prieta	0.94	584	0.3	-68
Northridge	0.83	966	0.5	-40

Sa = spectral acceleration

V = maximum base shear

V/W = base shear to effective weight ratio

Percent of Difference = difference between the spectral acceleration and the base shear to effective weight ratio

Table 22. Base shear analysis results: MW.

Earthquake	S_a	V	V/W	Percent of Difference
-	(g)	(kips)	(g)	(%)
Centro	0.87	1737	0.9	3
Loma Prieta	0.95	1762	0.91	-4
Northridge	1.35	2319	1.2	-11

Sa = spectral acceleration.

V = maximum base shear.

V/W = base shear to effective weight ratio.

Percent of Difference = difference between the spectral acceleration and the base shear to effective weight ratio.

In general, the first mode controls the behavior of a building frame without irregularities that can cause torsion, like the analyzed frame. Therefore, the spectral acceleration Sa for a linear single-dof and V/W fir a multi-dof model of the structure can be compared to look for differences; they are presented as the percent of difference. First, for the RCR system the percent of difference is on average greater than 50 %, which means that the system is dissipating energy through inelastic deformations, decreasing the lateral forces. For the MIF system, this did not happen because it is a linear system, which produces a similar response than the response spectrum predicts. In this case the small spectral differences are generated by the multiple degrees of freedom of the structure, which causes than more than one mode of vibration contributes to the response. However, from the tables it can be noticed that the difference does not exceed 11%, which suggests that the fundamental mode controls the response.

Another important aspect that must be pointed out is the difference between the maximum values of the base shear. For example, for the El Centro earthquake, the base shear of the MIF system was 3.72 times the response of the RCR shear wall. This means that it is possible to reduce the size of the frame sections by using the RCR shear wall system instead of the MIF. It can be seen from the graphs of the base shear that the response of the MIF is much greater than the RCR base shear. The same pattern is observed in the top acceleration plots.

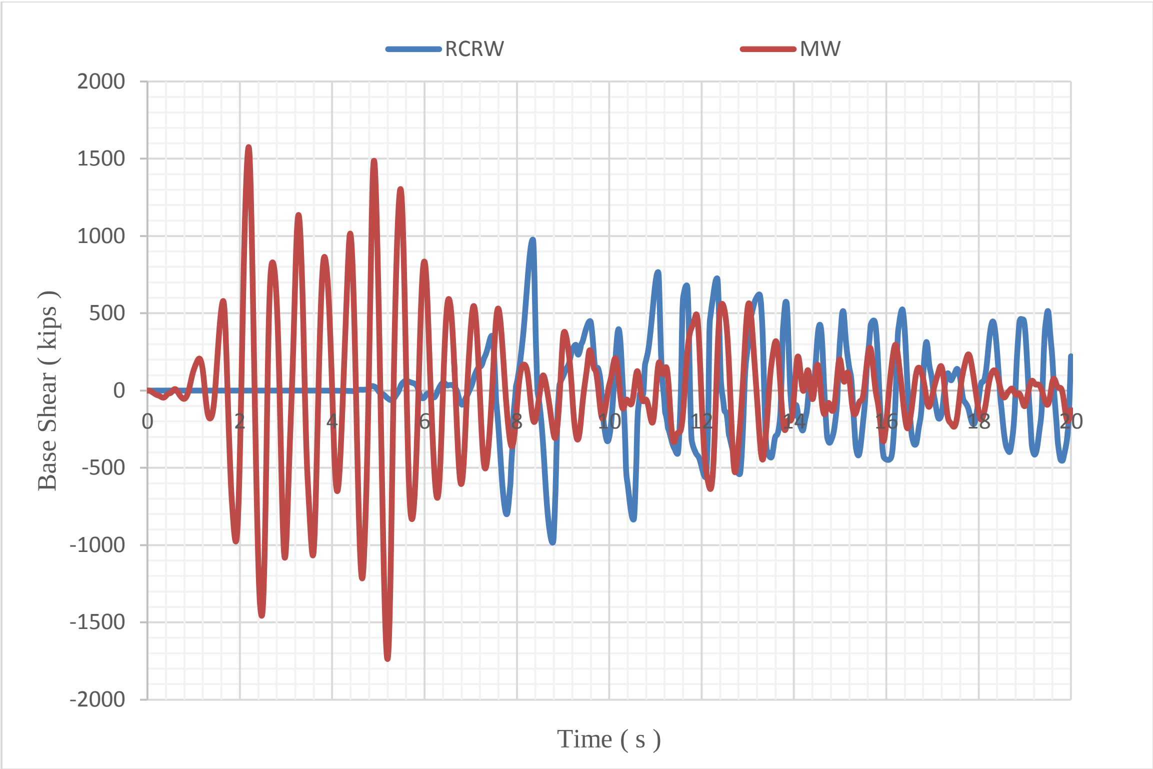

Figure 53. Frame base shear response – Centro

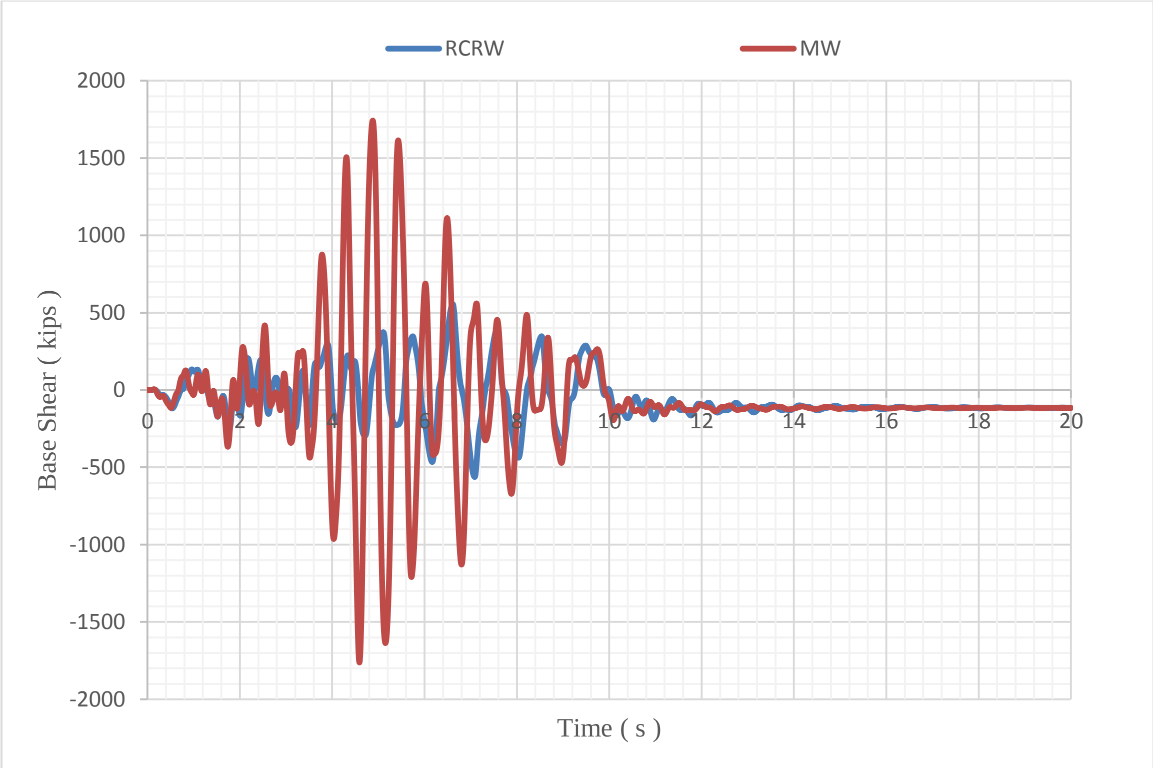

Figure 54. Frame base shear response – Loma Prieta

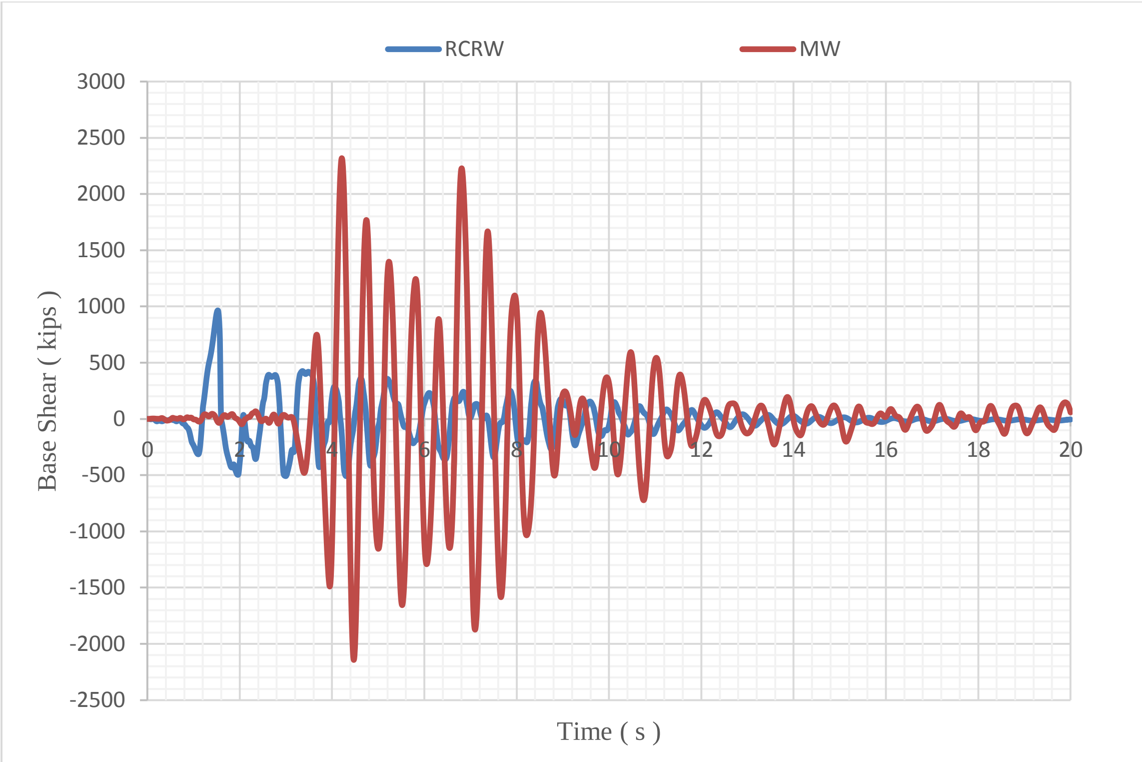

Figure 55. Frame base shear response – Northridge

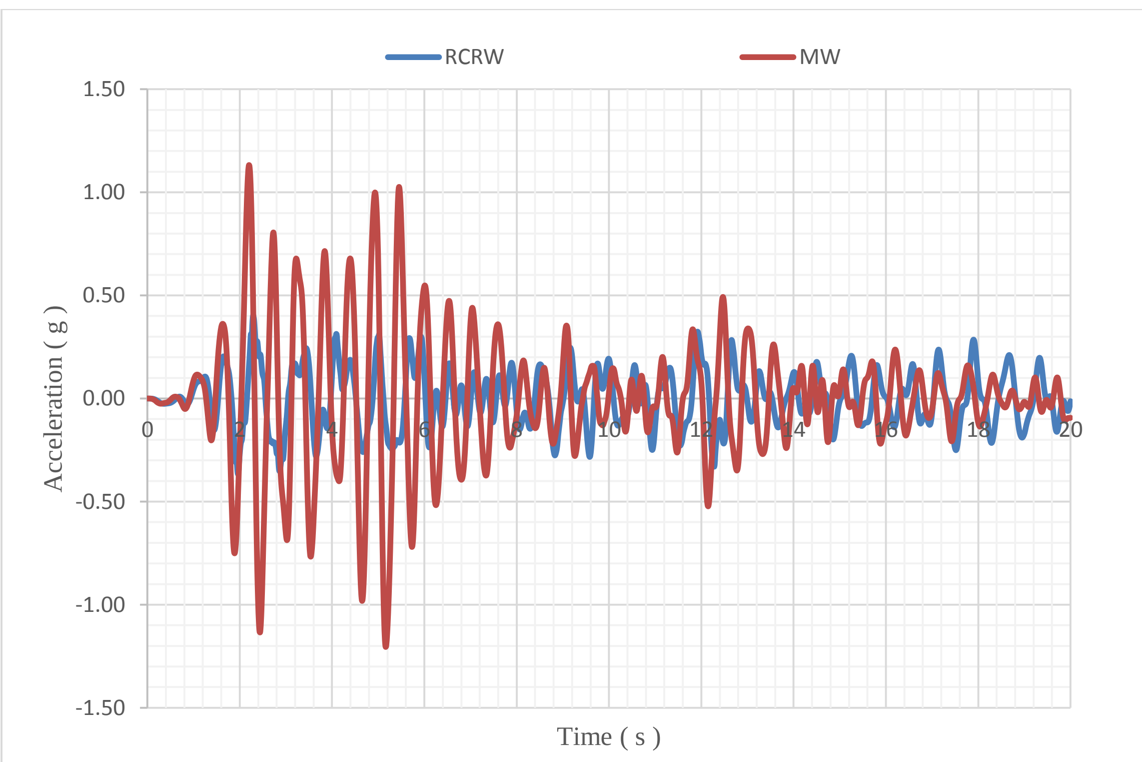

Figure 56. Top acceleration: El Centro

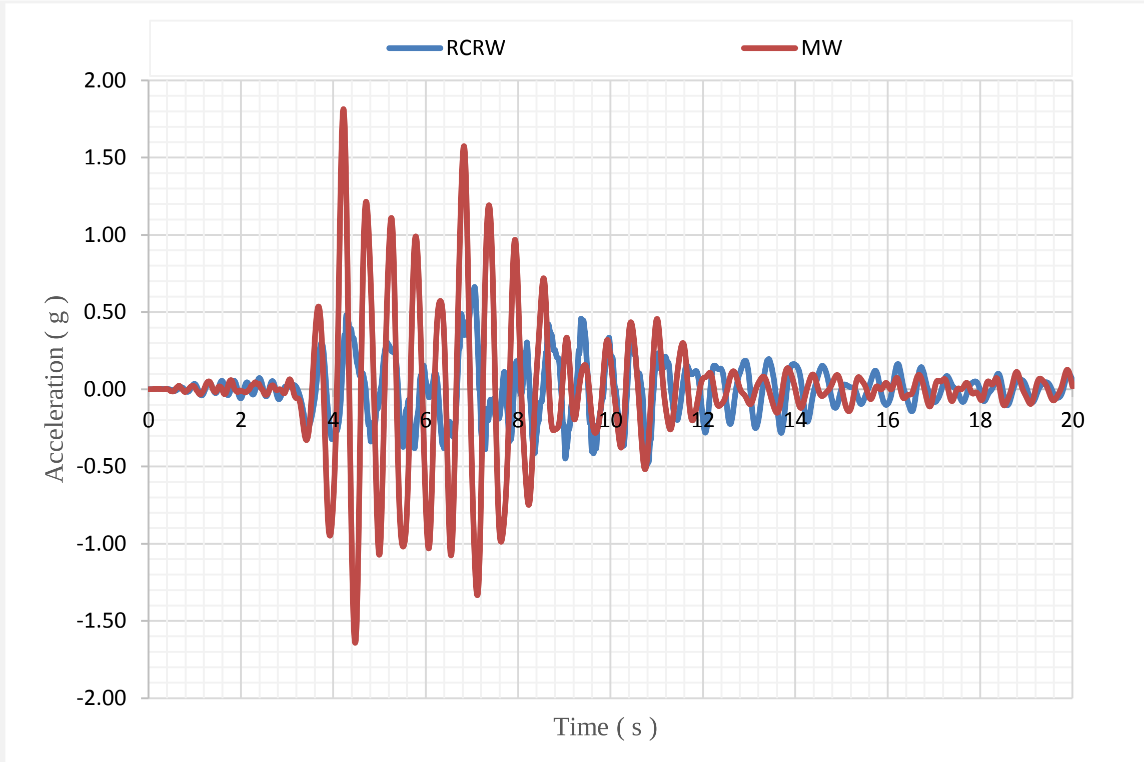

Figure 57. Top acceleration: Loma Prieta

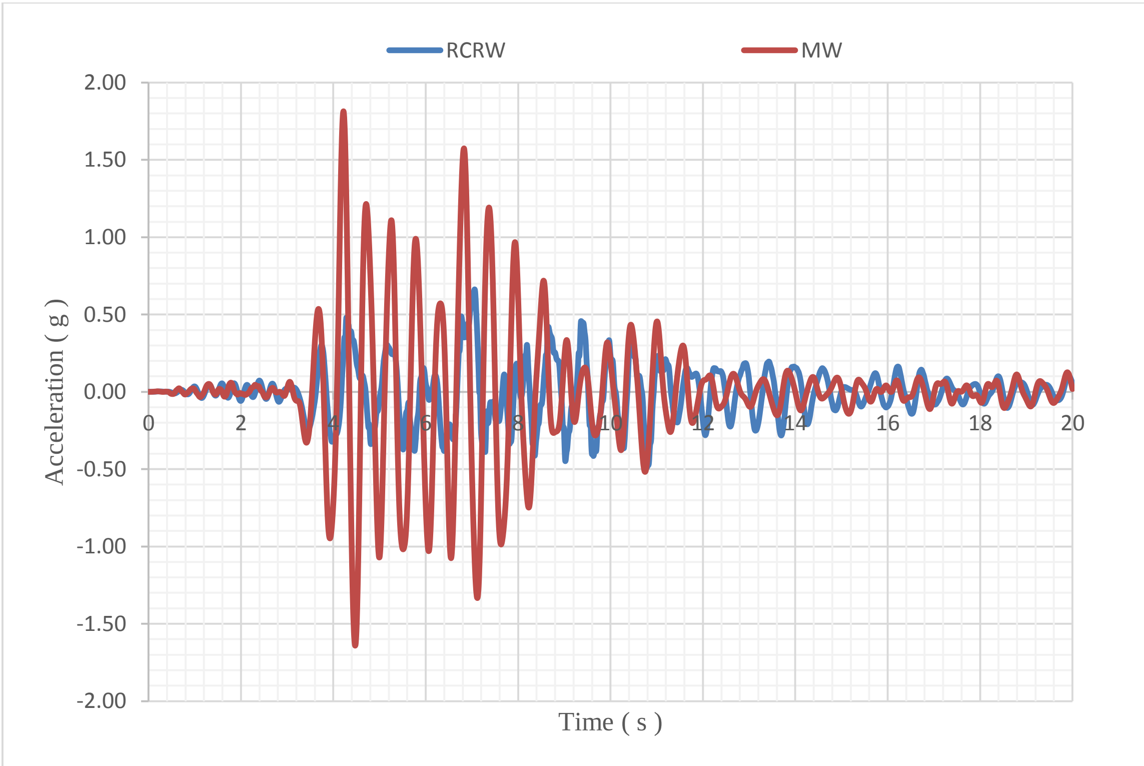

Figure 58. Top Acceleration: Northridge

5.3.2.2 FORCE VS DISPLACEMENT CURVES BEHAVIOR

Figure 59 through Figure 61 present the behavior of the axial force-displacement curves of the base links. The figures show the vast energy dissipation that the RCR shear system provides through the plastic cycles; whereas the masonry wall has a linear elastic behavior with no energy dissipation, because of the typical behavior of unreinforced masonry discussed previously. This effect forces the RCR shear wall system to decrease its response. For example, in the previous section was seen that the base shear and top acceleration had a dramatic decrease.

In addition, the base link experienced a maximum deformation of 3.09 in for the Northridge earthquakes. Having in mind that the yield deformation of the system was 0.25 in., the response of the link exhibited a ductility of 12.5. Therefore, this suggests that the RCR shear wall is a good system to resist earthquake loads, because: (1) the system can dissipate energy through hysteresis, meaning that the design can be done for lesser forces, (2) it is capable of sustaining a large deformation as it shows a ductile behavior before creating a collapse mechanism. From the axial force-displacement plots (see Figure 59 to 61) it can be noticed that for the three earthquakes, the masonry link exceeds 1,000 kips. Recalling that the ultimate strength of the masonry wall, obtained from the FEMA 306 in section 5.3.2, was 96 kips, the masonry wall fails in compression, because it barely represents 10 % of the required strength. On the other hand, the inelastic response of the RCR shear wall provided a maximum capacity of 588 kips (see section 5.2.3 and Figure 52), which is greater than the maximum force of 545 kips generated in the base link of the RCR shear wall model due to the Northridge earthquake.

5.3.2.3 STORY DRIFTS

Finally, the story drifts in percent of both systems are tabulated in Table 23. In general the drifts are similar for both systems. However, for the Northridge earthquake, the RCR shear wall system had a story drift of 2.63 %, which exceeds the maximum 2 % of drift established by ASCE 7-05, as discussed previously. This is not critical taking into account that the Northridge earthquake was devastating. Although

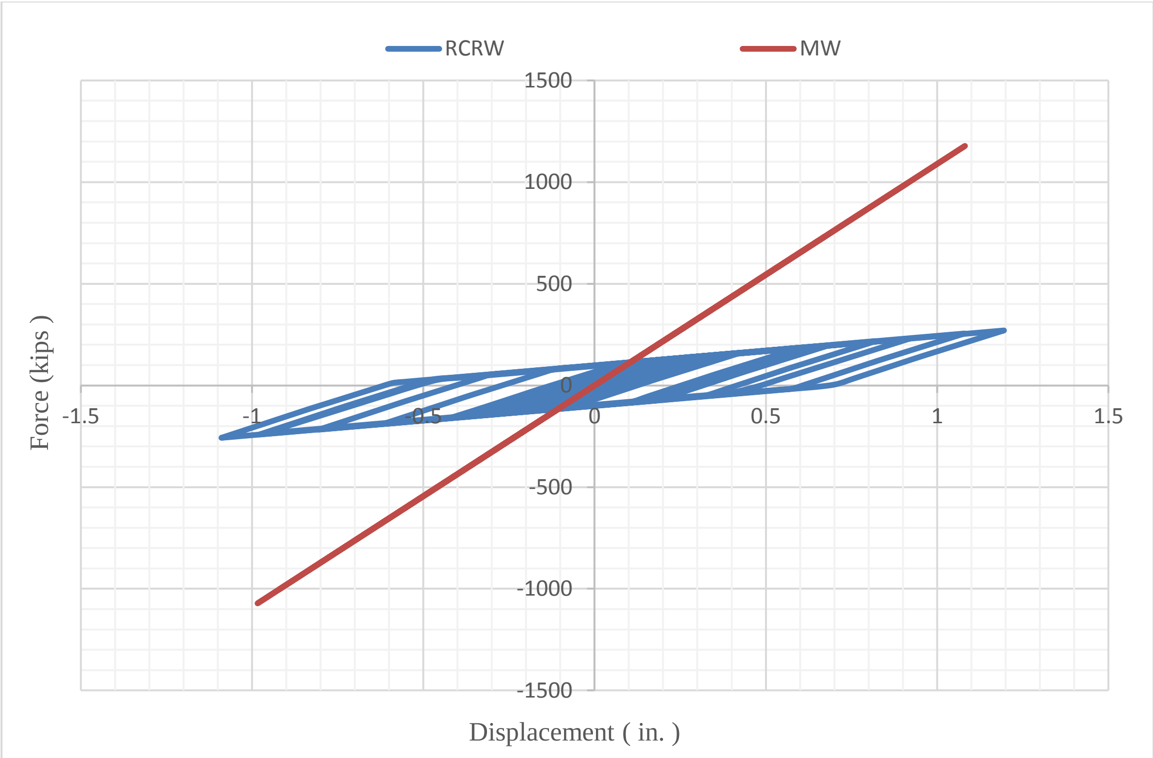

Figure 59. Force-Displacement base link curve: El Centro

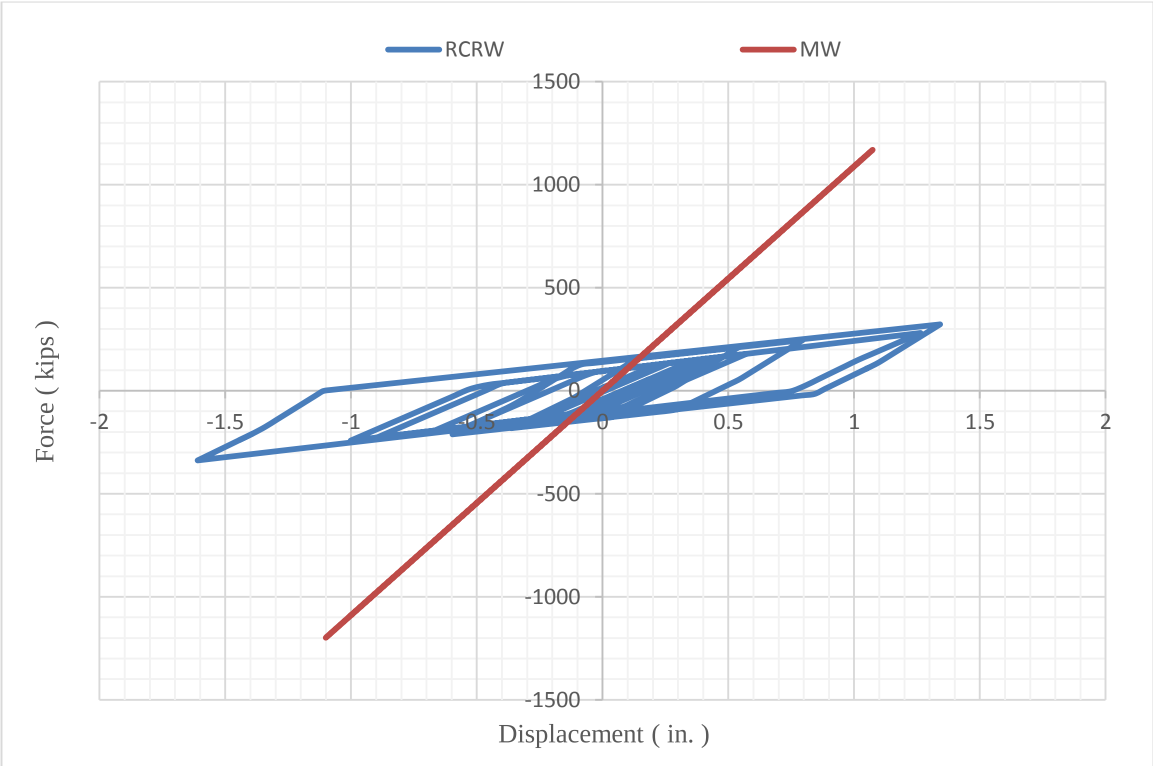

Figure 60. Force-Displacement base link curve: Loma Prieta

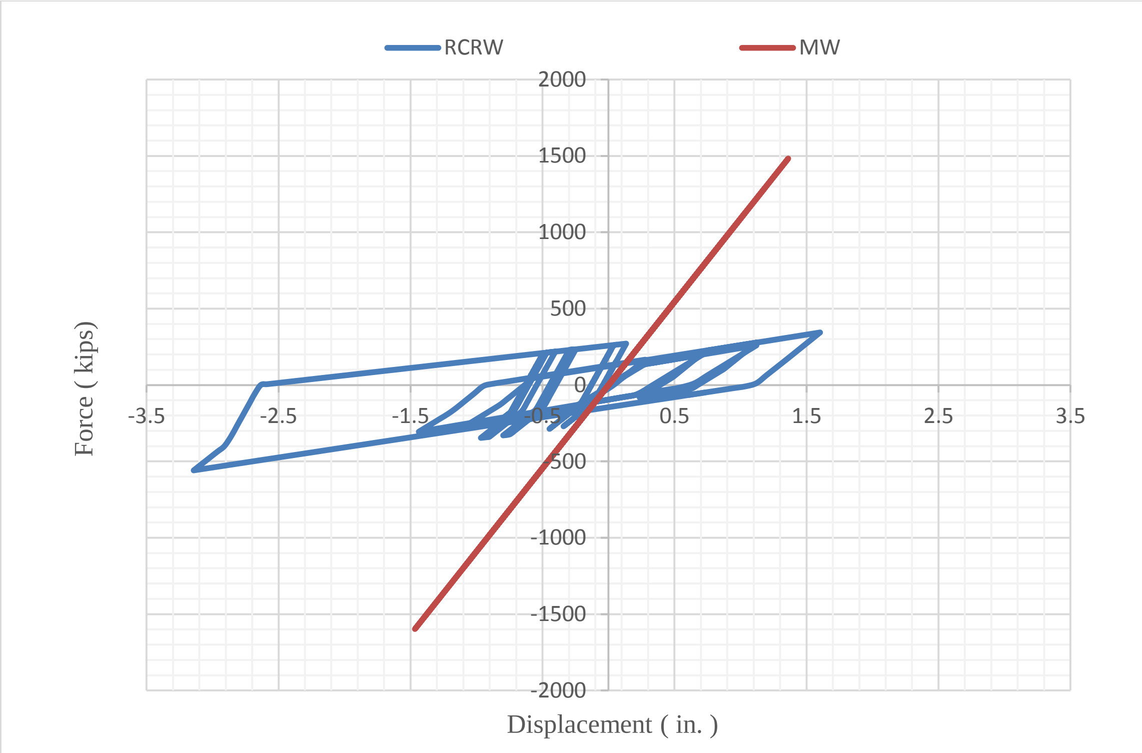

Figure 61. Force-Displacement base link curve: Northridge.

the other earthquakes were strong, the story drifts did not exceed the maximum drift established by ASCE 7-05 for the type of structure analyzed in this investigation.

In Section 5.2.2.3 was discussed the equation to obtain the maximum drifts for the RCR shear wall system. However, for masonry infill frames, the applicable equation of the ASCE 7-05 to calculate the maximum allowable drift is:

$$\Delta_x = 0.015\, h_{sx} \qquad \textbf{(39)}$$

Continuing the discussion of section 5.2.2.3 and recalling the equation (31), it follows that the maximum allowable drift is 1.5 % and 2.0 % for the masonry and RCR wall systems, respectively. Therefore, looking at Table 23, the maximum allowable drift was exceeded for the Northridge earthquake, which means that both systems do not meet the code. However, this is more critical for the masonry system

Table 23. Frame story drifts.

	RCRW shear wall system			Masonry infill frame system		
Story	**El Centro**	**Loma Prieta**	**Northridge**	**El Centro**	**Loma Prieta**	**Northridge**
-	(%)	(%)	(%)	(%)	(%)	(%)
1	1.05%	1.34%	2.63%	1.22%	1.20%	0.92%
2	0.79%	0.73%	1.93%	0.98%	1.05%	1.61%
3	0.29%	0.26%	0.77%	0.58%	0.66%	1.34%

due to the lack of ductility, leading to sudden failures; while the RCR wall system still conserves a deform capacity before collapse.

5.4 WIND LOAD ANALYSIS

An analysis of wind load using ASCE 7-05 standard guide for the X direction was performed to verify that the RCR shear wall system is controlled by the earthquakes loads. The Simplified Procedure presented in Section 6.4 was performed. The following discussion is based on the Section 6.4 of the ASCE 7-05. The equation to obtain the lateral pressure in the Simplified Method is:

$$p_s = \lambda * K_{zt} * I * p_{s30} \quad \textbf{(40)}$$

where

λ= height and exposure adjustment coefficient, obtained from the Figure 6-2. It is equal to 1.47 for a 37 ft building height, and a exposure category C (defined in Section 6.5.5).

Kzt = topographic factor as defined in Section 6.5.7. It is 1.0 for flat terrain.

I = importance factor as defined in Section 6.2. It is 1.15 for Occupancy Category III.

p_{s30} = simplified design wind pressure for Exposure B, at h = 30 ft., and for I = 1.0, from Figure 6-2. It is equal to 33.4 psf.

Performing the calculations in equation (40), a simplified design pressure of 56.46 psf was obtained. To determine the frame line load, the pressure was multiplied by 60 ft which is the Y distance in the building plan view, and finally was divided by two, to obtain the loads due to the tributary area. This gives a line load of 1.69 k/f, as shown in Figure 62. Using the following load combinations the maximum total base shear V_t for wind loads was obtained:

$$V_t = 1.2\,D + 1.6\,W + L \tag{41}$$

$$V_t = 0.9\,D + 1.6\,W \tag{42}$$

where

D = dead load

W = wind load

L = live load

From the equations, the maximum base shear was 100 kips which is just 55 % of the 182 kips seismic base shear obtained with the Equivalent Lateral Load Analysis. Therefore, the wind conditions do not control the design of the RCR shear wall system.

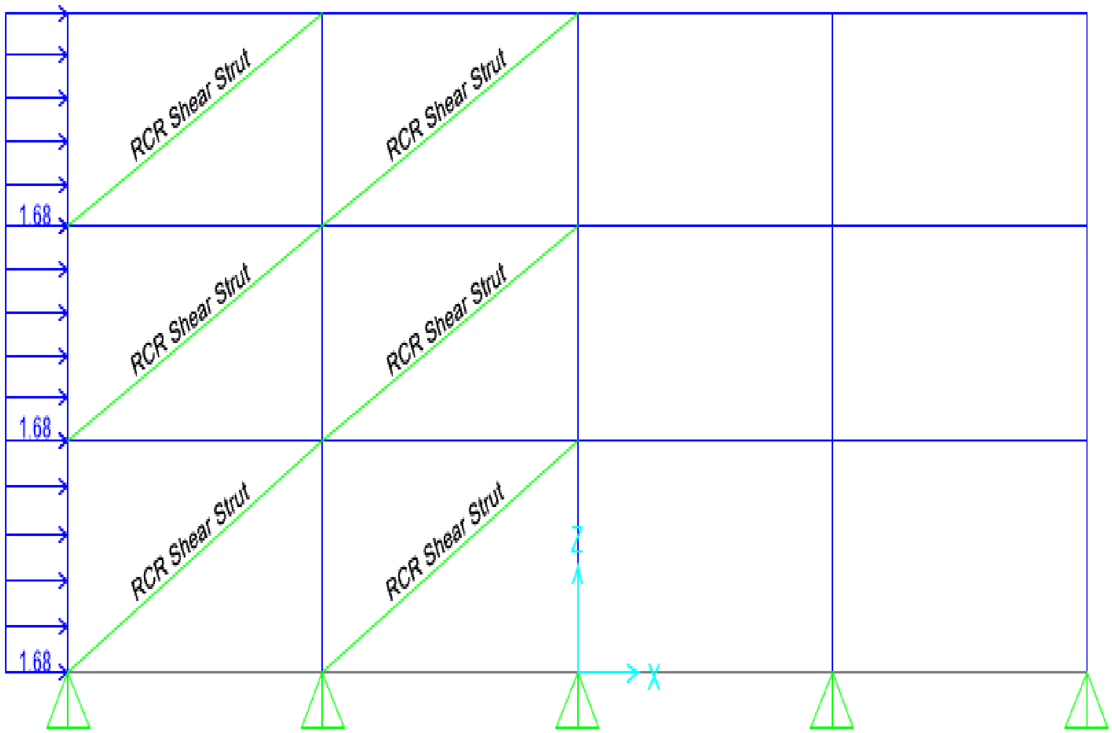

Figure 62. Wind frame line load.

CHAPTER 6

CONCLUSIONS AND RECOMMENDATIONS

6.1 INTRODUCTION

The following conclusions and recommendations are aimed to demonstrate that the objectives of this research were fulfilled. These conclusions are divided into experimental results and analytical predictions. The former discusses the most important results obtained from the experimental tests using crumb rubber. The latter are conclusions derived from the time history performed for the Reinforced Crumb Rubber shear wall and Masonry Infill Frame building, using three different earthquakes motions. Recommendations for future works using crumb rubber are suggested at the end.

6.2 CONCLUSIONS

6.2.1 EXPERIMENTAL RESULTS

1. From the Axial Cyclic Load Test performed on the crumb rubber it was obtained that:
    - The average ultimate compression stress of the crumb rubber block was 114.8 psi.
    - The average modulus of elasticity was 335.54 psi, with a maximum of 424.84 psi and a minimum of 257.08 psi, demonstrating a considerable variability.
    - The average ultimate strain was 42 %, meaning that the block can be compressed almost half its length before it fails.
    - The crumb rubber block ultimate tension stress was 30.0 psi, which represents 26 % of the ultimate average compression stress.
    - The ultimate tension strain obtained was 14.8 %.

- Tension and compression failures showed the typical 45° cracks that emerge from specimens subjected to pure axial loads. Furthermore, bulges were generated at the sides of the compression specimens.
- Two geometric configurations for the test were used, yielding similar stresses, suggesting an isotropic behavior.
- Stress-strain curves cycles showed little or no energy dissipation through hysteretic cycles since the material behavior was similar to a linear elastic material, and in the plots there were no area under the curves.
- Under the laboratory conditions, and the applied stress levels, the crumb rubber presented no signs of a time dependent response behavior, because the compression response did not change dramatically with changes in load velocity rate.

2. The average specific weight of the crumb rubber block was 61.05 lb/ft^3, which is in agreement with the manufacturer's tests.
3. From the Confined Crumb Rubber Steel Rebars Compression Test it was obtained that:
    - The crumb rubber confinement helped to improve the compression strength of slender steel rebars. The maximum increment obtained was 80 %, similar to the Cadamuro's results. This increase was measured in regard to the compression strength of the tested rebars with no confinement.
    - In general, as more area of confinement was used, a greater increase on the compression strength was obtained.
    - Elements with large slenderness ratio, exhibited higher compression strength.
4. From the Crumb Rubber Infill Test it was obtained that:
    - The crumb rubber panel, acting as an infill frame, was very sensitive to the slenderness ratio and the boundary condition. Specimens with large slenderness failed very quickly by buckling and out-plane bending moment, generated by the out-plane rotation of the

panel. The use of a confinement element at the borders of the panels improved the strength of the panel up to 22 %.

- From the test curves, it was shown that the panel continued behaving linearly elastic, with no energy dissipation or hysteretic cycles.
- The maximum lateral stress obtained was 28.89 psi.
- The maximum lateral rigidity of the infill panel was 128.57 psi.

5. In Plane-Resistance of Reinforced Crumb Rubber shear panel:

- Basically, the plain specimen showed a linear elastic behavior throughout all the cycles, resulting in little or no dissipation of energy through hysteretic cycles.
- The plain specimen shear modulus was 181.17 psi.
- The reinforced specimens presented a bilinear behavior, with a yield point, dissipating energy through inelastic hysteretic cycles.
- The more steel and stiffness, greater hysteric cycles were reached.
- A maximum initial stiffness, Gk_1, of 1,282.0 psi was achieved, reinforcing the panel with a reinforcement ratio of 2.07 %. It represents an increment of 390 % the stiffness of the plain specimen. The second part of the curve of the reinforced specimens showed an average stifness, Gk_2, of 250.8 psi, with a maximum of 348.2 for the 2.07 % reinforcement ratio, suggesting that the stiffness of the second part of the curve is provided by the crumb rubber, after the steel yield.
- The maximum yield shear stress reached by the wall was 40.06 psi, and the maximum ultimate stress was 175.00 psi.
- The maximum ductility was 13.46.
- Failure: The failure was controlled by the steel plasticization at the supports. The deformed shape looks like a typical deformed shear wall, and the rebars cut the rubber. In addition, some of the rebars were broken due to cyclic stresses. Therefore, the hysteretic

behavior is mainly associated to the steel plasticization, the breakage of the rebars, and the cutting of the rubber block by the movement and deformation of the rebars.

6.2.2 ANALYTICAL RESULTS

1. Using the Reinforced Crumb Rubber shear wall system it was possible to reduce the base shear of the structure in comparison to the base shear obtained for the Masonry Infill Frame system. The base shear reduction range was 42-73 %. This percent of reduction is attributed to two factors: (1) the hysteretic behavior, which contributes to dissipate energy, providing a greater damping that reduces the amplitude of the system response, and (2) following the philosophy of ASCE 7 whereas the period of the structure increases, the seismic response coefficient decreases, which is based on the general trend of earthquakes spectra, the response of the Reinforced Crumb Rubber shear wall was lower because had a longer period compared with the Masonry Infill Frame.
2. The Reinforced Crumb Rubber shear wall system base shear obtained from the non-linear time history showed a reduction of 40 – 68 %, regarding the earthquake elastic spectra with a damping of 5 %, which means that the system response decreases due to the inelastic response of it.
3. The reduction behavior is also manifested at the top building acceleration. For example, the maximum acceleration for the Masonry Infill Frame in the Northridge earthquake was 1.74 g, while for the Reinforced Crumb Rubber shear wall was 0.69 g, which represents a reduction of 60%.
4. In general the drifts were similar for both systems. However, for the Northridge earthquake the Reinforced Crumb Rubber shear wall system had a story drift of 2.63 %, which exceeds the maximum 2 % of drift established by ASCE 7-05. Nevertheless, this data was not considered critical since the required ductility for this case was 12.5 and the maximum ductility achieved on the experimental tests was 13.46. Therefore, the system continues having a deformed capacity. However, the Masonry Infill Frame exceeded the 1.5 % drift stated by the ASCE 7-05, which is critical for this case due to the lack of ductility of masonry.

5. The advantages of using an Reinforced Crumb Rubber shear wall were: (1) decreasing the base shear of the structure by the flexibility and the hysteretic behavior offered by the material inelastic response, which in turn results in a reduction of the frame element sections, (2) the ability of the system to deform with a maximum ductility of 13.46, which offers a ductile response, and (3) a reduction in the quantity of waste scrap tires that every year end in the landfills, and contributes to one of the biggest environmental problems.

6.3 RECOMMENDATIONS

1. Determine the mechanical properties of the crumb rubber with high quality manufacturing control of the material and in standardized form in future works.
2. Develop a statistical study suggesting designing values of the crumb rubber and the properties variability.
3. Extend the works of slender elements for several slenderness ratios and different confinement configurations, as for example: a bending test over a crumb rubber beam with a core composed of a steel truss with elements.
4. Carry out experimental tests to determine the capacity of the double shear system, varying the reinforcement ratio, steel rebars diameter and yield stress and size (height, length, thickness) of the Reinforced Crumb Rubber wall.
5. Perform a scale size in-plane cyclic load test in a Reinforced Crumb Rubber wall to verify whether in fact the use of a double shear wall system capacity increases by increase the length and the area of the wall.
6. Construct a scale model of Reinforced Crumb Rubber shear wall system building to perform an experimental time history using a shaking table in order to verify whether the system behaves as predicted in the non-linear time history analysis performed with SAP2000.

7. Conduct a study to define the response modification coefficient R for the RCR shear wall system.
8. Perform a dynamic test to determine the equivalent damping ratio of the recycled crumb rubber.

REFERENCES

American Society of Civil Engineers (ASCE) (2005). "Minimum Design Loads for Buildings and Other Structures". Reston, VA.

Botero, J., et. al. (2005). "Gomas Trituradas: Estado del Arte, Situación Actual y Posibles Usos como Materia Prima en Puerto Rico." *Rev. Int. de Desastres Naturales, Accidentes e Infraestructura Civil.*, 5(1), 69–86.

Cadamuro, J. (2009). "A study on the use of recycled crumb rubber in reinforced rubber piles." MS thesis, The Cooper Union Albert Nerken School of Engineering, New York, NY.

Centers for Disease Control and Prevention (CDC). "Mosquitoes' Main Aquatic Habitats." <http://www.cdc.gov/dengue/entomologyEcology/m_habitats.html>. (September 10, 2009)

CDC. "Dengue, Entomology & Ecology." <http://www.cdc.gov/dengue/entomologyEcology/m_habitats.html>. (July 26, 2010)

Federal Emergency Management Agency (FEMA). (1997). *NEHRP guidelines for the seismic rehabilitation of buildings*. FEMA-273, Building Seismic Safety Council, Washington, D.C.

FEMA. (1998). *Evaluation of Earthquake Damaged Concrete and Masonry Wall Buildings*. FEMA-306 Building Seismic Safety Council, Washington, D.C.

Holmes, M. (1961). "Steel Frames with brickwork and concrete infilling." *Proceedings of the Institute of the American Society of Civil Engineers*, 19, 473-478.

International Code Council (ICC). (2009). *International Building Code*. Country Club Hills, IL.

Kadir, M. R. (1974). "The structural behavior of masonry infill panels in framed structures." PH.D. thesis, University of Edinburgh, Edinburgh, Scotland.

Lawless, D., and Hawk, D. (2013). "BCSI Guidelines for Continuous Lateral Restraint & Diagonal Bracing of Metal Plate Connected Wood Trusses." *Structural Building Component Magazine*, April, 10–11.

Lecuchars, J., and Scrivener, J. (1976). "MASONRY INFILL PANELS SUBJECTED TO CYCLIC IN-PLANE LOADING." *Bulletin of the New Zealand National Society for Earthquake Engineering*, 9(2), 122–131.

Liaw, T., and Kwan, K. H. (1984). "NONLINEAR BEHAVIOR OF NON-INTEGRAL INFILLED

FRAMES." *Computer and Structures*, 18 (3), 551–560.

Mainstone, R. J. (1971). "On the stiffness and strengths of infilled frames." *Proceedings, Institution of Civil Engineers*, Supplement IV, 57–90.

Narendra, T. (2010). *Design of Reinforced Masonry Structures*. 2nd ed. McGraw-Hill.

Office of Environmental Health Hazard Assessment (OEHHA). (2007). *Evaluation of Health Effects of Recycled Waste Tires in Playground and Track Products*. Sacramento, CA.

Paulay, T., and Priestley, M. (1992). *Seismic Design of Reinforced Concrete and Masonry Buildings*. 1st ed. John Wiley & Sons Inc.

Polyakov, S. V. (1960). *On the interaction between masonry filler walls and enclosing frame when loading in the plane of the wall*. Earthquake Engineering Research Institute, San Francisco, 36–42.

Salmon, C., J., and Malhas, F. (2008). *Steel Structures Design and Behavior*. 5th ed. Prentice Hall.

Santiago, I. (2002). "Seismic Retrofitting of Structures using Recycled Plastic." University of Puerto Rico, Mayagüez Campus, Mayagüez, Puerto Rico.

Shing, P. B. et. al. (1990). "In-Plane Resistance of Reinforced Masonry Shear Walls." *Journal of Structural Engineering*, 116(3), 619–640.

Stafford, S., and Carter, C. (1969). "A method of analysis for infill frames." *Proc. Inst. Civil Engrs*, 44, 31-48

Stafford Smith, B. (1961). "Behavior of Square Infilled Frames." *Journal of Structural Division*, Proceedings of the American Society of Civil Engineers, 92, 381–403.

Velásquez, E. (2001). "Reciclaje de Neumáticos: Una Gran Industria." *Dimensión*, Colegio de Ingenieros y Agrimensores de Puerto Rico, CIAPR, 4, 29–32.

Williams, A. (2011). *Steel Structures Design*. 1st ed. McGraw-Hill, United States.

World Health Organization (WHO). "Impact of Dengue." <http://www.who.int/csr/disease/dengue/impact/en/>.

Yura, J. (2001). "Fundamentals of Beam Bracing." *Engineering Journal*, 38(1), 11–26.